THE PRESSURE DEPENDENCE OF SPONTANEOUS MAGNETIC FIELDS IN LASER PRODUCED PLASMAS

Ronald Stanley Bird

NAVAL POSTGRADUATE SCHOOL
Monterey, California

THESIS

The Pressure Dependence of Spontaneous Magnetic Fields in Laser Produced Plasmas

by

Ronald Stanley Bird

Thesis Advisor: A. W. Cooper

Approved for public release; distribution unlimited.

The Pressure Dependence of Spontaneous Magnetic Fields in Laser Produced Plasmas

by

Ronald Stanley Bird
Lieutenant Commander, United States Navy
B.S., University of Florida, 1964

Submitted in partial fulfillment of the
requirements for the degree of

DOCTOR OF PHILOSOPHY

from the
NAVAL POSTGRADUATE SCHOOL
June 1973

ABSTRACT

A plasma has been produced by irradiation of an aluminum slab with a 6.6 joule, 22 nanosecond (10^{10} watt/cm^2) pulse of 1.06 micron radiation. Magnetic fields were observed to arise spontaneously when the laser-produced plasma was formed. The space and time behavior of the spontaneous magnetic fields and their relationship to the plasma density profile for expansion into various background pressures of H_2, He, N_2 and Ar was investigated using magnetic and electrostatic (double) probes. The magnitude and direction of the magnetic fields was found to depend on the background gas pressure. The generation of spontaneous magnetic fields at the front of the expanding laser plasma was observed long after laser irradiation ceased. These fields were axially symmetric and in a direction opposite to the initial field direction. Reverse fields were observed only above a "critical" background gas pressure. Magnetic fields were also observed to arise when a laser plasma impinged on a glass plate.

The observed increase of the magnitude of the initial spontaneous magnetic fields is interpreted as arising from the momentum interaction between the expanding laser plasma and the pre-ionized ambient background plasma. The reverse field is attributed to the development of an axial electron temperature gradient at the plasma front due to snowplowing of the ambient plasma.

TABLE OF CONTENTS

LIST OF TABLES

LIST OF FIGURES

ACKNOWLEDGEMENT

I wish to thank Mr. Hal Herreman for assisting in the maintenance of the laser system and for his help in the setting up of the plasma diagnostic systems. To my colleague Larry McKee I would like to extend my sincere gratitude. Without his initial investigation of the spontaneous magnetic fields and his invaluable assistance in interpreting the data obtained in the present investigation, this thesis would not have been possible. I would like to thank Professor Schwirzke for suggesting complimentary experiments which helped in the interpretation of the experimental results and Professor Cooper for helping me to put the interpretation into words.

To my wife, Pen, I wish to convey my deep appreciation for her continual encouragement and patience.

This research was sponsored by the Office of Naval Research.

I. INTRODUCTION

Since the first theoretical considerations on plasma production by means of laser beams in 1963, a considerable amount of research has been devoted to the subject of high power laser interaction with solid targets. In metals, the light is absorbed by interaction with electrons. An electron in the conduction band will be excited to a higher energy level when it absorbs an incident photon. This energy will eventually be shared with other electrons and ions through collisions. Since the mean free time between collisions of electrons in a conductor is of the order of 10^{-13} sec, the electrons which absorb the incident photons will make many collisions, both among themselves and with lattice phonons, in times of the order of the duration of the laser pulse (nanosecond laser pulse). The optical energy can therefore be regarded as instantaneously turned into heat at the point at which the light is absorbed. One can invision, therefore, the possibility of heating a small amount of solid material to a very high temperature in a very short time. It has been this possibility that has motivated much of the work on laser-produced plasmas; the goal being attainment of controlled thermonuclear fusion through laser irradiation of solids.

In investigating the formation and subsequent development of the highly ionized plasma which results when the incident laser radiation (irradiance $\geq 10^9$ W/cm^2) is absorbed by the target material, it has generally been assumed that the only magnetic fields present were those induced by external sources. However, it has recently been discovered that a magnetic field may arise spontaneously when a laser plasma

(laser-produced plasma) is produced either by the laser induced breakdown of a gas [Ref. 21] or by the laser irradiation of a solid target [Ref. 13] . These investigations imply that spontaneous magnetic fields may arise under very general conditions during the production of a laser plasma. Since the largest spontaneous fields observed have been of the order of kilogauss at a distance of several millimeters from the "point" of the laser impact on the target surface, much larger fields have been predicted in the region where absorption of the laser radiation occurs (within $\sim$1 mm from the target surface). In fact, in a recent computer simulation experiment, Widner [Ref. 22] has observed a spontaneous field intensity of the order of 1 MG near the laser impact point. Magnetic fields of this magnitude can have a significant influence on the dynamics of a laser plasma (for example, by influencing electronic heat conduction and the generation of plasma instabilities). By inhibiting shock compression of the target, such spontaneous fields could exert a critical influence on the approach to thermonuclear conditions in laser-fusion experiments.

This thesis contains the first study of the effect of the presence of various background gases on the spontaneous magnetic fields (produced by irradiation of an aluminum slab with a 300 MW (6.6 J in 22 nsec) Nd-doped glass laser) and of the relationship of the spontaneous magnetic fields to the laser plasma density profile. It is a continuation of the investigation begun by L. L. McKee [Ref. 12] on the spatial and temporal behavior of the spontaneous magnetic fields associated with a Mylar $(C_{10}H_8O_9)_n$ laser plasma expanding into a background of nitrogen gas.

The spontaneous fields were detected using magnetic probes (inductive

loops). The probe coils consisted of five turns of #40 Formvar copper wire and had a diameter of about 1 mm. The probe circuit response was linear for frequencies below about 30 MHz. The plasma density profiles were diagnosed with electric double probes. The double probes were maintained at a fixed bias of sufficient magnitude (10 volts) to insure collection of saturation ion current. Since the expansion velocity of the laser plasma (10^7 cm/sec) was greater than the ion thermal velocity, the probe current was proportional to the product of the ion density and the plasma expansion velocity. The expansion velocity was obtainable from the probe signals so that the relative density of the plasma could be calculated.

This thesis is divided into nine more sections. Section II discusses the previous experimental work connected with the spontaneous magnetic fields. The thesis problem is stated in Section III. Section IV presents the basic theory of laser-produced plasmas including the influence of an ambient background gas on the laser plasma expansion dynamics. The theory of the initial production of the spontaneous magnetic fields is developed in this section. Section V contains the details of the experimental procedures. The experimental results are presented in Section VI. They include the spatial mapping of the magnetic fields and their density profiles, the pressure dependence of the magnetic fields associated with laser plasmas expanding into ambient backgrounds of N_2, Ar, He and H_2, and the observation of the production of fields in a direction opposite to the initial field direction at sufficiently high background gas pressures. This production of reverse field occurred long after the cessation of the laser pulse and it occurred at the front of the expanding laser plasma. In addition, reverse field was

observed when the expanding laser plasma impinged on a glass plate. In Section VII the experimental results are compared with the model proposed by McKee to explain the strong dependence of the magnetic fields on the pressure of the background gas. The model is shown to be incorrect in that it cannot be used to explain the results of the present investigation. In Section VIII a model is developed to explain the pressure dependence of the spontaneous magnetic fields and this model is compared with the experimental results in Section IX. The summary and conclusions are contained in Section X.

II. PREVIOUS RESEARCH

A. THE DISCOVERY OF THE FIELDS

During the latter part of 1970, as part of a study of the interaction between a laser plasma and the ambient background plasma through which it was streaming, Stamper et al. [Ref. 13] discovered that magnetic fields were spontaneously generated in the laser-produced plasma. They used a neodymium doped glass laser with an output of 60 J in 30 nsec, a beam diameter of 32 mm, and a full angle, half power beam divergence of 200 μ rad to produce a plasma by irradiation of a 250 μm diam (approximate diam of focal spot) fiber of Lucite $(C_5H_8O_2)_n$. Experiments were also conducted using silver and aluminum discs. The spontaneous fields were observed with magnetic probes (inductive loops) as the plasma streamed into various pressures of nitrogen background gas. They reported that:

(1) The magnetic fields were seen as pulses which propagated with the same velocity as the front of the laser plasma.

(2) The magnitude of the fields was insensitive to background pressure in the range from 50 mTorr to 200 mTorr.

(3) The fields were primarily azimuthal (cylindrical-polar coordinates) and corresponded to conventional current flow in the direction of the laser beam.

(4) The maximum fields varied as r^{-1} in the radial direction for distances less than 1 cm from the target.

(5) The duration of the fields at probe positions near the laser impact point was approximately that of the laser pulse.

(6) The maximum fields observable were of the order of a kiloguass at about r=0.5 cm.

(7) Magnetic fields were also spontaneously generated in the laser plasmas produced by irradiation of the aluminum and silver discs. The maximum fields produced by laser irradiation of aluminum were an order of magnitude larger ($\sim 10^3$ gauss) than those produced by irradiation of silver.

The generation of these fields was explained in terms of thermoelectric currents associated with large temperature gradients existing near the target surface during the time the laser irradiates the target. In their theoretical analysis of the origin of the fields, they neglected any interaction that might occur between the laser plasma and the ambient background plasma, although they pointed out that because of the strong (observed) coupling of the expanding laser plasma to the ambient background plasma, their simplified model would need re-examination at later times in the expansion of the laser plasma. They derived an equation for the development of the magnetic field by starting with a generalized Ohm's law, neglecting electron inertia and ion pressure. Their result was

$$\frac{\partial \vec{B}}{\partial t} = \nabla\times(\vec{V}_e\times\vec{B}) + \frac{1}{\mu_o\sigma}\nabla^2\vec{B} + \vec{S}(\vec{r},t) \qquad (1)$$

where $S(\vec{r},t)$, the source term, was shown to have a non-zero value if $\frac{\nabla kT_e}{e} \times \frac{\nabla n_e}{n_e} \neq 0$ (a complete discussion of the derivation of Eq. (1) is given in Section IV. C).

B. THE DISCOVERY OF THE PRESSURE DEPENDENCE OF THE SPONTANEOUS MAGNETIC FIELDS

Shortly after the discovery of the spontaneous magnetic fields by Stamper *et al.* an extensive study of such fields was begun by L. L. McKee

at the Naval Postgraduate School [Ref. 12] . In particular, the dependence of the magnitude of the fields on the power of the incident laser beam and on the ambient pressure of nitrogen background gas was studied. A detailed spatial mapping of the fields for pressures of 0.1 mTorr, 5 mTorr and 250 mTorr was conducted. The study was carried out using a 300 MW (7.5 J and 25 nsec) neodymium-doped glass laser, a Mylar disc target of 5 mil thickness, and glass enclosed inductive loops for field characterization. During McKee's investigation the following observations were made:

(1) The maximum fields detected at a fixed position exhibited a systematic dependence on the nitrogen background pressure.

(2) The fields were symmetric about the target normal (the z-axis in Fig. 1), although the laser beam was incident at an angle of 30° with respect to the target normal (Stamper had reported azimuthal symmetry for the case of normal incidence).

(3) The total magnetic field energy at any given time in the expansion phase of the laser plasma was dependent on the nitrogen background pressure.

(4) The maximum magnetic field signals occurred earlier in time at 250 mTorr N_2 than at 0.1 mTorr N_2 for axial positions close to the target (distances less than about 1 cm). As a result of this, on the spatial plots of the fields the axial position of the maximum fields at 250 mTorr N_2 appeared to "propagate" ahead of those for 0.1 mTorr N_2 at early times in the expansion of the laser plasma ($t < 200$ nsec).

(5) After several hundred nanoseconds, a relatively small magnitude field in a direction opposite to the direction of the initial

field appeared behind the initial fields. This reverse field appeared sooner in time for a pressure of 250 mTorr than for 0.1 or 5 mTorr.

To explain the observed pressure dependence McKee noted that Dean [Ref. 8], using the same experimental arrangement as Stamper et al., had apparently observed the formation of a density shell at the front of a laser plasma streaming into an ambient nitrogen background plasma. Dean found that:

(1) A well defined expanding interaction front existed.

(2) The dynamics of the expansion of the front were dependent on the pressure of the ambient nitrogen background gas.

(3) The density gradients in the shell depended on the pressure of the ambient nitrogen background gas. The shell thickness, δ, scaled approximately as the inverse cube root of the nitrogen background pressure, decreasing from 2.4 mm at 25 mTorr to 1.2 mm at 200 mTorr.

(4) The dynamics of the expansion suggested a strong momentum coupling between the laser plasma and ambient background plasma. The average expansion velocity of the front during laser irradiation of the target was inversely proportional to the cube root of the ambient pressure from about 30-250 mTorr N_2 pressure.

McKee used Dean's results, arguing that in his experiment the ambient nitrogen plasma would be "swept-up" at the front of the expanding laser plasma and a density shell would be formed. He never actually described the overall shape of the plasma spatial density profile that he had in mind, but from his discussion a profile similar to the one depicted below can be inferred.

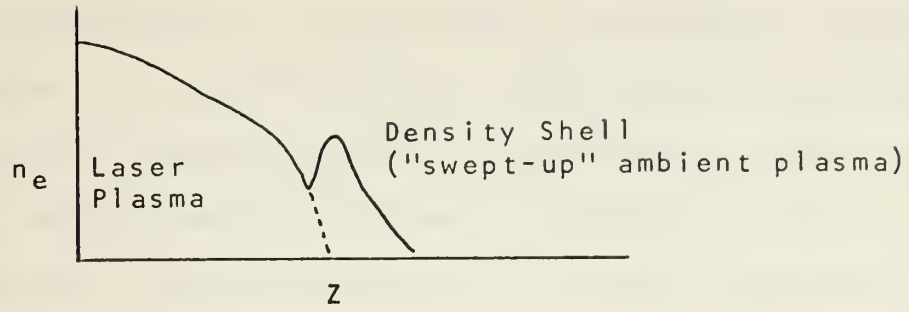

This profile is symmetric about the z-axis (which extends out from the center of the laser impact area as shown in Fig. 1).

The shell would contain a density gradient in the same direction (i.e., the negative z-direction) as exists at the front of the laser plasma. McKee suggested that the interaction between the laser plasma and the ambient plasma would cause the "swept-up" background to be heated in the density shell in such a way as to produce an electron temperature gradient in the same direction (i.e., the negative radial direction) as the temperature gradient produced by laser irradiation of the target.

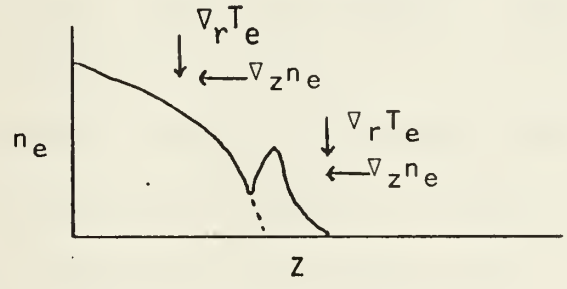

Therefore, he stated that additional fields would be produced in the density shell and they would be in the same direction as the fields produced at the front of the laser plasma, since $\frac{\partial \vec{B}}{\partial t} \propto \vec{S}$ and $\vec{S} \propto \nabla T_e \times \frac{\nabla \vec{n}_e}{n_e}$ (the first two terms on the right hand side of Eq. (1) are not magnetic field source terms; both terms are functions of $\vec{B}$ and they vanish in the absence of a magnetic field). The magnitude of these additional fields would vary as $\nabla_r T_e \times \frac{\nabla_z n_e}{n_e} \sim \frac{|\nabla_r T_e|}{\delta}$. This explains the

observed pressure dependence, since Dean had already shown that δ was inversely proportional to the cube root of the nitrogen background pressure. McKee stated that $|\nabla_r T_e|$ would be independent of the ambient density since it resulted from the relative velocity between the laser plasma and ambient background plasma and, furthermore, that it would be of approximately the same magnitude as the radial temperature gradient produced by the laser irradiation of the target. McKee also argued that the observation of the axial positions of the maximum fields at 250 mTorr N_2 "propagating" ahead of those for 0.1 mTorr at early times in the expansion could be explained by his model, since at 250 mTorr N_2, most of the fields would be produced in the density shell at the front while for 0.1 mTorr N_2 the fields would be produced behind the front of the expanding laser plasma. Although he did not elaborate the discussion further, he appears to have meant the following. For a background of 0.1 mTorr N_2 no shell forms and the maximum fields are formed near the front of the expanding laser plasma and convected away with the plasma as it expands. For a background of 250 mTorr N_2 the maximum fields are produced in and convected away with the density shell as the laser plasma expands. Since (according to McKee) the density shell is initially found at greater axial distances ($t \lesssim 200$ nsec) than is the field producing region for plasma expansion into 0.1 mTorr N_2, the axial position of maximum fields for expansion into 250 mTorr N_2 "propagates" ahead of the axial position of maximum field for expansion into a background of 0.1 mTorr N_2.

To explain the appearance of reverse fields at late times, McKee argued that, since the density gradient behind the shell was in the opposite direction to the density gradient at the front of the shell,

the sign of the source term would change. To explain the occurrence of reverse field earlier at 250 mTorr he argued that collisional heating would take place behind the density shell at 250 mTorr thus increasing the magnitude of the radial temperature gradient.

III. THE THESIS PROBLEM

McKee's explanation of the observed pressure dependence of the fields was based almost entirely on the results obtained by Dean. This was necessary since he had no experimental information concerning the interaction between the laser plasma and the ambient background plasma. Indeed, he had no way of determining the position of the magnetic fields relative to the streaming plasma.

The initial problem in the present investigation was to develop a technique to obtain density data in addition to field profiles in an attempt to verify the McKee model. In addition, McKee had observed a significant z-component of the fields during his investigation and its origin required further investigation. Since the pressure dependence of the fields had only been examined for a Mylar laser plasma streaming into a nitrogen background plasma, the pressure dependence of the fields for various background gases required examination.

This thesis reports the results of an investigation in the problem areas cited above. In particular, the location of the magnetic fields relative to an aluminum laser plasma was spatially mapped for pressures of 0.1, 5, 250 and 700 mTorr N_2. It was during this mapping that a significant discovery was made, namely that at high pressure ($\geq$ 250 mTorr) spontaneous fields were created long after laser shut-off and in a direction opposite to that of the initial fields. An examination of the corresponding density profiles showed that these "reverse fields" were developing at the front of the laser plasma. This discovery was significant because it provided a direct test of the McKee model and also

because it demonstrated that field production was not specific to a laser-produced plasma, but might also occur in fast moving plasmas generated by other means, as for example, by a theta-pinch or a plasma gun.

IV. THEORY

A. LASER-PRODUCED PLASMAS

The production of a plasma by irradiation of a solid with a Q-switched laser has received considerable attention in the last ten years and an excellent review of the papers published on this subject, both theoretical and experimental, is presented in Ref. 1. A theoretical treatment of the production of the plasma in a vacuum is quite complicated since many phenomena must be considered. To describe plasma production by a Q-switched laser with a flux density in excess of 10^9 W/cm^2, the initial absorption of the laser radiation by the solid, the thermal ionization of the ablated target material, the subsequent absorption of the laser radiation by the target blow-off material, and the re-radiation by the hot plasma should all be included. Several theoretical models have evolved, each emphasizing one particular aspect of the laser-plasma interaction and each giving reasonable treatment of the phenomenon with which it deals [Ref. 2] . Although, at present, there are no models that combine all the phenomena mentioned above, a reasonably consistent picture of the processes and interactions that occur when a high-power Q-switched laser beam interacts with a solid surface, in vacuo, has emerged.

The plasma is first created by the heating and vaporization of the target material.[1] It expands at a relatively constant velocity

---

[1] For a Nd-doped glass laser (1.06 μ) impinging on a copper target, the skin depth is the order of 10^{-6} cm [Ref. 5] .

until the electron density in the front drops below the critical density n_c.[2] It then accelerates as the radiation is absorbed in the front. Shortly after the arrival of the peak intensity of the laser pulse at the target (as the incident light flux begins to decrease), the plasma front again propagates at constant velocity [Refs. 2 and 3] . Thus, three distinct stages appear during the course of the expansion of the ablated target material.

The last two stages appear quite differently when the expansion is into an ambient background gas rather than into vacuum. The expansion of the plasma in the presence of a background gas will be treated in the next section.

A simplified one-dimensional model treating the observed (vacuum) heating and acceleration of the plasma (second stage) and fashioned after the treatment by Haught and Polk [Ref. 4] has been given by Ready [Ref. 2] . In this treatment it is assumed that:

(1) The target is initially a cold fully ionized plasma (the ionization process can be neglected).

(2) The plasma expands in one direction away from a surface located in the plane z=0 (see Fig. 1).

(3) The plasma absorbs the incident laser radiation via free-free transitions of the electrons in the presence of the ions (inverse bremsstrahlung).

---

[2] The critical density for the laser plasma is the density at which the electron plasma frequency is equal to the frequency of the laser radiation ($n_c = \omega^2 m_e \varepsilon_o / e^2$. At electron densities above the critical density the laser plasma reflects most of the incident radiation. The critical density for 1.06 μ radiation is $\sim 10^{21}$ cm^{-3}.

(4) Radiation losses can be neglected.[3]

(5) The pressure can be approximated by $P=P_s(1-\frac{z}{Z})$, where P_s is the plasma pressure at the target surface and Z is the position of the plasma front.

(6) The electrons and ions share a common temperature.[4]

(7) T is independent of position (no temperature gradients exist).

(8) The plasma expansion velocity has the time independent form $v=\frac{dZ}{dt}(\frac{z}{Z})$.

(9) The power absorbed by the plasma is $W=\Phi A(1-e^{-\int_z^0 K_\nu dz})$ where Φ is the laser irradiance, K_ν is the absorption coefficient [Ref. 5], and A is the cross-sectional area of the beam.

The plasma temperature can be determined by equating the rate at which the plasma absorbs energy to the sum of the rate of change of plasma thermal energy and the rate at which work is done by the plasma in its expansion:

$$\frac{1}{A}\frac{dW}{dz} = \frac{1}{2}\frac{d}{dt}(n_e + n_i)kT - \frac{\partial P}{\partial z}\frac{dz}{dt} \quad . \qquad (2)$$

---

[3] The temperature of the plasma treated here can be shown to be of the order of 100 eV. Although considerable line radiation from ions predominantly in charge states III and IV is observed from such plasmas, the bremsstrahlung continuum in the range 20-6000 A will dominate the radiation energy loss. If one assumes a temperature of 100 eV, an average ion number density of approx 10^{20} cm^{-3}, an average ion charge state of three, and a plasma volume of approximately 10^{-5} cm^3, then bremsstrahlung radiation is emitted by the plasma at the rate of approximately 10^7W during the time of the laser pulse. The volume was estimated by assuming a total of 10^{16} Al^{3+} ions are produced by the laser irradiation (see Section IV. E) and requiring that $n_e \sim 10^{21}$ cm^{-3}.

[4] The equipartition time for transfer of absorbed energy from electrons to ions can be approximated by $\tau^{\varepsilon}_{ei} \sim 25\,(\frac{m_i}{m_p})\,T_e^{3/2}\,(K)\,[n_e(cm^{-3})\,z]^{-1}$ [Ref. 5]. For the same conditions assumed in footnote 3, $\tau^{\varepsilon}_{ei} \ll 1$ nsec.

The work done by the plasma in the expansion increases the plasma kinetic energy so that

$$\frac{-\partial P}{\partial z}\frac{dz}{dt} = \frac{d}{dt}\left\{\frac{1}{2}(n_i m_i + n_e m_e)\left(\frac{dz}{dt}\right)^2\right\} \qquad (3)$$

By integrating Eqs. (2) and (3) from zero to Z and using the result $N = A\int_0^Z n_s\left(1 - \frac{z}{Z}\right) = An_sZ/2$, where N is the total number of ions or electrons in the plasma and n_s is the corresponding number density at the surface of the target, Ready obtained the equations

$$T = \left[(N_i m_i + N_e m_e)Z/6k(N_i + N_e)\right]\frac{d^2Z}{dt^2} \qquad (4)$$

$$\frac{d^3Z^2}{dt^3} = \left[24(N_i m_i + N_e m_e)\right] W \qquad (5)$$

These coupled equations were solved numerically by McKee for the conditions of this experiment. The maximum temperature obtained was of the order of 100 eV and this maximum occurred a few nanoseconds after the arrival of the maximum laser intensity at the target.

In this simplified model, the plasma temperature and the position of the plasma front have been calculated for the case of a laser-produced plasma expanding under vacuum conditions (i.e., if a background is present, it is of such a low density that no interaction occurs between the laser plasma and the background). However, in the present investigation, the presence of a background gas (pressures above 1 mTorr) is observed to influence the plasma expansion dynamics and the production of a spontaneous field. Therefore, one cannot neglect the effect of the presence of an ambient background gas on the expansion dynamics.

B. THE INFLUENCE OF A BACKGROUND PLASMA ON THE LASER-PLASMA EXPANSION DYNAMICS

The optical radiation flux from a dense, hot laser plasma is known to be rich in lines of highly stripped ions in the far ultra-violet and near X-ray regions. This flux, in addition to the bremsstrahlung

radiation mentioned previously is energetically capable of ionizing an ambient background gas (the longest wavelength energically able to ionize helium is approximately 540 Å).

Koopman [Ref. 6] has investigated the photoionization (background of He, H_2, Ar and Xe) produced from a plane copper target irradiated by an 8 J, 20 nsec ruby laser. His study indicated that the background gas was completely ionized to distances of the order of a centimeter and that at large radii the degree of photoionization fell as r^{-2}. He estimated the total optical energy emitted between 1000 and 200 Å to be approximately 1 ± 0.5 J (5%–15% of the laser energy converted to ionizing UV radiation). In a previous report [Ref. 7] using a 6 J, 30 nsec ruby laser and various target materials, Koopman reported a similar result. Therefore, when a laser-produced plasma expands into an ambient background gas, one must consider the effects of plasma–plasma interactions on the expansion dynamics.

The fact that an interaction between the laser plasma and the ambient background plasma does occur at early times in the plasma expansion has been well established [Refs. 3, 6, 7, 8 and 9] .

Dean [Ref. 8] found that:

(1) During the period of laser irradiation of the target (early time), the average expansion velocity of the plasma luminous front varied inversely as the cube root of the ambient background pressure between 30 mTorr N_2 to 250 mTorr N_2, while the radius of the front (for a given pressure) varied as $t^{0.6}$.

(2) At later times the radius of the luminous front varied inversely as the cube root of the ambient pressure (same pressure range) and directly (given pressure) as $t^{0.4}$.

Dean suggested that the results could be explained by a model which supposes that the early-time dynamics of the laser plasma expansion correspond to the propagation of a radiation-driven detonation wave and that at later times the plasma expands as a blast wave. This model assumes that early in the expansion there is momentum transfer between the expanding front and the ambient background plasma and that, as the front propagates into the background plasma, further energy from the laser is absorbed behind the front and is transported to the front by heat conduction. At later times (after the end of the laser pulse) all the momentum in the driving laser plasma piston is assumed transferred to the "swept-up" background plasma which propagates as a blast wave. Dean also suggested that if the observed coupling is strong, i.e., if the background plasma is being excluded by and moved by the front, then slowing down and transition from detonation wave to blast wave should occur approximately at a radius such that the mass of displaced ambient plasma equals the initial piston mass.

Earlier, Ramsden and Savic [Ref. 10] had proposed a similar model to explain the results of their investigation of the development of a laser-induced spark in air. They used a .2 J, 20 nsec ruby laser to produce gas breakdown in 200 mTorr of air. By using streak and image converter photography they were able to show that a luminous front developed which propagated back toward the laser. During the period of laser irradiation they observed that the radius of the front varied as $t^{.65}$ while after irradiation ceased the radius of the front was proportional to $t^{.38}$. They interpreted the initial phase of the expansion of the spark as corresponding to the propagation of a radiation driven shock wave while the late time propogation was interpreted as

corresponding to the propagation of a blast wave. They derived an expression for the average expansion velocity of the radiation-driven detonation wave given by

$$\bar{V} = \frac{2(\gamma^2 - 1)W}{\pi r^2 \Delta t}^{1/3} \rho_o^{-1/3} \qquad (6)$$

where W is the energy absorbed from the laser beam throughout the time interval, Δt, during which the wave is driven, r is the focal spot radius, and ρ_o is the ambient gas (plasma) density. Actually, the equation they derived, which was also used by Dean, was incorrect in that they mistakenly used the density behind the front instead of ρ_o in their derivation of $\bar{V}$ [Ref. 11] .

Hall [Ref. 9] investigated the dynamics of the expansion of a laser plasma into an ambient background of argon. The plasma was produced by irradiation of a tantalum slab with a .5 J, 20 nsec ruby laser. Using an image-converter camera and double probes for diagnostics, he found that the late time expansion dynamics of the laser plasma could be explained by blast-wave theory, i.e., $r \propto (\frac{1}{\rho_o})^{1/5} Z^{2/5}$

Thus, the presence of a background gas (pressures above 30 mTorr) influences the expansion dynamics of a laser-produced plasma, even as the laser is irradiating the target. The effect of this interaction between the laser plasma and the ambient background (plasma) on the production of spontaneous fields will be discussed in Section VIII. In the following sub-section, the equation governing the development of the spontaneous magnetic fields will be developed.

C. INITIAL PRODUCTION OF SPONTANEOUS MAGNETIC FIELDS

As mentioned earlier, the accepted model for production of the laser plasma requires absorption of the laser energy by the electron fluid. The ions are subsequently heated via electron-ion collisions.

Thus, during the initial heating and acceleration of the laser plasma, one can assume that $T_e \gtrsim T_i$ and the electrons can be considered to exist in a background of stationary ions.

The equation of motion for the electron fluid is

$$n_e m_e \left(\frac{\partial \vec{V}_e}{\partial t} + (\vec{V}_e \cdot \nabla)\vec{V}_e\right) = -n_e e(\vec{E} + \vec{V}_e \times \vec{B}) - \nabla \cdot \overleftrightarrow{P}_e + \vec{C}_{ei} \qquad (7)$$

where $\vec{V}_e(\vec{r},t)$ is the average electron velocity, $\vec{E}(\vec{r},t)$ and $\vec{B}(\vec{r},t)$ are the averaged electromagnetic fields, $\overleftrightarrow{P}_e$ is the kinetic stress tensor, and $\vec{C}_{ei}$ represents the momentum per unit volume per unit time transferred to the electrons by the ions through collisions.

This equation can be simplified through the use of several approximations. If one assumes that the random velocity distribution within the volume under consideration is isotropic (i.e., the electron-electron collision time τ_e is much less than the characteristic time for field production) then $\nabla \cdot \overleftrightarrow{P}_e$ reduces to the electron pressure gradient, ∇P_e. If the macroscopic flow velocity of the electron fluid element is small with respect to the random thermal velocity of the electrons $\left[\frac{kT_e}{m_e}\right]^{1/2}$ then the convection of the electrons can be neglected and the convective derivative $\frac{\partial \vec{V}_e}{\partial t} + (\vec{V}_e \cdot \nabla)\vec{V}_e$ reduces to $\frac{\partial \vec{V}_e}{\partial t}$. For the aluminum laser plasma produced in the present investigation, the asymptotic expansion velocity of the plasma front was of the order of 10^7 cm/sec (assuming no interaction). Assuming an electron temperature of 100 eV, one can show that $\left|\vec{V}_e\right| \cdot \left[\frac{kT_e}{m_e}\right]^{-1/2} \sim 10^{-2}$ and the above approximation would appear acceptable. The left-hand side of Eq. (7) can be reduced further if the frequencies of interest can be shown to be low enough so that electron collective effects are not important, i.e., $\omega \ll \omega_{pe}$ where ω_{pe} is the electron plasma frequency. If this is the case, the electrons can be considered massless (react instantaneously to applied fields) and the left-hand side of Eq. (7) can be set equal to zero.

One can approximate the ratio ω/ω_{pe} by $1/\omega_{pe}(n_e)\tau$ where $\omega_{pe}(n_e)$ is the plasma frequency at the critical density and τ is the rise time of the laser pulse. Thus $\frac{\omega}{\omega_{pe}} \sim 10^{-7}$ ($\omega_{pe}(n_e) \sim 10^{15}\text{sec}^{-1}$ and $\tau \sim 10^{-8}$sec) and setting the left-hand side of Eq. (7) equal to zero appears acceptable. If one approximates $\vec{C}_{ei}$ by the Joule or resistive drag term, $\frac{n_e e \vec{J}}{\sigma}$, then Eq. (7) can be written

$$\vec{E} = \frac{\vec{J}}{\sigma} - \vec{V}_e \times \vec{B} - \frac{1}{n_e e} \nabla P_e \qquad (8)$$

One can obtain an equation describing the initial development of the spontaneous magnetic fields by taking the curl of Eq. (8) and using the Maxwell equations. The result is

$$\frac{\partial \vec{B}}{\partial t} = \nabla \times (\vec{V}_e \times \vec{B}) + \frac{1}{\mu_o \sigma} \nabla^2 \vec{B} + \frac{\nabla k T_e}{e} \times \frac{\nabla n_e}{n_e} \qquad (9)$$

The first two terms on the right hand side are the flow and diffusion terms. The generation of an initial magnetic field requires that the last term, the thermal source term ($\vec{S}$) be non-zero [Ref. 12] . In deriving Eq. (9) use was made of the vector identity $\nabla \times (f\nabla A) = \nabla f \times \nabla A$. Also, in writing $P_e = n_e k T_e$, the isotropic velocity distribution has been assumed to be Maxwellian.

During most of the times of interest in this investigation, the ratio of the flow term to the diffusion term in Eq. (9), known as the magnetic Reynold's number, R, can be shown to be greater than one[5] so that field diffusion can be neglected. Thus Eq. (9) can be reduced to

$$\frac{\partial \vec{B}}{\partial t} = \nabla \times (\vec{V}_e \times \vec{B}) + \frac{\nabla k T_e}{e} \times \frac{\nabla n_e}{n_e} \qquad (10)$$

Physically, Eq. (10) expresses the fact that the rate at which the the fields vary in a region depends on the rate at which the fields are created in the region and the rate at which the

---

[5] The magnetic Reynold's number can be approximated by $R = \mu_o \sigma L V_e$ where L is a characteristic length. Thus, for $V_e = 10^5$ m/sec, $T_e = 10$ eV and L = 1 cm, R = 60.

fields flow out of the region. It also expresses the fact that the initial generation of spontaneous fields by the thermal source term can occur only if non-adiabatic conditions exist in the field production region.

For adiabatic expansion, $Tn_e^{1-\gamma} = \text{const.}$ $(T=T(n_e))$ and the source term vanishes ($\nabla T_e \times \nabla n_e \propto \nabla n_e \times \nabla n_e = 0$). Thus, non-adiabatic conditions are required for the generation of the magnetic fields by the thermal source term. This means that the energy must be supplied to the electrons at a sufficiently high rate that there is an imbalance between the rate per unit volume at which internal energy is supplied to the electrons and the rate per unit volume at which they do work ($\frac{dU}{dt} \not\propto - \frac{dW}{dt}$). Stamper has suggested that the ratio $\frac{dQ/dt}{dU/dt}$ might serve as a useful measure of the non-adiabaticity of the plasma production process, where $\frac{dQ}{dt}$ is the rate per unit volume at which the laser energy is supplied to the electrons. Stamper approximated $\frac{dQ}{dt}$ by the product of the absorption coefficient (K_ν) and the radiation intensity (Φ), while $\frac{dU}{dt}$ was approximated by $\frac{n_e kT}{\tau^{\varepsilon}_{ei}}$, τ^{ε}_{ei} being the electron-ion thermalization time. During the time the plasma is absorbing the incident laser radiation, $\frac{dQ/dt}{dU/dt}$ is of the order of one [6] (for the conditions of this investigation) and the plasma, indeed, appears non-adiabatic.

The question arises as to whether the thermal source term can actually generate field intensities of the order of those observed.

---

[6] $\frac{dQ/dt}{dU/dt} = \frac{K_\nu \Phi \tau^{\varepsilon}_{ei}}{n_e kT} \sim \frac{\tau^{\varepsilon}_{ei} \Phi \bar{n}}{\tau_{ei} n_e kTc}$ where $K_\nu \sim \frac{\bar{n}}{c\tau_{ei}}$, τ_{ei} is the electron-ion collision time, and $\bar{n}$ is the index of refraction of the plasma (which can be approximated by one).

If so, how large are the maximum fields and where are they located with repect to the laser impact area? In a recent investigation by computer simulation, Widner [Ref. 22] , using the thermal source term for the magnetic fields, has obtained very large magnetic fields (megagauss) in the focal spot region. The laser-target configuration considered assumed cylindrical geometry with axial symmetry and a semi-infinite planer target. The laser beam was assumed to possess uniform spatial intensity, constant temporal intensity, and a finite radial extent. The beam impinged axially on the target, which had an initial, finite, axial density gradient. Both field diffusion and field convection were neglected, and the plasma expanded into a vacuum. The thermal conduction time-scale was assumed to be much faster than the hydrodynamic time scale. Widner found that the spontaneous magnetic fields were being driven by a temperature gradient near the target surface in the negative-radial direction as had been suggested by Stamper. This temperature gradient is a consequence of the finite radial extent of the laser beam and occurs near the radial edge of the laser heated region of the plasma. Because of the fast thermal-conduction timescale, the temperature gradients rapidly decay after laser shut-off.

From Widner's "experiment" one can conclude that the radial temperature gradient occurring at the edge of the laser impact region can generate (through the thermal source term) very large azimuthal magnetic fields during the time the laser irradiates the target. These fields are in the same direction as the spontaneous fields observed by Stamper and McKee.

V. EXPERIMENTAL PROCEDURES

A. LASER

The laser used in this investigation was a Korad-K-1500 Q-switched neodymium-doped glass laser. The laser consisted of an oscillator and a single amplifier stage. The Q switch was a Pockels Cell. The laser system was operated at a power level of 300 MW, which was obtained with a pulse width (full width of half-maximum) of 22 nsec. The output of the system varied within about 10 per cent of 300 MW and no data were accepted if obtained at power levels outside this range.

B. LASER MONITORING TECHNIQUES

The beam was monitored with a Korad K-D1 photodiode. This photodiode provides a signal proportional to the laser power and also integrates this output to give another signal which is proportional to the laser-pulse energy.

About one per cent of the beam was reflected by a beam splitter to a MgO diffusing block for viewing by the photodiode (see Fig. 2). The scattered light then passed through a 0.1 per cent neutral density filter before entering the photodiode. The power signal was displayed on a Tektronix 7904 oscilloscope and the energy signal was displayed on a Tektronix 564B storage oscilloscope.

The photodiode energy signal was calibrated by L. L. McKee [Ref. 12] by using a Westinghouse RN-1 Laser Radiometer. The radiometer provided an absolute measure of the energy incident at the target which allowed calibration of the diode's integrated signal.

The energy output of the laser was monitored on every shot, while the pulse width was checked at the beginning and end of each data taking session. For energy outputs within 10 per cent of 6.6 J, the pulse width (full width at half-maximum) was consistently 22± 1 nsec.

The arrival time of the laser pulse at the target was computed by taking into account the various cable delays and the laser beam path length. The zero time in this investigation was taken as the arrival time of the laser pulse, which was defined to occur 22 nanoseconds prior to the arrival of the maximum intensity at the target.

C. PLASMA CHAMBER

The target was located in a chamber which was specially constructed by McKee to facilitate the diagnosis of the laser plasma by use of probes and by optical means (see Fig. 3). The inside volume of the chamber was cylindrical with a diameter of 10 inches and a height of 6 inches. All ports shown in Fig. 3 are circular.

The beam entered the chamber after passing through a 28 cm focal length lens and struck the target at an angle of 30° to the flat target's normal. Since the laser plasma expands along the target normal [Ref. 2], illuminating at a 30° angle permitted probing the plasma along the z-axis (at axial distances greater than 4 mm) without the laser beam striking the probes.

The target was a flat disc of aluminum 1/32 inches thick and about 2 inches in diameter. The target was rotated after approximately 20 shots to prevent severe cratering of the target in the laser impact area, although there was no noticeable effect on the character of the probe signals after the same impact area was irradiated as many as 40 times.

The chamber was pumped to a vacuum of about 5×10^{-5} Torr of air by an oil diffusion pump. Vacuum pressures lower than 1 mTorr were measured with an ionization gauge. Pressures in the range from about 1-1000 mTorr were measured with a thermocouple gauge, while above 1 Torr pressures were monitored by a manometer filled with diffusion pump oil (octoil).

D. MAGNETIC PROBES

1. Probe Construction and Calibration

The magnetic probe used in this investigation consisted of five turns of #40 Formvar copper wire with a diameter of about 1 mm. The probe circuit response was linear, with an effective area of the inductive loop of 7.2×10^{-6} cm^2, for frequencies below about 30 MHz (see Fig. 47). The effective area (nA) of the probe was determined by insertion of the inductive loop into calibrated Helmholtz coils and recording the voltage signal output (V_p) across the impedance of the cable connecting the probe and scope. The details of the construction and calibration of the coils and probe are described by McLaughlin [Ref. 19].

2. Probe Signal Integration

The response of the inductive magnetic probe is given by

$$V_p = nA \frac{dB_\perp}{dt} \qquad (11)$$

where $\frac{dB_\perp}{dt}$ is the time rate of change of the component of the magnetic field normal to the plane of the coil and it has been assumed that the magnetic induction is constant over the coil area. In order to obtain signals proportional to the magnetic field itself, the output of the probes was integrated with a passive RC integrator. This integrating unit and its relations to the other probe circuit components is illustrated below:

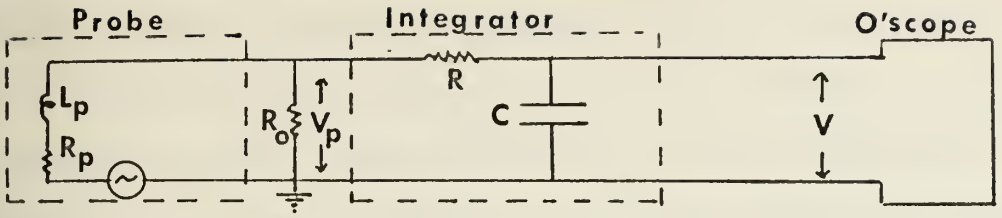

V_p represents the voltage signal output from the probe across the impedance of the cable, R_o, and V represents the voltage of the integrated output from the RC integrator. V is simply the voltage across the capacitor, C, and is given by

$$V = \frac{1}{C} \int_0^t \frac{V_p - V}{R} \, dt \qquad (12)$$

where $\frac{V_p - V}{R}$ is the current in the circuit passing through R.

If RC is large compared to the integration time, V will be much smaller than V_p, and the integrand simplifies to $\frac{V_p}{R}$. To see that this is so, consider the simple example of a constant voltage, V_p, applied at t=0. Then the voltage drop across the capacitor, C, is given by

$$V = V_p (1 - e^{-t/RC}) = V_p (t/RC - \tfrac{1}{2}(t/RC)^2 + \ldots) \qquad (13)$$

If $t/RC < 0.1$, then the second order and higher terms may be dropped, and the error introduced is < 5%. The rule of thumb whereby V can be neglected compared to V_p is then that RC exceed the total observation time by a factor of at least 10.

When the expression for V_p in Eq. (11) is substituted into Eq. (12), the result (assuming a linear probe response) is

$$V = \frac{nA}{RC} B \qquad (14)$$

The integrator time constant was checked by McKee by integrating sinusoidal signals of frequencies comparable to those of the spontaneous magnetic fields (1-10 MHz). The time constant is then given by $V_i / 2\pi f V_o$

assuming, of course, that the requirement $t/RC < .1$ is satisfied. Here, V_i is the sinusoidal input (V_p) to the RC integrator and V_o is the integrated output. McKee determined the value of the time constant to be $RC=3.7 \times 10^{-6}$ sec. Therefore, the requirement that $2\pi f RC \gtrsim 20$ was satisfied. Since the magnetic fields were observed as long as 1 μsec, their lowest fundamental frequency was about $f=10^6 sec^{-1}$ so that $2\pi f RC \gtrsim 20$ and the RC time constant was acceptable.

The conversion factor between the magnetic field and the output of the RC integrator becomes

$$B = 5.2V \qquad (15)$$

where B is in gauss and V is in millivolts. Since the circuit response is linear only to frequencies of about 30 MHz, magnetic field signals with risetimes less than 30 nsec will be seriously distorted and Eq. (15) will not be valid.

3. Probe Signal Reliability and Sensitivity

Several steps were taken to insure that the magnetic probe signals were meaningful. The probe was carefully shielded by covering it with metallic braid to reduce electrostatic noise pickup. To check the effectiveness of the shielding, the probe signals were monitored under experimental conditions for which no target was in place to verify that a null signal was obtained. Also, the probe coil was rotated by 180° and the probe signals were checked to make sure that they reversed in polarity. This demonstrated that the signals were not electrostatic in nature. Further, the signals obtained by passive RC integration were checked by McKee to insure that the RC integrator gave results comparable with those obtained by numerical integration of the direct $\frac{dB}{dt}$ signals.

The values of B obtained by the two methods agreed to within 5%. The magnetic field signals were recorded on a Tektronix 7904 oscilloscope with a maximum vertical sensitivity of 1 mV/division (centimeter divisions). Since the minimum discernible signal was less than 1 mV, magnetic fields as low as 1 gauss in magnitude could be resolved.

E. ELECTRIC DOUBLE PROBES

1. Probe Theory

When a potential difference is applied between two electrodes immersed in an ionized but macroscopically neutral gas, the positive ions will be attracted towards the negative electrode and the electrons will be attracted towards the positive electrode. That is, the applied electric field attempts to destroy the neutrality of the plasma by separating the positive and negative charges. This charge separation will occur in the immediate neighborhood of the two electrodes, the bulk of the plasma remaining charge neutral. The regions adjacent to the two electrodes in which plasma neutrality no longer exists are known as the "sheath regions" and it is in these regions that most of the applied potential difference is developed. When the two electrodes are of comparable surface area and the entire system (electrodes plus biasing potential) is isolated from ground, i.e., the entire system "floats" with the plasma and therefore follows the change of plasma potential, the system is called a double probe system.

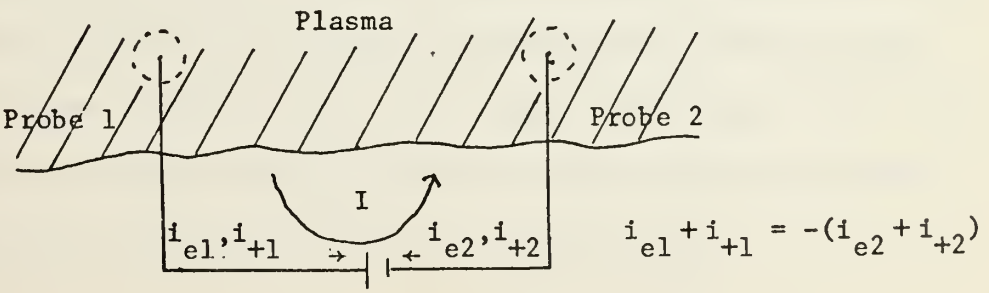

Assume that the double probe is immersed in a plasma and that initially V=0. If the electron and ion temperatures are equal, then the random electron flux (J_-) to the probe tips will be much larger than the random ion flux. The probe tips will collect a net electron current until the electron and ion fluxes to each tip are equal. The probe tips will then be at a potential below the plasma potential.

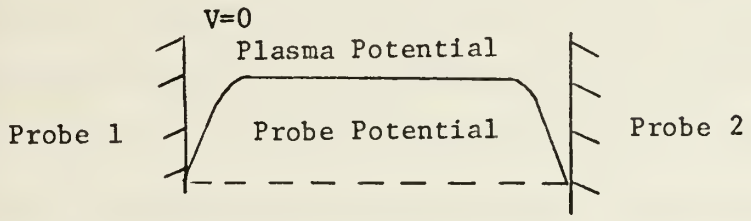

As V is increased, eventually all the electrons will be repelled from probe 2, which will then be collecting the random ion current J_+A. This is the maximum current that can be drawn by the isolated double probe system.

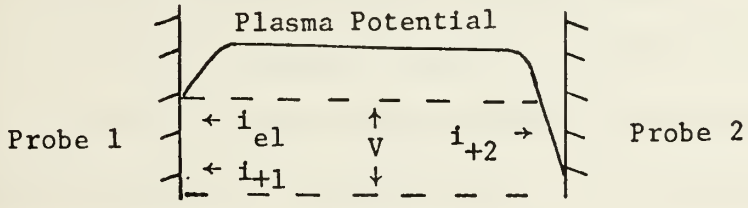

Notice that since $|J_-| > |J_+|$, probe 1 will still be at a negative potential with respect to the plasma.

As previously mentioned, the initial thermal energy of a laser produced plasma is rapidly converted to ordered flow kinetic energy at least for plasma expansion into near vacuum conditions. The conversion appears to have taken place by the time the plasma has expanded to dimensions on the order of .01 to .10 cm [Ref. 14] .

In the flowing plasma, the charge neutrality condition $n_e = \sum n_i Z_i$ requires that the mean flow velocity of the electrons and ions be equal. Therefore, the ordered kinetic energy of the plasma is largely due to the ions because of their greater masses.

If one assumes that the ions and electrons of an aluminum laser plasma have a common temperature of 100 eV and a streaming velocity of 5×10^6 cm/sec, then the ratio of the ion kinetic energy to the ion thermal energy is approximately 4, the ratio of the electron kinetic energy to the electron thermal energy is approximately 7×10^{-5}, and the ratio of the electron thermal velocity to the ion streaming velocity is approximately 100. Consequently, the ion current to a probe placed in this streaming laser plasma is dominated by the ion directed velocity while the electron current to the probe is dominated by the electron random thermal velocity. Actually, the conditions assumed above are somewhat pessimistic, as for most of the data taken in this investigation the ion temperature is probably less than 100 eV and the ion streaming velocity is greater than 5×10^6 cm/sec. Since the maximum current drawn between the elements of a double probe is limited by the ion current to the probe [Ref. 20], the current measured by a probe biased at saturation and in an environment such as the one discussed above is

$$I \sim A_\perp \overline{n_i Z} e V_{LP} \qquad (16)$$

where $A_\perp$ is the probe area perpendicular to the directed plasma flow, $\overline{n_i Ze}$ is the average ionic charge per unit volume in the laser plasma, and V_{LP} is the magnitude of the plasma streaming velocity.

In writing Eq. (16), it has been tacitly assumed that the areas of the probe tips are equal, that the plasma parameters are uniform

across the probe tips, and that plasma-probe interactions such as secondary electron emission due to ion bombardment can be neglected.

Since the probe used in this investigation had tips of equal area which were always placed in a plane perpendicular to the axis of symmetry of the expanding plasma, the first two conditions were satisied. The secondary electron emission coefficient due to ion bombardment (γ_i), defined as the average number of electrons ejected per incident ion, has been measured by Koopman [Ref. 21] for similar experimental conditions and falls in the range of 0.0-0.5. Therefore, secondary electron emission will contribute to the total current drawn between the probe tips. However, γ_i is a very weak function of the ion kinetic energy in the range of energies expected in the present investigation and its contribution to I can be taken to be a constant over the range of ion kinetic energies encountered [Ref. 26] . Consequently, Eq. (16) becomes

$$I \sim (1+\varepsilon) A_{\perp} \overline{n_i Z} \, e \, V_{LP} \qquad (17)$$

To minimize the secondary electron emission current drawn by the double probe, the probe was operated at a potential just above saturation.

Since I, $A_{\perp}$ and V_{LP} are measurable quantities and ε is a constant, one can use Eq. (17) to obtain relative density profiles ($\overline{n_i Z}$) which are felt to be reliable. To obtain the absolute magnitude of the ion densities one must know both Z and ε.

2. Probe Construction and Sensitivity

The isolated double probe is the logical choice for use in probing a laser plasma at distances of the order of a few centimeters from the laser impact point for two principal reasons. First, one does not have to allow for rapid fluctuations in the plasma potential because

the isolated double probe maintains a fixed potential difference between the electrodes irrespective of the plasma potential. Also, the maximum current drawn by the probe is limited by the ion saturation current, which is much less than the electron saturation current. This is especially advantageous in the dense, hot environment of a laser plasma. The probe design shown in Fig. 4 has been found satisfactory for the work described in this investigation. The probe circuit is similar to that used by Koopman [Ref. 7] to obtain density measurements in laser-produced plasmas with single Langmuir probes. The probe circuitry was inclosed by an aluminum housing attached to the probe and the entire system was isolated from ground. The minimum time response of the circuit was estimated by measuring the rise times of the fastest detected signals and was of the order of a few nanoseconds. The diameter of the cylindrical tips was about 1 mil, they had a length of 1 mm and were about 1 mm apart. The double probe signals were recorded on a Tektronix 7904 oscilloscope. The minimum discernable signal was approximately 200 mV (0.2 relative units in Figs. 14-39).

3. Probe Operating Conditions

Since the probe was to be used to detect the passage of the front of the laser plasma, the probe was biased to collect the saturation ion current corresponding to the passage of the front. The characteristic curve for a background of 700 mTorr N_2 and at a point 3 mm behind the front is shown in Fig. 5. The probe appears to collect saturation currents at a bias of 8 volts. Therefore, in order to insure collection of saturation current with a minimum contribution to the current from secondary electron emission, all data were taken with the

probe biased at 10 volts. For zero bias, the probe draws a current only as the front passes. The probe current signal is first positive and then becomes negative and decays to zero at the back of the front. This behavior may be the result of an asymmetric probe perturbation associated with the passage of the plasma front and it is responsible for the non-zero value of the current at zero probe bias in Fig. 5.

F. DATA COLLECTION AND ERROR ESTIMATES

By far the most critical parameter affecting the reproducibility of the results obtained in this investigation was probe positioning. If a probe was maintained at a fixed position and the signals detected at that position were monitored over a series of several shots, then it was found that for laser power outputs of between 285-315 MW, the magnitudes of the signals fluctuated by less than 5% and the time of arrival of characteristic features of the detected signals such as signal maxima, fluctuated by at most a few nanoseconds. If the probe was removed from the chamber and then re-introduced at ostensibly the same position, the time of arrival of the signal characteristics was reproducible within the same few nanoseconds, but the signal amplitudes might be found to vary as much as 30% from the amplitudes previously recorded. This variation was a result of the rather crude method of positioning the probe, which consisted initially of locating the probe relative to three mutually perpendicular planes of reference by measuring distances from those planes to the probe tip with a plastic ruler graduated in millimeters. This was the technique used by McKee in his investigation of the spontaneous fields. To reduce the errors associated with reintroduction of the probe into the chamber at each position, a probe holder was designed so that once the probe was in position, it

could be relocated an any axial position along a line of constant r and θ by sliding the holder along a graduated scale. The holder was situated on top of the vacuum chamber (see Fig. 3) and probe data were taken by introducing the probes from the top of the chamber with the probe shaft in the $\theta = 0^{\circ}$ plane and parallel to the target surface. The probe position could be changed while the chamber was evacuated and this permitted making an entire series of moves along the z-axis without re-pressurization of the chamber. Initial probe positioning was accomplished by centering the probe on the point made by intersection of the mapping line with the target surface. The mapping of the fields along a constant surface was then carried out by setting the pressure and sliding the probe to the various axial data points; the pressure was changed and the procedure was repeated. Once the fields were mapped, the magnetic probe was replaced by the double probe and the procedure was repeated. The laser system was aligned just prior to a mapping series so that no re-alignment would be necessary during the course of the "run." Using this procedure, it was possible to reproduce the mapping results to within a magnitude of 10%, provided, of course, that the probe remained fixed in the holder.

The pressure curves of Fig. 10 were obtained by fixing the magnetic probe at the position (0.4, 0, 0.4) and varying the gas pressure. The individual data points are not shown for clarity purposes, but it is again estimated that the difference in magnitude between the "true" value of $B_{\theta\ MAX}$ and the value plotted in Fig. 10 is less than 10%.

VI. EXPERIMENTAL RESULTS

A. INITIAL FIELD ORIENTATION AND CHARACTERISTICS

The initial spontaneous magnetic fields were found to be mainly in the azimuthal direction and symmetric about the z-axis (see Fig. 6) as previously reported by McKee [Ref. 12] . The direction of the fields corresponds to conventional current in the negative z-direction along the axis of the coordinate system (fields in the clockwise direction in Fig. 1). Figures 6, 11 and 40 are typical magnetic field signals detected with the probe at various positions and pressures. The maximum of the magnetic field signal occurred later in time as the magnetic probe was moved out to positions of larger axial distance.[7]

Mention was made in McKee's thesis of the measurement of a z-component of the magnetic fields. That this z-component was the result of probe perturbation of the plasma can be seen by examination of Figs. 7 and 8.

Figures 7 and 8 demonstrate the influence of the probe on the measured value of the z-component field. The component of the field measured by an open probe (i.e., inductive loop not glass enclosed) at the position ($r=0.5$, $\theta=0$, $z=0.5$ cm) was smaller than that measured by an enclosed probe by a factor of 6 (see Fig. 7). Figure 8 demonstrates that the direction of the measured z-component of the magnetic field depends on the direction from which the probe is inserted into the chamber.

---

[7] The maximum of the magnetic field signals was observed to occur earlier in time as the probe was moved out at high background pressures of nitrogen. This phenomenon will be discussed further in Section VI.B.

When the open probe was inserted from the right side the measured component was opposite in direction to that measured by the same probe when it was inserted from the left; in both cases the probe was in a plane parallel to the plane of incidence of the laser radiation. It can be seen from Figure 8 that the smallest measured z-component was obtained by introducing the probe from the top of the chamber (probe in a plane perpendicular to the plane of incidence).

Thus it appears that the measured z-component resulted from probe perturbation of the plasma and that the magnetic fields of the unperturbed plasma possess no significant z-component.

B. PRESSURE DEPENDENCE OF THE MAGNETIC FIELDS

Figure 9 displays the manner in which the maximum azimuthal magnetic fields detected at the position (0.4, 0, 0.4) depend on the background pressure of nitrogen for aluminum and Mylar targets. This figure indicates that although the magnitudes of the fields at any pressure depend on the target material, the field amplification for a given target material depends only on the background gas. The fields produced by irradiating an aluminum target are a factor of eight larger than those obtained by irradiating Mylar in the pressure independent region of the curves. That the fields are larger for the aluminum target is in accord with the computed higher maximum temperature of the aluminum laser-produced plasma.[8]

---

[8] As previously mentioned, the maximum temperature of the aluminum plasma was computed to be of the order of 100 eV using the one-dimensional program written by McKee. He obtained a value of the order of 10 eV for the maximum temperature of his Mylar plasma, using the same program.

Figure 10 displays the manner in which the maximum azimuthal magnetic fields at the position (0.4, 0, 0.4) depend on the background pressure for various gases. Below approximately 1 mTorr the fields are independent of the background gas as one would expect by inspection of Fig. 9. Above 1 mTorr the shape of the pressure curve is dependent on the background gas present. The important features of Fig. 10 appear to be that:

(1) Below about 1 mTorr the maximum fields are independent of the background gas.

(2) In the range from 50 mTorr to about 250 mTorr, the maximum fields appear to be a function of the density of the background gas, being larger for higher density backgrounds.

(3) While the maximum fields decrease sharply with pressure above about 250 mTorr for N_2 and Ar and 450 mTorr for H_2, they continue to increase for a background of He up to a pressure of 1 Torr.

Figure 11 shows the manner in which the magnetic fields detected at the position (0.4, 0, 0.4) vary as the background pressure increases from 250 mTorr N_2 to 70 Torr N_2. This figure clearly shows that as the pressure increases the time at which the fields attain their maximum value decreases. The fields attain their maximum value at approximately 100 nsec for 250 mTorr N_2 while the maximum value of the fields for 70 Torr N_2 occurs at about 45 nsec. This figure also clearly shows that as the pressure increases, the time of onset of "field reversal" shifts toward the origin and that the maximum value of the reverse fields increases as the pressure increases through 5 Torr N_2. Thus, the generation of reverse field appears pressure dependent. The above investigation

was repeated at the position (0.4, 0, 0.6) and the times of arrival of the maximum fields were compared with those obtained at (0.4, 0, 0.4). The results are plotted in Fig. 12. At very high pressures the maximum fields arrive sooner at the position (0.4, 0, 0.6), while at lower pressure they arrive later. This "behavior" of $B_{\theta MAX}$ demonstrates that at least at very high pressures, one cannot assume that $B_{\theta MAX}$ "propagates" with the plasma. All propagation speeds presented in the thesis were obtained from double probe data. The individual signals obtained at (0.4, 0, 0.6) exhibit the general characteristics of those detected at (0.4, 0, 0.4). They differ in that the maximum fields are reduced from those obtained at corresponding pressures at (0.4, 0, 0.4) while the maximum reversed fields are larger than those detected at (0.4, 0, 0.4) for pressures between 2.5 and 10 Torr. No significant reverse field is observed at (0.4, 0, 0.6) for 70 Torr N_2.

These results suggest that whatever the mechanism for production of reversed fields, it is "turned-on" sooner at higher pressures. Figure 13 is a plot of the axial position of onset of "strong" field reversal versus background pressure along the line r=0.4 cm, $\theta = 0^\circ$. The points were obtained by successively moving the magnetic probe (axially) toward the target at a fixed pressure until the magnetic probe signal resembled the signal obtained at 2.5 mTorr N_2 in Fig. 11. The field reversal was arbitrarily taken to be strong when the probe signal at the particular pressure resembled the signal obtained at 2.5 Torr N_2 in Fig. 11. Again the results seem to indicate that the mechanism for field reversal occurs sooner at higher pressures for a particular background gas. This figure also demonstrates that to produce strong field reversal at a given position requires a greater pressure of He than of N_2.

C. SPATIAL MAPPING OF THE MAGNETIC FIELDS AND THEIR DENSITY PROFILES

The magnetic fields and the corresponding double probe profiles were mapped along the line r=0.4 cm, $\theta=0^{\circ}$ for pressures of 0.1, 5, 250 and 700 mTorr N_2. The results of this mapping are displayed in Figs. 14-39. To obtain the density profiles two assumptions were made in Eq. (17). First, it was assumed that the ion charge state was the same throughout the laser plasma. There is some experimental evidence, however, that the ions of highest charge state are located at the front of the laser plasma and that the average ion charge state decreases toward the "back" of the laser plasma [Ref. 2] . In addition, it was assumed that $\overline{V_{LP}}$ was a constant. By examination of Eq. (17) it can be seen that to obtain absolute ion densities from the relative densities in Figs. 14-39, one must evaluate $n_i=n_{iREL.} \times \overline{ZV}_{LP}/ZV$, where Z and V are the actual charge state and magnitude of the plasma expansion velocity at the point in question.

As a result of the above assumptions, the relative density profiles obtained with the double probe are useful only for locating the position of the plasma front (and back) relative to the magnetic fields or for detecting a steepening or slowing of the (narrow) front of the plasma. From an examination of Figs. 14-39 it appears that:

(1) At t=20 nsec, which is about the time the peak of the laser pulse is reaching the target surface, the magnetic field profiles along the 4 mm line are pressure dependent (Figs. 14, 19, 24 and 32).

(2) Since the plasma front does not reach the probe until a time later than t=20 nsec, the fields at t=20 nsec are in the ambient background plasma. The "density profiles" in Figs. 14, 19,

24 and 32 do not represent the photoionized background plasma, since they do not change significantly as the background pressure is increased by a factor of 700. These profiles are the result of the existence of an initial pulse in the double probe signal. This pulse (see the double probe signal depicted in Fig. 11) occurs at all axial positions and between the times t=0 and t=60 nsec. It will be discussed further in Section IX.

(3) The magnetic fields appear to be tied to the laser plasma for expansion into backgrounds of 0.1 and 5 mTorr N_2 (Figs. 14-18 and 19-23), i.e., the magnetic field maxima propagate with the expanding plasma. For t=300 nsec, the field maximum is located closer to the plasma front for expansion into 250 and 700 mTorr N_2 than for expansion into 0.1 or 5 mTorr N_2 (compare Figs. 18 and 28) at times greater than 300 nsec the generation of reverse field at the front of the laser plasma shifts the initial (clockwise) field maximum back into the laser plasma (compare Figs. 28 and 30).

(4) The onset of field reversal occurs at the front of the plasma and it occurs earlier in space and time at 700 mTorr than at 250 mTorr (Figs. 29, 36 and 40).

(5) Field reversal is coincident with a strong interaction between the laser plasma and the ambient background as is evidenced by a steepening and slowing of the front of the expanding plasma (compare, for example, Figs. 18 and 36).

(6) Reverse field is also present at the "back" of the laser plasma and it appears sooner at higher pressures (Figs. 28 and 36).

Although the density profiles were mapped only out to a distance of z=2.8 cm, the magnetic fields were mapped out to z=6 cm. This mapping showed that no field reversal occurs for pressures of 0.1 and 5 mTorr. However, a small magnitude of reverse field is present at the back of the laser plasma for all pressures and it occurs at later times for pressures of 0.1 and 5 mTorr. This reverse field was also observed by McKee (as was mentioned previously) and he also noted that it occurred earlier at higher pressures.

The field reversal was also mapped in the radial direction. Figure 40 shows the magnetic field signals detected at the positions z=1.6 cm, r=0.1, 0.2, 0.4 and 0.8 cm for a background pressure of 700 mTorr N_2. The largest reverse fields were detected at about r=0.4 cm. The maximum reverse fields arrive later as r increases, while they decrease in magnitude for probe positions on either side of r=0.4 cm. The maximum reverse field at the position (0.4, 0, 1.6) occurs at a time corresponding to the arrival of the density maximum. Reverse field arrives ahead of the plasma front and is preceded by a component of field in the direction of the initial fields (i.e., clockwise).

D. PRODUCTION OF REVERSE FIELD IN A LASER PLASMA IMPINGING ON A GLASS PLATE

Since the field reversal occurring at the front of the laser plasma appears to be a consequence of the interaction between the laser plasma and the ambient background plasma (which results in a slowing down and steepening of the plasma front), one should be able to induce the production of reverse field by simply causing the plasma front to rapidly decelerate.

Magnetic field reversal was observed several hundred nanoseconds after laser shut-off by allowing the expanding laser plasma to impinge upon a glass plate. The results of an experiment conducted in a background of 700 mTorr N_2 and with a glass plate located in the plane z=1.15 cm are depicted in Fig. 41. The right side of this figure displays the magnetic fields (B_θ) detected by a probe located at the position r=0.4 cm, $\theta = 0^\circ$ and z=1 cm with and without a glass plate located in the plane z=1.15 cm. The left side displays the plasma density profile in the absence of a glass plate and at a time corresponding to the arrival of the largest reverse fields at the magnetic probe. Reversal appears to onset after about 150 nsec when the plate is in place and reaches its largest value 320 nsec into the expansion process. Figure 42 shows the results of the same experiment conducted in a background of 5 mTorr. Reversal again appears to onset after about 150 nsec and the reverse fields attain their largest value at t=350 nsec. The rate of onset of reversal is larger for a background of 700 mTorr N_2 than for a background of 5 mTorr N_2.

E. TARGET MASS REMOVAL

To estimate the maximum temperature of the laser plasma and the kinetic energy of the streaming laser plasma, one must know the mass of the plasma. The mass of the ablated aluminum target material was determined by cleaning and weighing the target disc before and after a total of 234 shots. The average power of the incident pulse was 300 MW and a total mass of 1.0 mg was removed from the disc. Therefore, about 10^{17} aluminum atoms and ions (4.3 μg) were removed from the target disc per shot.

In a previous experiment cited by Ready [Ref. 2] it was determined that the ionization efficiency of a Q-switched ruby laser (10^9 W/cm^2) incident on a thin aluminum coating was about 1%. The total number of aluminum atoms and ions removed per shot in that experiment was estimated to be 5×10^{16}. In another experiment cited by Ready, a 100 MW, 30 nsec ruby laser was employed to produce a carbon plasma. The electron density 1 mm from the target surface increased rapidly to a maximum of 1.66×10^{19} cm^{-3} and decreased by a factor of 10 after 500 nsec. The neutral atom density reached a peak around 1.6×10^{20} cm^{-3} then decreased as the opaque blowoff plasma shielded the target surface and later went through another maximum as the initial blowoff plasma became transparent and the laser light again reached the surface. The neutral atoms were detected for about 1 nsec after the end of the laser pulse and the relative number densities indicated that only about 10% of the total vaporized material became ionized. Most of the ionized plasma was contained in the initial blowoff which was nearly 100% ionized.

Therefore, it will be assumed here that the initial blowoff material is 100% ionized and contains 10^{16} aluminum ions.

VII. APPLICABILITY OF THE "SHELL" MODEL

According to the model suggested by McKee, the pressure dependence of the self-generated magnetic fields is a result of the formation of a density shell at the front of the expanding laser plasma. Since the pressure dependence is evident during target irradiation, the model requires that the density shell form while the laser is still irradiating the target and that it be present even several hundred nanoseconds later (McKee explains the field reversal at late times by arguing that it occurs at the back of the density shell and also explains the continued increase of total field energy with time for expansion into 5 mTorr N_2 by arguing that magnetic fields are being created at the front of the density shell for several hundred nanoseconds after laser shut-off). He was unable to experimentally confirm the existence of the shell, since the only diagnostics at his disposal were magnetic probes. McKee's model was not unreasonable, however, since Dean [Ref. 8] had previously reported observing what appeared to be the formation of a density shell at the front of a laser plasma created under similar experimental conditions. In his conclusions McKee pointed out that, although his explanation of the pressure dependence of the spontaneous fields was plausable, it relied heavily on Dean's work and that "the relationship of the magnetic field to the laser plasma density and to the ambient plasma density must be thoroughly studied" to verify or to disprove the explanation that he had put forward.

The results of this investigation do not support the model developed as a result of McKee's investigation.

A difficulty in attempting to apply this model to explain the results of the present investigation is that it does not predict field reversal at the front of the plasma. The model requires that the interaction between the laser plasma and ambient background plasma cause the electrons in the shell of displaced background to be heated to a higher temperature on axis than off axis with the result that a radial electron temperature gradient of the same magnitude as exists in the laser plasma is formed in the density shell. The heating mechanism is not discussed, but it is stated that as long as there is an interaction between the two plasmas field production can continue at the front of the plasma. However, the results of the present investigation suggest that a strong interaction between the two plasmas is accompanied by the production of fields in the opposite direction at the front of the plasma (Figs. 34-37). If the initial field amplification is to be the result of the production of additional magnetic fields at the front of the density shell (in the manner proposed by McKee), then the observation of the production of reverse field at the front at later times in the expansion requires that the direction of the radial electron temperature gradient reverse. It is hard to believe that a radial temperature gradient in the density shell would initially grow in one direction due to the interaction between the laser plasma and the ambient background plasma and would then reverse its direction as the interaction continued. One might argue that the reverse fields are really being generated at the back of the density shell and that the shell merely is not resolvable. However, the width of the density shell should be comparable to the spatial width of the reverse fields and, therefore, of the order of several mm (Figs. 30, 31 and 36-39). For an expansion velocity of

3×10^6 cm/sec and a spatial half-width of 3 mm, the probe system would require a rise time of less than 100 nsec to resolve the density shell. This is much longer than the observed probe rise time.

Another difficulty associated with the shell model is that it predicts the production of reverse fields at the back of the density shell at early times in the expansion of the laser plasma (even for background pressures less than 250 mTorr). This prediction results from the fact that the density gradient is reversed at the back of the shell (in +z direction) so that one would expect reverse field production to accompany growth of the initial fields. Since the quantity $\frac{\nabla_z n_e}{n_e}$ might be smaller at the back of the density shell, production of reverse field could occur on a smaller scale than production of the additional field at the front of the shell. However, even if the source term behind the shell is not strong enough to actually reverse the fields, it should act to distort the shape of the magnetic probe signals detected at, say, (0.4, 0, 0.4) as the pressure is increased to 250 mTorr. No distortion of the signals is detected.

A very strong argument used to support the shell model was that it explained the existence of the maximum fields in a background of 250 mTorr N_2 at greater axial distances than those in 0.1 and 5 mTorr at early (fixed) times in the expansion phase (see Section II.B).

Double probe signals have been obtained in the present investigation at positions along the line r=0.4 cm, $\theta = 0^\circ$ for a Mylar laser plasma expanding into a nitrogen background gas. The experimental conditions were similar to those existing during McKee's investigation. The following observations were made:

(1) There was no evidence of the formation of a density shell for laser plasma expansion into 250 mTorr N_2.

(2) There was evidence of an interaction between the laser plasma and the ambient background; for example, at t=200 nsec the plasma front was located at (0.4, 0, 1.5) for plasma expansion into 5 mTorr N_2 and at (0.4, 0, 1.0) for plasma expansion into 250 mTorr N_2. In the figure below, the positions of the plasma fronts are superimposed on McKee's Fig. 52(b), which is a plot of the axial variation of B_θ along the line r=0.4 cm, $\theta = 0^\circ$

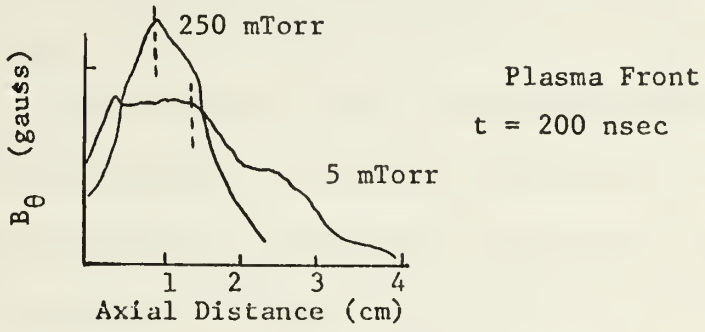

This figure indicates that $B_{\theta MAX}$ is located at the plasma front for expansion into a background of 250 mTorr N_2, while for expansion into a background of 5 mTorr N_2 $B_{\theta MAX}$ is located about 1 cm behind the plasma front. This result was predicted by McKee with the exception that he suggested the presence of a shell at the front for a background pressure of 250 mTorr N_2. It should be mentioned that the formation of density shells (of the order of 1 millimeter in thickness) has been observed in the present investigation. These shells were only observed when an aluminum laser plasma streamed into a background of H_2 and only at background gas pressures above 450 mTorr H_2.

The figure below represents the double probe and magnetic probe signals obtained at the position (0.4, 0, 2.0) when an aluminum laser plasma streamed into an ambient background of 450 mTorr H_2.

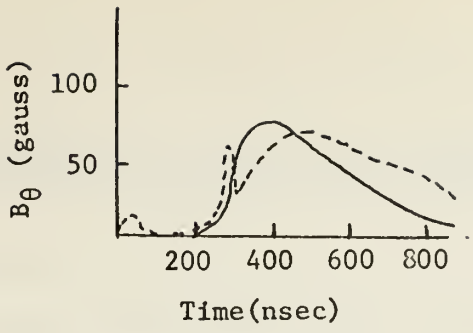

No region of increased B_θ is observed in the vicinity of the shell and, in fact, the shell appears to have no perturbing effect on the spontaneous fields residing in the vicinity of the density shell.

The principal diagnostic techniques used by Dean to observe the density shells which formed when the plasma (produced by irradiating a cylindrical fiber of lucite) expanded into a nitrogen background gas were fast photography, shadowgraphy and coaxial floating electric double probes. Evidence of the existence of the shells was obtained independently using all these techniques. Thus, there appears to be little doubt that the density shells actually existed. One must conclude, therefore, that either the formation of a density shell at the front of a laser plasma expanding into an ambient background is not a universal characteristic of the streaming laser plasma or that the probe employed in the present investigation only recorded the existence of the density shell over a specific range of hydrogen background gas pressures. The latter conclusions appear unacceptable in view of the known sensitivity and time resolution of the probe.

From the above discussions, it appears that the shell model cannot satisfactorily explain the results of this investigation and that no shell was present in McKee's investigation.

VIII. THEORETICAL MODEL FOR THE PRESSURE DEPENDENCE

A. INTERACTION MODEL

That an interaction between the laser plasma and the ambient background plasma does occur at sufficiently high ambient plasma densities has been well established. Koopman [Ref. 6] has suggested that the observed interaction is the result of multi-coulomb collisions occurring between the two plasmas. If a strong momentum transfer interaction is a dominant form, one would expect "snowplowing" or displacement of the ambient plasma by the leading edge of the laser plasma piston, with a corresponding "pile-up" of piston plasma behind the interface between the laser plasma and the background plasma. The ambient and piston plasmas would be intermixed in the region of the interface. That is, the model is one in which the background plasma is "captured" at the front of the expanding laser plasma, increasing the total mass of the streaming plasma and, by conservation of momentum, decreasing the expansion velocity of the plasma front. Thus it will be assumed that there exist three distinct regions characterizing the expansion of a laser plasma into an ambient background plasma: ambient plasma, interface, and laser plasma (see Fig. 43).

A one dimensional expansion model can be justified on the basis of the following considerations. The diameter of the laser beam at the target surface is about 6 mm and the laser radiation is absorbed within a distance of the order of 0.01-0.1 mm from the target [Refs. 2 and 14]. Therefore, the ablated target material will initially have larger dimensions parallel to the target surface than perpendicular to it. Since

the expansion is driven by pressure gradients (see Eq. (3)) and $|(\nabla P)_z| \sim \frac{P}{\delta_z} >> |(\nabla P)_r| \sim \frac{P}{\delta_r}$, δ_z and δ_r being characteristic axial and radial dimensions, initially there will be a more rapid expansion perpendicular to the surface than parallel to it. Thus, the expansion will be considered to be one dimensional.

When the laser plasma expands into the ambient background plasma, the axial position of the plasma front will be governed by the interaction between the two plasmas, i.e., $Z=Z(\rho_o, t)$ where Z is the axial position of the plasma front and ρ_o is the ambient plasma density. An empirical expression for the late time dependence of the axial position of the plasma front on time and on the ambient nitrogen plasma density can be obtained from Figs. 44 and 45, the result being

$$Z \propto (\frac{1}{\rho_o})^{0.1} t^{0.5} \qquad (18)$$

The dependence of the radial position of a plasma front on time has been determined in many investigations of the interaction of a laser-produced plasma with an ambient background. A brief description of some of these investigations has already been given in Section IV.B. Ramsden and Savic [Ref. 10], Bobin et al. [Ref. 3] and Dean [Ref. 8] assumed spherical geometry when comparing theory and experiment (supported by photographs of the propagation of nearly spherical luminous fronts). Hall [Ref. 9] argued that because of the presence of the target slab, the expansion did not possess spherical symmetry. He modified the spherical blast wave model [9] used by the above authors, taking into

---

[9] An approximate expression for the position of the front of a spherical blast wave as a function of ρ_o, t, and the actual energy, E, released in the explosion is $r=(E/\rho_o)^{0.2}t^{0.4}$

account that the main flux of target ions was biased toward the target normal, by assuming that the general form of the blast wave was a spherical segment and that E was a function of the angle subtended by the spherical segment. For this model one replaces E by $E^*=2E/(1-\cos(\frac{1}{2}\theta))$. Hall's model "predicted" that $r \propto t^{0.4}$ while he observed that $r \propto t^{0.42}$ for background pressures above 600 mTorr Ar.

Since in the present investigation, $Z \propto (\frac{1}{\rho_o})^{0.1} t^{0.5}$ the plasma front does not propagate like an ideal blast wave. The reason for the deviation can be understood by reviewing the basic assumptions made in ideal blast wave theory.

In ideal blast wave theory, a finite amount of energy is released suddenly within a small volume. The initial mass contained within this volume is assumed to be negligible in comparison with the mass of the displaced ambient background and, therefore, there is rapid transfer of the kinetic energy from the initial mass to the ambient background. The initial energy of expansion is gradually converted into random thermal energy and the blast wave slows down. For a laser-driven blast wave, the energy input is from the ablated material. Consequently, the total mass of the laser plasma ions must be less than the mass of the displaced background plasma if blast wave theory is to hold. This requirement appears to have been satisfied in the regimes for which blast wave-like propagation was observed. This requirement was, in general, not met in the present investigation. For example, at a background pressure of 250 mTorr N_2, the axial position at which the mass of the swept-up ambient plasma is equal to the mass of the plasma piston (assuming that the estimated 10^{16} laser plasma ions sweep up all the ambient plasma ions contained in a cylinder of 3 mm radius) is z=5 cm.

B. LOCATION OF THE FIELD PRODUCING REGIONS

During the absorption of the incident laser radiation by the blow-off plasma, the plasma temperature will initially be much less than the maximum estimated temperature of 100 eV. Any spontaneous magnetic fields created early in the absorption phase will then be subject to rapid diffusion from the region of production into the ambient background, i.e., the diffusion term $\frac{1}{\mu_o \sigma} \nabla^2 \vec{B}$ on the right-hand side of Eq. (9) cannot be neglected when $\sigma(T_e)$ is low. As the temperature in the field-producing region increases, the rate of field diffusion decreases due to the $T_e^{3/2}$ dependence of σ and for the maximum temperature estimated here, diffusion of the fields can be neglected. In a reference frame moving with the laser plasma front, one can then write

$$\frac{\partial \vec{B}}{\partial t} = \frac{\nabla k T_e}{e} \times \frac{\nabla n_e}{n_e} \qquad (19)$$

A very significant consideration in field production is the "geometrical factor" in the cross product of the thermal source term. Since the initial density profile is determined, to a large extent, by the target geometry while the temperature profile is determined by thermal heat conduction, one might expect that it would be possible to change the direction of the initial fields by altering the target geometry or by shaping the laser pulse. Experimental evidence supporting this prediction has recently been reported [Ref. 17] .

The targets employed in the present investigation were planar. Thus, the isothermal and iso-density contours appear to be nearly orthogonal near the edge of the focal region [Ref. 16] . Therefore, the important region for field production is the edge of the focal spot where one expects both $\nabla_r T_e$ and $\nabla_z n_e / n_e$ to be large.

Because the expanding laser plasma is axially symmetric, the thermal source term vanishes along the target normal. Therefore, a toroidal doughnut of azimuthal magnetic field will be created primarily at the edge of the focal spot in the blow-off portion (front) of the laser plasma and carried with the expanding plasma.

Support for the suggestion that the important region for field production lies near the edge of the focal spot was obtained by measuring the fields produced by irradiating a .001 inch aluminum foil. The target was irradiated several times without changing its orientation. The first shot produced a hole of about 3 mm in diameter in the foil. While succeeding shots did not noticeably change the diameter of the hole, they yielded fields down in magnitude by only a factor of 3 and produced a noticeable change in the appearance of the target surface over an area within a 3 mm radius from the center of the laser impact point. This experiment was first conducted by R. Case at the A.F.W.L. Kirtland A.F.B., New Mexico, who obtained a similar result.

C. HEATING IN THE INTERACTION REGION

In a coordinate system moving with the interface between the laser and ambient plasmas, a considerable part of the kinetic energy of the ambient plasma ions entering the interface will be converted into heat through the action of ion viscous forces. This, of course, assumes that the ambient plasma ions are "captured" within the interface. As the laser plasma piston displaces the ambient background plasma it slows. Thus the energy available for conversion to heat drops and the maximum temperature to which successive increments of ambient plasma ions are raised will decrease. The change in electron temperature in the interface due to the identical process for the incident electron gas

will be smaller than the change in the ion temperature by a factor on the order of $\frac{m_e}{M_{AP}}$, where M_{AP} is the mass of the ambient plasma ion. Therefore, one would expect the electrons to be heated primarily by electron-ion collisions in the interface. However, the characteristic time for transfer of energy between the electrons and the ions as a result of multi-coulomb collisions (τ^{ε}_{ei}) is larger than the characteristic time for energy transfer between the ions (τ^{ε}_{i}) by a factor of about $(\frac{M_i}{m_e})^{\frac{1}{2}}$ [Ref. 18] , so that the ambient plasma electrons in the interface will be heated by another process (other than electron viscous heating) during the early stages ($t < (\frac{M_{AP}}{m_e})^{\frac{1}{2}} \tau^{\varepsilon}_{AP}$) of the expansion (see Appendix A for a discussion of the characteristic times τ^{ε}_{ei} and τ^{ε}_{i}). That process appears to be compressional heating as can be seen from a heuristic argument. In the interface, the displaced ambient background plasma is highly compressed. The electron gas is compressed in the same manner as the ion gas. Therefore, the dominant heating mechanism for the ambient plasma electron gas in the interface can be considered to be adiabatic compression of the electrons for times less than $(\frac{M_{AP}}{m_e})^{\frac{1}{2}} \tau^{\varepsilon}_{AP}$. The interface will also contain laser plasma electrons and ions and the above discussion also applies to them. Since the ion masses are similar, it would seem acceptable to consider a single ion temperature to exist within the interface.

If one assumes, as did McKee, that a well defined shell of "swept-up" ambient plasma forms at the front of the laser plasma even as the laser is irradiating the target, and that the temperature within the shell is of the order of the temperature within the laser plasma (100 eV), then the ion density within the shell would necessarily be of the order of 10^{19} cm^{-3} for the electrons to be heated non-adiabatically (via

electron-ion collisions) during this time interval.[10] Therefore, it would seem that there would be little contribution to the observed field amplification as a result of field production within a shell of compressed ambient plasma during this time interval. It should also be noted that McKee's model required the production of a large radial temperature gradient in the shell, while for the geometry assumed here any interaction mechanism would drive a large axial temperature gradient.

Up to this point, little consideration has been given to the effect of the pile-up of the laser plasma on the heating within the laser plasma. As a result of the pile-up, there will also be strong viscous heating of the laser plasma ions. As the front slows down, the pile-up of the laser plasma will probably be the dominant mechanism driving the production of a large axial ion temperature gradient, not only at the front, but throughout the piled-up laser plasma. As the density of the ambient plasma is increased, the rate at which the laser plasma piles up (re-thermalizes) will increase. In the extreme case for which $M_{AP} \to \infty$, which can be simulated by allowing the plasma to impinge upon a glass plate, the very large axial ion temperature gradient which is produced near the plate is entirely the result of a rapid pile-up of the laser plasma ions near the plate. Since $\tau_{ei}^{\varepsilon} \propto \frac{T_e^{3/2}}{n_e}$, the increase in n_e accompanying an increase in the pile-up rate will reduce the characteristic electron heating time so that one would expect the rate at which the electrons are heated to increase.

---

[10] This number was arrived at by assuming that $\tau_{eA}^{\varepsilon} \sim 20$ nsec, $T_e = 100$eV, $Z=3$ and using the expression in footnote 4 for τ_{ei}^{ε}.

For the analysis to be valid the ion-ion viscous heating time due to pile-up of the laser plasma should be at most of the order of the time that has elapsed since laser shut off. If one assumes that the density of the aluminum laser plasma ions in the piled-up region is 10^{16} cm (the 10^{16} ejected Al ions in a volume $\pi(.3)^2(1)$), Z=3 and T_i=100eV, then the ion-ion equipartition time (τ_i^{ε}) can be calculated from the expression $\tau_{LP}^{\varepsilon} \sim 3\cdot10^6 \left(\frac{M_i}{M_{proton}}\right) \frac{T_i^{3/2}(eV)}{n_i Z^4}$ [Ref. 18]. The result is $\tau_{LP}^{\varepsilon} \sim$ 15 nsec. Thus, the characteristic time for collisional transfer of energy among the ions appears to be much shorter than the times corresponding to the onset of the strong reversal observed in this investigation.

In summary, it appears that:

(1) The electron viscous heating rate will be less than the ion viscous heating rate in the ambient plasma. Thus, electron heating would be expected to be mostly the result of electron-ion collisions.

(2) Ion-electron collisional heating is very slow compared to the ion thermalization rate so that for early times the electrons behave adiabatically and the dominant electron heating mechanism is (adiabatic) compression.

(3) Therefore, the initial field amplification does not result from additional fields produced in the displaced ambient plasma.

(4) Viscous heating of the piled-up laser plasma ions causes the production of an axial ion temperature gradient which is transmitted to the electrons via electron-ion collisions.

(5) Since the electron-ion collision time decreases as the electron density increases, the electron heating rate which results from the pile-up of the laser plasma increases as the pile-up rate increases

D. THE INITIAL FIELD AMPLIFICATION

The initial field amplification appears to develop while the laser is illuminating the target ($B_{\theta MAX} \sim 75$ gauss in Fig. 14 while $B_{\theta MAX} \sim$ 400 gauss in Fig. 24) and to be fully developed by the end of the laser pulse. During this time a large radial temperature gradient is maintained by the laser near the target surface. This temperature gradient will not be significantly influenced by the density of the ambient background plasma since the expansion of the blowoff is directed along the target normal. However, the axial density gradient in the field production region can be expected to increase as the mass of the displaced background plasma increases. If one assumes that during the time of the laser pulse, the quantity $\frac{\nabla_z n_e}{n_e}$ can be approximated by $\overline{V_{LP}}^{-1}$ where $\overline{V}_{LP}$ is the average expansion velocity of the front of the laser plasma during the time (τ) the laser is irradiating the target, then Eq. (19) can be written

$$B_{\theta MAX} \sim \frac{\nabla_r kT_e}{e\,\overline{V}_{LP}} \qquad (20)$$

Equation (20) assumes that the steepening of the density gradients of the laser plasma in the field production region, $\delta \sim \frac{n_e}{|\nabla_z n_e|} \sim \overline{V}_{LP}\,\tau$ (as a result of snowplowing of the ambient plasma) is proportional to the average expansion velocity of the plasma during the time the laser is irradiating the target. It is by no means clear that δ should scale as $\overline{V_{LP}}$. However, one would expect that $\overline{V_{LP}}$ could be used as a measure of the effect of the interaction on the expansion dynamics of the laser plasma. Thus, as $\overline{V_{LP}}$ decreases the initial fields should increase. Since $\overline{V_{LP}}$ is also a measure of the steepening of the density gradients in the laser plasma, different background plasmas should yield the same maximum fields for the same measured value of $\overline{V_{LP}}$.

At pressures too small for a strong interaction to occur there will be no steepening of the density gradients in the field production region and, therefore, no enhancement of B_θ .

E. FIELD REVERSAL

As the laser plasma expands into a low density background plasma, the gradients at the front relax and field production becomes insignificant. However, if the expansion is into a background plasma of sufficient density to strongly influence the laser plasma a different situation results. The viscous heating in the interface will "drive" large axial temperature gradients in the ion fluid, which will eventually be transmitted via collisions to the electron fluid. Therefore, field production will again occur near the "outer edges" of the interface. The equation describing this "late time" field production is

$$\frac{\partial \vec{B}}{\partial t} = \nabla_z \frac{kT_e}{e} \times \frac{\nabla_r n_e}{n_e} \qquad (21)$$

This equation "predicts" that the fields at the front will be produced in a direction opposite to the direction of the initial fields. It also predicts that the field reversal will occur sooner and grow to a larger magnitude as the background pressure increases, since the increased background density will increase the rate at which the laser plasma is piled-up in the interface, thus increasing n_e and decreasing the characteristic time for energy transfer between the ions and the electrons.

Notice that the source term in Eq. (21) contains an axial temperature gradient while the source term in Eq. (20) contains a radial temperature gradient. The radial temperature gradient is driven by the laser irradiation of the target. After cessation of the laser pulse,

this gradient can be expected to decay rapidly as a result of electronic heat conduction. In fact, there is evidence that the initial plasma becomes transparent to the incident laser radiation during illumination of the target [Ref. 2] . In that case the radial temperature gradient in the blowoff will begin to relax while the laser is still illuminating the target. The only temperature gradient that is driven (in the initial plasma) after cessation of the laser pulse is the axial temperature gradient which results from the interaction between the laser plasma and the ambient background. Therefore, the temperature gradient appearing in Eq. (21) is the axial temperature gradient.

IX. COMPARISON OF THEORY AND EXPERIMENTAL RESULTS

To compare the scaling of $B_{\theta MAX}$ with $\overline{V_{LP}}$ predicted in Eq. (20) to the experimental results, one must know the average expansion velocity of the plasma front during laser illumination of the target. It was not possible to measure $\overline{V_{LP}}$ during this time interval by the double probe technique employed in this investigation. Since the functional dependence of the position of the plasma front on the ambient background gas density appears to change after cessation of the laser pulse (see Section IV. B.), Eq. (18) cannot be used to evaluate V_{LP} during the initial expansion phase. Many authors [Refs. 3, 8 and 10] have reported observing that $\overline{V_{LP}} \propto \rho_o^{-1/3}$ during laser illumination of the target and they have interpreted the plasma expansion in this time interval as corresponding to the propagation of a radiation-driven detonation wave. If this functional dependence is assumed for the present investigation, then Eq. (20) predicts that $B_{\theta MAX} \propto \rho_o^{1/3}$. In Fig. 49 this predicted scaling of $B_{\theta MAX}$ as the cube root of the background gas pressure is compared with the measured values of $B_{\theta MAX}$ at the position (0.4, 0, 0.4) for the case of a Mylar laser plasma expanding into various pressures of nitrogen background gas, i.e., the Mylar curve in Fig. 9. A Mylar laser plasma was chosen for comparison purposes because in arriving at Eq. (20), the effects of the generation of reverse field at the front of the expanding laser plasma were neglected and McKee observed no field reversal at the front of the Mylar laser plasma produced in his investigation (pressures below 250 mTorr N_2). The computed values of $B_{\theta MAX}$ in Fig. 49 agree with the experimental values to

within 20% at pressures below 250 mTorr N_2. Above 250 mTorr N_2 the computed and experimental values of $B_{\theta MAX}$ diverge. This is due, in part, to the generation of reverse field at the front of the laser plasma. In Fig. 50 the predicted scaling is compared to the Al curve of Fig. 9. The computed values are well above the measured values of $B_{\theta MAX}$. This result is not surprising in view of the production of reverse field which is known to occur at the front of the aluminum laser plasma. If the computed values of $B_{\theta MAX}$ in Fig. 50 do represent the fields one would measure in the absence of the generation of reverse field, then one can equate the difference in the magnitudes of the computed and observed fields to the magnitude of the reverse field (B_R).

Figure 51 is a plot of B_R versus nitrogen background gas pressure obtained from Fig. 50 using this technique. The reverse field appears to scale as $P^{3/4}$. One can test the validity of the interpretation given to Fig. 50 (and Fig. 49) by attempting to predict the pressure at which reverse field should be observed at the position (0.4, 0, 0.4) for the aluminum laser plasma. This can be done by finding the pressure at which B_R is equal to the computed value of $B_{\theta MAX}$ in Fig. 50. At this pressure the measured field at the front of the laser plasma should be zero. The pressure is found by solving the equation $250 + 105\,(P-1)^{1/3} = 10(P-1)^{3/4}$. Thus, reverse field should occur at a pressure of approximately 500 mTorr N_2. As can be seen from Fig. 11, reverse field is first observed at the position (0.4, 0, 0.4) at a pressure of about 2.5 Torr N_2, i.e., at a pressure five times the predicted pressure. In view of the rather crude approximations which were necessary in arriving at this prediction, the order of magnitude agreement between predicted and measured pressure is not unreasonable, and tends to lend

credance to the qualitative interpretations. As a further check, the scaling law $B_r \propto P^{3/4}$ has been applied to two values in the range of well developed field reversal in Fig. 11, 2.5 Torr and 5 Torr. The scaling law applied to the value B_R=25 gauss at 2.5 Torr predicts B_R=42 gauss at 5 Torr, differing by 20% from the measured value of 50 gauss.

To compare the results depicted in Fig. 10 to the theory of the last section, one must again be able to calculate $\overline{V_{LP}}$ over the time interval, τ, of the laser pulse. Although it was not possible to measure $\overline{V_{LP}}$ during this interval, it was possible to measure $\overline{V_{LP}}$ at distances greater than 1 cm from the target. Table I shows the values of $B_{\theta MAX}$ at the probe position (0.4, 0, 0.4) for various background gas pressures as a function of $\overline{V_{LP}}$, where $\overline{V_{LP}}$ is the average expansion velocity of the plasma front along the line r=0.4 cm, $\theta=0^\circ$ from z=1.0-2.0 cm. These values of $\overline{V_{LP}}$ should be a measure of the interaction occurring between the laser plasma and background plasma during the early part of the expansion phase.

TABLE I

$B_{\theta MAX}$ AS A FUNCTION OF $\overline{V_{LP}}$ FOR VARIOUS BACKGROUND PRESSURES

Pressure	$B_{\theta MAX}$(gauss)	V_{LP} (cm/sec)
250 mTorr N_2		4.0×10^6
1000 mTorr H_e	630	4.5×10^6
180 mTorr A_r		4.0×10^6
450 mTorr H_2		8.3×10^6
35 mTorr A_r	470	8.3×10^6
230 mTorr H_e		7.7×10^6

The data shown in Table I support the prediction made in the last section that different background gases should produce the same maximum fields for the same measured values of $\overline{V_{LP}}$, although there $\overline{V_{LP}}$ is the average value of V_{LP} over the interval z=1-2 cm while $B_{\theta MAX}$ is the maximum field at the position (0.4, 0, 0.4). If the field amplification depicted in Fig. 10 results from the steepening of the density gradients in the field producing regions of the laser plasma, then it is not unreasonable to predict that the maximum obtainable fields will be the same regardless of the background gas present, although, of course, the pressure at which the maximum fields occur will vary from gas to gas. The maximum fields are of the order of 650 gauss for backgrounds of H_e, N_2, and A_r in agreement with the above prediction. The apparent anomolous behavior of H_2 will be discussed in a following subsection.

For all the curves of Fig. 10, the maximum observed fields first increase as the pressure increases and then sharply decrease as the pressure continues to increase. It has been suggested [Ref. 15] that this rather sharp decrease in the magnetic field is a result of collisional effects (ohmic losses) which come into play at the higher pressures.

The diffusion of the self-generated magnetic fields is controlled by the term, $\frac{1}{\mu_o \sigma} \nabla^2 \vec{B}$ in Eq. (19). This term has previously been shown to be negligibly small, at least for times of the order of several hundred nsec and for pressures below a few hundred mTorr. For this regime it is the high conductivity of the laser plasma which allows one to neglect the diffusion term. As the background pressure increases the expansion velocity of the plasma front decreases (Eq. (18)), decreasing the rate at which the expanding plasma cools. This decreases

the rate at which the conductivity ($\sigma(T_e)$) falls off. In fact, the electron temperature of the laser plasma can be expected to increase as a result of the interaction between the two plasmas. Thus one is not justified in arguing that the decrease in $B_{\theta MAX}$ observed in Fig. 10 is a result of collisional damping. That is, one cannot simply argue that at high background pressure the diffusion term will be the dominant term in Eq. (9). Rather, the decrease appears to be the result of field production in a direction opposite to the initial field direction. Reverse field production can be seen in Fig. 11. As the background pressure is increased from .25 Torr to 2.5 Torr, the value of $B_{\theta MAX}$ decreases and the field peak shifts toward the origin. At 5 Torr N_2, the production of reverse field at the front of the laser plasma has actually reversed the field direction. As the pressure is increased above 10 Torr N_2, the field peak continues to shift toward the origin.

This shift of $B_{\theta MAX}$ to earlier times as the background pressure is increased appears to be the result of field cancellation due to the generation of reverse field at the plasma front. For all pressures in Fig. 10, the earliest time at which spontaneous fields are detected coincides with the arrival of the laser pulse at the target, i.e., magnetic fields are detected at (0.4, 0, 0.4) before the plasma front arrives (this can also be seen by examination of Figs. 14, 19, 24 and 32 as was pointed out in Section VI.C.). As mentioned in Section VIII. B., the spontaneous fields created early in the absorption phase will be subject to rapid diffusion from the region of production into the ambient background, the result being that magnetic fields will be detected at a given position before the arrival of the plasma front. This explains the "instantaneous" arrival of the magnetic field signal

in Fig. 11. As the background pressure is increased above 250 mTorr N_2, the generation of reverse field at the plasma front (see, for example, Figs. 36-39) causes $B_{\theta MAX}$ to decrease. This decrease is the result of algebraic cancellation of the initial fields by the reverse fields. As the background pressure is increased above 2.5 Torr N_2, the production of reverse field continues to shift the time of "arrival" of reverse field at the probe to earlier times. For expansion into a background of 70 Torr N_2, reverse field has diffused into the ambient background ahead of the plasma front and caused an even earlier occurrence of reverse field at the probe position. The net result is that $B_{\theta MAX}$ occurs earlier in time in a background of 70 Torr N_2 than in a background of 250 mTorr N_2. This discussion demonstrates that one cannot attribute any physical significance to the location of $B_{\theta MAX}$, at lease at pressures for which the production of reverse field occurs; for example, one cannot use $B_{\theta MAX}$ to locate the position of the plasma front. This is further demonstrated in Fig. 12. At low pressures, the maximum magnetic fields are located near the front of the laser plasma and little reverse field production is occurring at the front. Therefore, the maximum detected field arrives later at (0.4, 0, 0.6) than at (0.4, 0, 0.4), since to first approximation the maximum field can be considered to be frozen in the plasma. At a pressure of 70 Torr N_2, however, the maximum field detected at (0.4, 0, 0.6) is the "fast" diffusion field. The maximum value of this diffusion field "arrives" sooner at (0.4, 0, 0.6) than at (0.4, 0, 0.4).

The "spike" which can be seen in the double-probe signal in Fig. 11 for plasma expansion into a background of 70 Torr N_2 occurs for all pressures and for all background gases. It is not visible at low

pressures at distances less than about 6 mm from the target as it is masked by the signal from the laser plasma. This early signal was at first thought to be the result of a stream of energetic electrons induced by the interaction between the laser radiation and the target. Such electron currents have previously been reported [Refs. 23-25] . The signal was not detected when a glass slide was inserted in the chamber between the probe tips and the laser impact area or when the target was removed from the chamber and the laser was shone through the chamber (light in through port #1 and out through port #3 of Fig. 3) with the probe in place. Therefore, it was definitely not a form of circuit noise and the source of the signal was unable to penetrate a thin microscope slide.

If the source of this early probe signal is a laser-induced electron current, then one can estimate the associated magnetic field by assuming that it results from an axial electron current. The electron number density can be estimated from the magnitude of the probe signal (1 amp at (0.4, 0, 1.0)) by assuming that the probe current results from the net collection of secondary electrons by the probe. One must assume the current to be the result of the collection of secondary electrons (due to bombardment of the probe tips by the energetic electrons making up the laser-induced axial electron current), since no current flows in the circuit of an isolated double probe immersed in an electron beam. By assuming that $V_e \sim 10^8$ cm/sec, and that one secondary electron is ejected per incident electron, one can use Eq. (17) with $(1+\varepsilon) \rightarrow \varepsilon = 1$ to show that $n_e \sim 10^{15}$ cm^{-3}. If n_e is assumed to be constant out to the radial position r=4 mm, then the maximum "instantaneous" magnetic field detected at the position (0.4, 0 , 1.0) should be

about 1000 gauss ($B = \frac{\mu_o n_e e V_e r}{2}$). However, the maximum instantaneous field detected at this position was of the order of 10 gauss. Thus, the early double probe signal does not appear to result from a laser-induced electron current directed along the axis. Another possible source of the early probe signal is plasma radiation in the extreme ultraviolet or near X-ray region. Radiation in this frequency range would not be able to penetrate the thin glass slide. Photoemission of electrons from tungsten is known to occur in this frequency range. For example, the photoelectric yield is about 5 electrons/photon for incident photons of wavelength 620 Å (20 eV) [Ref. 26] . In this case the early probe signal would result from a repulsion of the photoelectrons emitted at the probe tip collecting the saturation ion current (probe #2 in Section V.E.) and an attraction of the photoelectrons emitted at the other tip. A probe current of 1 amp for 2×10^{-9} sec corresponds to photoemission of approximately 5×10^{11} electrons. This corresponds to absorption of about 10^{11} photons at wavelength 620 Å and represents a total energy of the order of 10^{-2} joules radiated at this wavelength into a solid angle of 2π steradians. Therefore, this signal source is energetically possible. Further support for this source is rendered by the fact that the early probe signal did not significantly change in shape or amplitude as the double probe was moved from the axial position z=2 cm to the position (1.5, 0, 2.0). This result suggests that the early signal source possesses spherical symmetry. One would expect the radiation flux from the laser plasma to be isotropic while a laser-induced electron current would probably be directed primarily along the axis.

Although detection of the actual reverse field only occurs at pressures in excess of .25 Torr, reverse field generation influences the

observed pressure dependence of the magnetic fields (Figs. 9 and 10) at lower pressures. The production of reverse field at the front of the laser plasma requires that the ratio $\frac{|\nabla_z T_e||\nabla_r n_e|}{|\nabla_r T_e||\nabla_z n_e|}$ be larger than one. This production of reverse field is driven by an interaction (momentum transfer) between the laser plasma and the ambient background plasma (Fig. 13). The interaction results in a steepening of the front of the laser plasma (pile-up) and, consequently, it drives large axial temperature gradients. No similar mechanism exists to drive a radial temperature gradient and, as described in Section IV.C., the initial laser-induced radial temperature gradient can be expected to decay rapidly. Although it was not possible to quantitatively determine the magnitude of the gradients in the above ratio, it is conceivable that the ratio would be larger than one as a result of the strong heating (very large $\nabla_z T_e$) taking place in the front.

One can estimate the electron temperatures required to produce the observed field reversal by dimensional analysis of Eq. (21). From that equation, one obtains the expression

$$\frac{kT_e}{e} \sim \frac{B_{\theta MAX}\delta_r\delta_z}{\tau}$$

where δ_r and δ_z are the radial and axial scale lengths and τ is the characteristic time for reverse field production. From Figs. 36-38, $\delta_z \sim 5$ mm, $\tau \sim 200$ nsec, and $B_{\theta MAX} \sim 50$ gauss. If one estimates δ_r to be 4 mm (see Fig. 40), then one obtains about 1 eV for the required electron temperature in the front. The ion temperature at the front can be estimated from the expression $\frac{1}{2}M_{LP}V_i^2 = \frac{1}{2}M_{LP}V_f^2 + \frac{1}{2}M_{AP}V_f^2 + 3/2(N_{LP} + N_{AP})kT_i$ where V_i and V_f are the initial and final propagation speeds of the plasma front, M_{LP} and M_{AP} are the masses of the laser plasma and swept up ambient plasma ions, and N_{LP} and N_{AP} are the total number of

laser plasma and swept-up ambient plasma ions. By the time reversal is apparent (Fig. 36), the front has propagated to z~ 1.5 cm, and $V_f \sim 3 \times 10^6$ cm/sec. Therefore, $N_{AP} \sim 10^{16}$ and the ion temperature in the front is of the order of 400 eV ($V_i \sim 1.1 \times 10^7$ cm/sec and $N_{LP} \sim 10^{16}$). If one assumes that the front contains 10^{16} Al^{3+} ions in a volume of $\pi (.3)^2(.5) \sim 1.4 \times 10^{-1}$ cm^3, then $n_e \sim 2 \times 10^{17}$ cm^{-3}. The plasma has also swept up on the order of 10^{16} electrons contained in the photoionized background. Assuming $T_e \sim 1$ eV, one obtains a value of approximately 100 nsec for τ_{ei}^{ε}, the electron-ion energy equipartition time. Thus, the electrons will be heated to the required temperature, at least on the basis of this simple analysis.

When the plasma encounters the glass plate, its directed kinetic energy is transformed into thermal energy via viscous ion heating as the plasma piles up at the plate. In effect, then, the glass plate acts as a very dense background gas. The reverse fields detected by the probe are larger and have a sharper onset in a background of 700 mTorr N_2 than in 5 mTorr. The reason for this is that for expansion into 700 mTorr N_2, the pile-up of the laser plasma at the front has resulted in production of reverse field before the steep front reaches the plate, thus reducing the magnitude of the initial fields. Also, the steep front will probably produce larger axial temperature gradients near the plate and produce them in a shorter period of time.

An order of magnitude estimate of the axial temperature gradient necessary to produce the observed fields again yields a value for T_e on the order of 1 eV.

Thus, it appears that to observe field reversal at the front of the laser plasma one need only cause a pile-up of the laser plasma (steepening of the front) at a sufficient rate to produce a large axial

temperature gradient. For the case of the laser plasma streaming into an ambient background plasma, the pile-up is a result of the observed coupling between the two plasmas. The reason the reversal occurs earlier in space and time as the background pressure increases (Fig. 13) is that the rate at which the pile-up occurs increases as the mass density of the snowplowed background increases and this increases $\nabla_z T_e$ in the front. This also explains why, in Fig. 13, the He curve lies to the left of the N_2 curve. One might also expect that the H_2 curve should lie to the left of the He curve in Fig. 13. However, Fig. 10 clearly shows the onset of reversal at (0.4, 0, 0.4) to occur at about 450 mTorr H_2; that is, at a value between the pressures corresponding to the onset of reversal for He and N_2. There is another apparent anomaly with the H_2 curve in Fig. 10. If the initial field amplification is the result of an interaction between the laser plasma and the ambient background plasma (during the time the laser is irradiating the target), then one would expect production of fields on the order of 600 gauss at sufficiently high hydrogen background pressure (see Eq. (20) and subsequent discussion). Therefore, if the present model is valid, another mechanism must be obtained by examination of Figs. 46 and 47. Figure 46 displays the magnetic field signals detected at the position (0.4, 0, 0.4) for background pressures of .45, 1, 2, 5 and 10 Torr H_2. As in Fig. 11, the field maximum shifts toward the origin as the pressure increases, but the structure of the signals has a different character. This structure was investigated by performing an axial sweep along the 4 mm line for a pressure of 5 Torr H_2. The results of this investigation are shown in Fig. 47. By the time the front has propagated a distance of 8 mm, the reverse field has attained a magnitude

of about 60 gauss with a spatial half width of about 2 mm. At a distance of 1 cm the reverse field has developed a definite double structure. The narrow "spike" of reverse field that first develops at the front appears to be responsible for the decrease in $B_{\theta MAX}$ observed above 450 mTorr H_2 in Fig. 10. The broader field reversal that develops later is characteristic of the reverse field signals detected in N_2, Ar, and He. If one plots the occurrence of the second field reversal in Fig. 13, the H_2 curve does lie to the left of the He curve (no reversal is observed for 2 Torr H_2, strong reversal onsets at z= 1 cm for 5 Torr H_2 and z=.6 cm for 10 Torr). The expansion velocity of the front was about 10^7 cm/sec during the time the initial reverse field was developing and it decreased to about 4×10^6 cm/sec during the time the broader field reversal was developing. Therefore, the broader reversal appears to be the result of a pile-up of the laser plasma, while the narrow reverse field structure is driven by some other mechanism.

This mechanism might be viscous heating of the swept up hydrogen background plasma contained in the interface. The hydrogen ions can be heated to temperatures of the order of 100 eV in times of the order of one nsec [11] at the interface, and, therefore, one can expect an electron-ion equipartition time of the order of 40 nsec at the front. It is, therefore, quite conceivable that the narrow "spike" of reverse field in Fig. 47 is being driven by a large axial electron temperature

---

[11] The ion-ion collision time can be approximated by $\tau_i = 3 \times 10^6 \left(\frac{m_i}{2m_p}\right)^{\frac{1}{2}} T_i^{3/2}(eV) \left[n_e \text{ cm}^{-3} Z^3\right]$ [Ref. 18]. Thus, for $n_e \sim 10^{18}$ and $T_i \sim 100$ eV, the characteristic time for the viscous heating of the hydrogen ions at the interface is ~ 1 nsec.

gradient produced at the interface as a result of collisional transfer of energy from the swept up hydrogen background plasma to the electrons.

The reverse field appearing at the "back" of the laser plasma (see Figs. 29-31 and 36-39) is not being driven by the axial electron temperature gradient which occurs as a result of the interaction between the laser plasma and the ambient background plasma since it is also present at a background pressure of 0.1 mTorr N_2. At this low pressure no interaction between the two plasmas is observed. This "secondary" component of reverse field appears to flow out of the region of the laser impact point after the emergence of the strongly heated blowoff plasma. That it appears sooner and grows to a larger magnitude as the pressure of the ambient background plasma is increased suggests that the generating mechanism for the secondary component of reverse field is influenced by the interaction between the laser and ambient plasma. If one assumes that the influence is the result of an increase in the axial density gradient at the back of the laser plasma, as indicated by Figs. 27 and 37, then Eq. (19) suggests that a small radial temperature gradient also exists at the back of the blowoff plasma. This explanation must be viewed with some skepticism at ambient background pressures for which a strong interaction is observed. The interaction will drive an axial temperature gradient even at the back of the blowoff plasma as a result of laser plasma pile-up. This axial temperature gradient should be much larger than any residual radial temperature gradient.

X. SUMMARY AND CONCLUSIONS

This investigation has been a continuation of the research started by L. L. McKee on the origin and properties of the spontaneous magnetic fields associated with laser produced plasmas. McKee's investigation was limited to the characteristics of the spontaneous magnetic fields associated with a Mylar laser plasma streaming into various mass densities of an ambient nitrogen plasma. The only diagnostic tools used in his investigation were magnetic probes (inductive loops). Using these probes he observed that the magnitude of the spontaneous magnetic fields exhibited a systematic dependence on the pressure of the ambient nitrogen plasma. Below background gas pressures of about 1 mTorr N_2 the maximum observed magnetic fields at a fixed probe position were independent of the background gas pressure. Between about 1 mTorr and 250 mTorr N_2 the maximum magnetic fields increased with pressure, while above 250 mTorr N_2 the maximum magnetic fields at a fixed probe position decreased with increasing background gas pressure. McKee developed what seemed to be a plausible model to explain the observed pressure dependence.

In the present investigation, electric double probes in addition to magnetic probes have been used to study the characteristics of spontaneous magnetic fields associated with an aluminum laser plasma expanding into backgrounds of H_2, He, N_2, and Ar and to study their spatial relationship to the plasma relative density profiles. The following conclusions have been reached as a result of this investigation:

(1) The model proposed previously to explain the systematic pressure dependence of the spontaneous magnetic fields was incorrect. That model required the formation of a density shell at the front of the expanding laser plasma for background gas pressures above about 1 mTorr N_2 and the subsequent production of spontaneous magnetic fields within the density shell. It was argued that these magnetic fields would be in the same direction as the axially symmetric fields residing in a laser plasma expanding into backgrounds of less than 1 mTorr N_2. However, in the present investigation no density shell was detected at the front of the Mylar laser plasma and the occurrence of reverse fields at the front of an aluminum laser plasma expanding into a sufficiently dense background could not be explained by the "shell" model.

(2) The model developed as a result of the present investigation attributes the increase in the magnitude of the initial spontaneous magnetic fields with increasing background gas pressure to the interaction which occurs between the laser plasma and the photoionized background plasma during the time the laser is irradiating the target. The interaction increases the axial density gradients at the front of the expanding laser plasma and this, in turn, increases the rate at which spontaneous magnetic fields are produced in the interaction region via the thermal source term, $\left.\frac{\partial \vec{B}}{\partial t}\right|_{\text{source}} = \frac{\nabla_r kT_e}{e} \times \frac{\nabla_z n_e}{n_e}$

(3) As the pressure in increased above a certain critical pressure, which appears to decrease as the mass of the background plasma ions increases, reverse field is generated at the front of the

streaming plasma. This reverse field generation appears to be the result of a pile-up (and re-thermalization) of the laser plasma as it sweeps up the ambient background plasma, and it continues long after laser shut-off. The pile-up drives an axial electron temperature gradient at the plasma front and, therefore, the spontaneous magnetic fields are produced in a direction opposite to the direction of the initial fields, i.e., $\left.\frac{\partial B}{\partial t}\right|_{source} = \frac{\nabla_z kT_e}{e} \times \frac{\nabla_r n_e}{n_e}$

(4) Reverse field can be produced long after laser shut-off if the laser plasma encounters a barrier. Therefore, one might expect to observe spontaneous magnetic fields whenever a streaming plasma encounters a barrier (for example, the solar wind encountering the earths magnetic field or the plasma ejected from a plasma gun and streaming into an ambient background).

(5) Reverse field is initially produced at the front of the laser plasma streaming into a background of H_2 at pressures above 450 mTorr before any significant pile-up of the laser plasma has occurred. This narrow component (spatial half-width of $\sim$ 2 mm) of reverse field appears to be generated in the swept-up hydrogen background plasma and it is followed by the appearance of a broad component of reverse field as the plasma front steepens and slows due to the interaction between the laser-plasma piston and the background.

APPENDIX A

Expressions for the characteristic times for ordinary collisions and for energy transfer among the charged particles making up a plasma as a result of these ordinary collisions can be obtained through some simple ideas based on the motion of the individual charged particles.

In the absence of a strong magnetic field, a particle's (here, an ion or an electron) path through a background medium (also ions or electrons) can be approximated by a broken line of randomly directed segments, each of length $\ell \equiv V\tau$, where V is the average speed with which the particle collides with the background and τ is defined as the average time between collisions. The quantity ℓ^{-1} is then the number of collisions per unit length made by the incident particle as it moves about in the background and one would expect, therefore, that $\ell^{-1} = n\sigma$, where n is the number of background particles per unit volume and σ is defined as the effective size of the scattering background particles. The size of the background particles can be taken to be πb^2 , where b is the distance of closest approach between a background particle and an incident "test" particle. The value one obtains for b clearly depends on the nature of the interparticle forces and on the energy of the background particle, incident particle system (here, the particles are considered as point charges with no internal structure and all collisions are therefore elastic).

If one assumes the active interparticle force to be the coulomb force (an assumption which appears valid for conditions of the present investigation) then $\frac{e^2 Z_1 Z_2}{b} = \varepsilon$ where ε is the relative kinetic energy of

the background particle, incident particle system at large separation distances (before the encounter). Now it turns out that because of the long range nature of the coulomb force, there will be many long range, small angle collisions between the particles and these collisions will increase the effective value of $\sigma = \pi b^2$ about an order of magnitude above the value $\pi[\frac{e^2 Z_1 Z_2}{\varepsilon}]^2$. Also, since b is generally obtained by assuming that the background particles are stationary, and that ε is the mean thermal energy of the incident particles, the mean free path for coulomb collisions is proportional to the square of the average energy (lab system) of the incident particles or to the square of their temperature if one assumes a Maxwellian distribution of velocities.

In this investigation, use is made of two characteristic times: τ_{ei}^{ε} , the characteristic time for energy equipartition between the plasma electrons and the plasma ions and τ the ion-ion collision time.

Because large fractional energy exchanges occur between like particles in a single collision, one can write $\tau_e^{\varepsilon} \sim \tau_e$ and $\tau_i^{\varepsilon} \sim \tau_e$, where τ_i^{ε} , τ_e^{ε} , and τ_e are respectively the ion-ion energy equipartition time, the electron-electron energy equipartition time and the electron-electron collision time. Since the relative velocity in electron-ion collisions is of the same order as in electron-electron collisions, and since recoil effects can be neglected in the relatively long range small angle collisions considered here, one may write $\tau_{ei} \sim \tau_e$. On the other hand, only a small fraction of the energy is transferred (the order of the mass ratio) in collisions of electrons with ions so that $\tau_{ei}^{\varepsilon} \sim \frac{m_i}{m_e} \tau_{ei} \sim \frac{m_i}{m_e} \tau_e$. Since the particle mean free path is proportional to the square of the temperature, if the ions and electrons are assumed to

have about the same temperature, then one can use the relationship $\tau = \frac{\ell}{V}$ to show that $\tau_i \sim (\frac{m_i}{m_e})^{1/2} \tau_e$. Therefore, substituting $\tau_e \sim (\frac{m_e}{m_i})^{1/2} \tau_i$ in the expression $\tau_{ei}^{\varepsilon} \sim (\frac{m_i}{m_e}) \tau_e$, one ean show that $\tau_{ei}^{\varepsilon} \sim (\frac{m_i}{m_e})^{1/2} \tau_i$. If the ion temperature is larger than the electron temperature, then τ_i inereases, but the eondition $\tau_i << \tau_{ei}^{\varepsilon}$ should still be satisfied as long as $\tau_i << (\frac{m_i}{m_e})^{1/2} T_e$.

Thus, beeause the electrons and ions making up a plasma have a mass ratio very different from unity, a loeal equilibrium (Maxwellian distribution) ean be established with the electron and ion fluids long before it is established between the two fluids, i.e.,

$$\tau_e^{\varepsilon} = (\frac{m_e}{m_i})^{1/2} \tau_i^{\varepsilon} = (\frac{m_e}{m_i}) \tau_{ei}^{\varepsilon}$$

In a mueh more rigorous analysis, Spitzer [Ref. 5] obtains the following expressions for the relaxation times:[12]

$$\tau_e = \frac{0.266\ T_e^{3/2}(K)}{n_e(cm^{-3})\ \ln \Lambda} \qquad \tau_i = \frac{11.4(m_{ion}/m_{proton})^{1/2} T_i^{3/2}\ (K)}{n_i(cm^{-3})\ \ln \Lambda}$$

where $\ln \Lambda$, the eoulomb logarithm is proportional to $\ln \frac{T_e^{3/2}}{n_e^{1/2}}$ and has a value of 11.9 for $n_e = 10^{16}$ em^{-3} and $T_e = 100$eV.

In computing the above relaxation times, Spitzer assumed the eleetrons and ions possessed a Maxwell-Boltzman veloeity distribution, but with different kinetic temperatures.

---

12 $$\tau_{ei}^{\varepsilon} = \frac{3.19 \times 10^{-3}\ (\frac{m_{ion}}{m_{proton}})\ \left[1836\ T_e(K) + \frac{m_{proton}}{m_{ion}}\ T_i(K)\right]^{3/2}}{n_i(cm^{-3})\ Z_i^2\ \ln \Lambda}$$

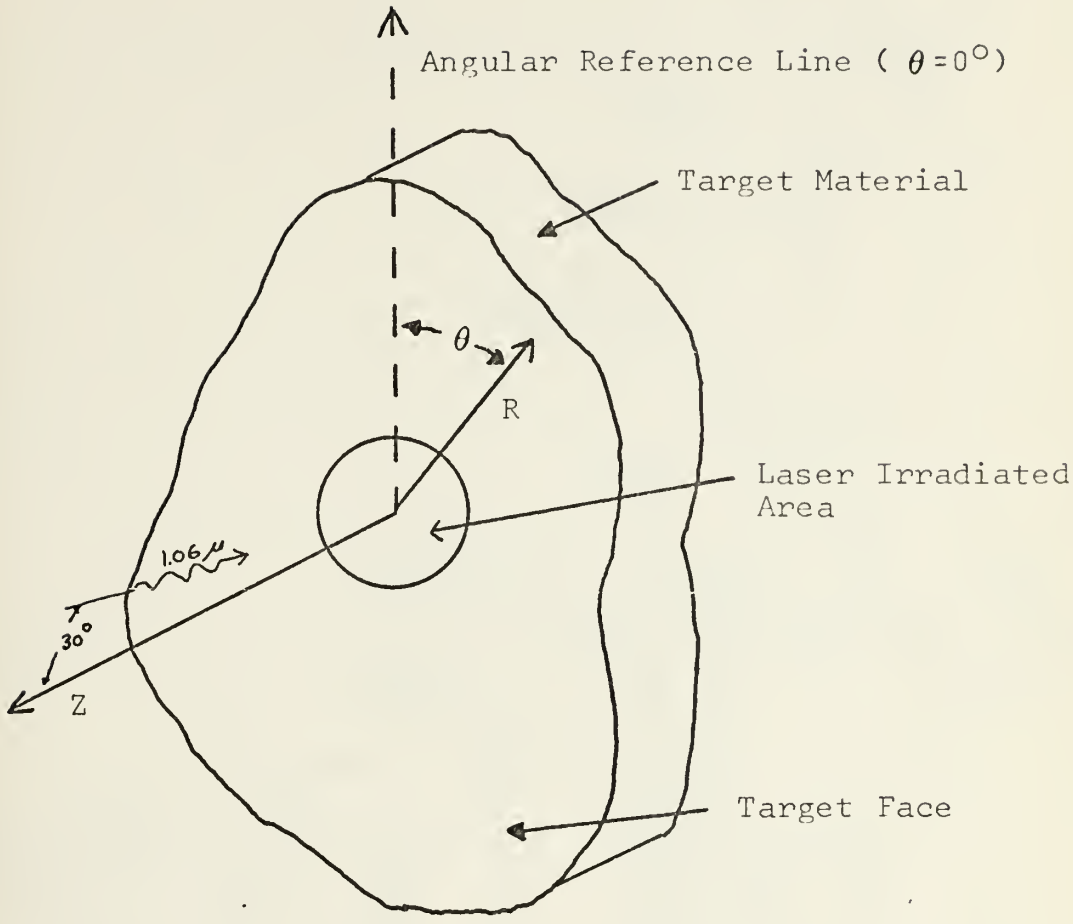

Figure 1. Cylindrical-polar coordinate system used.

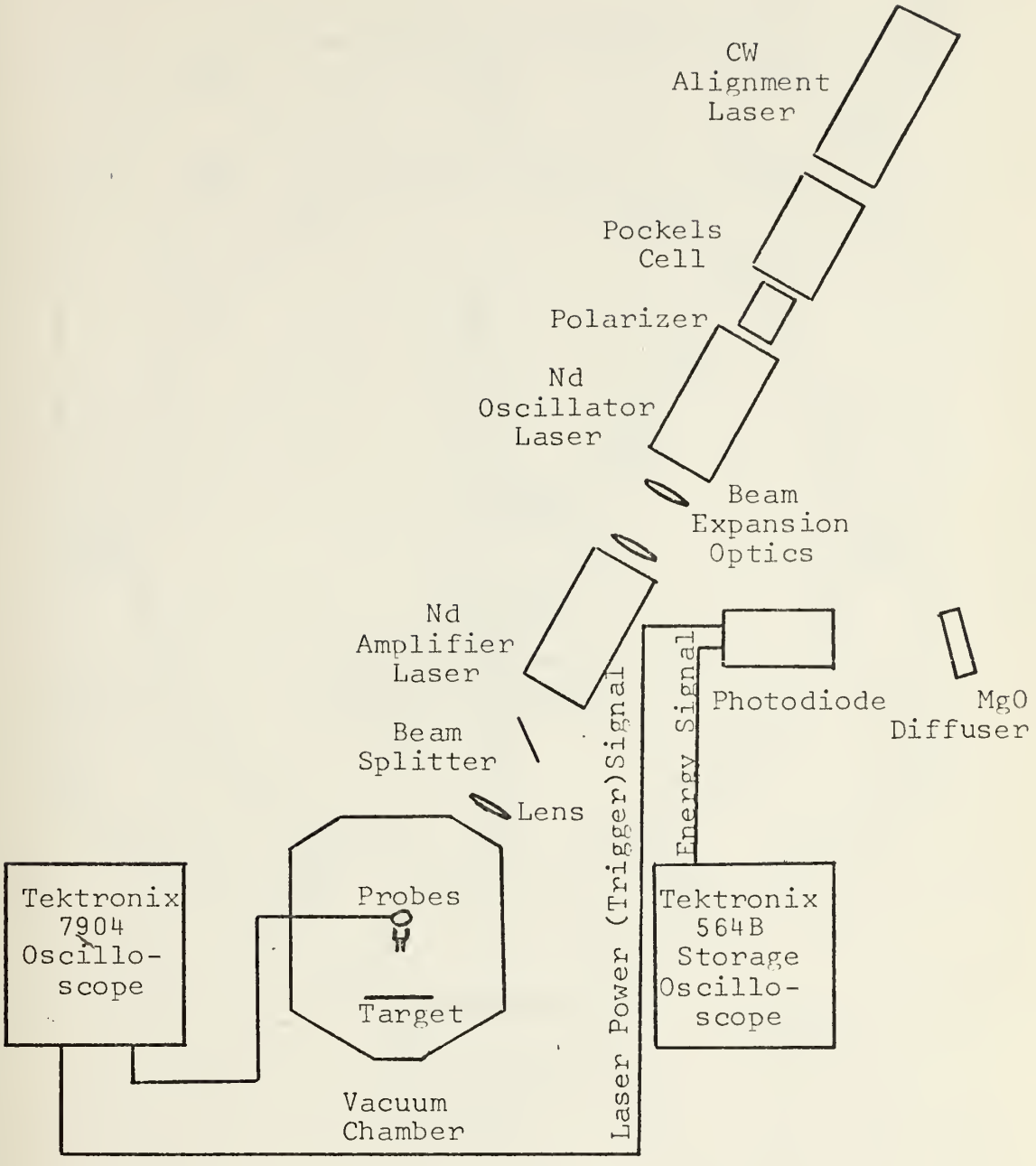

Figure 2. Block diagram of experimental layout.

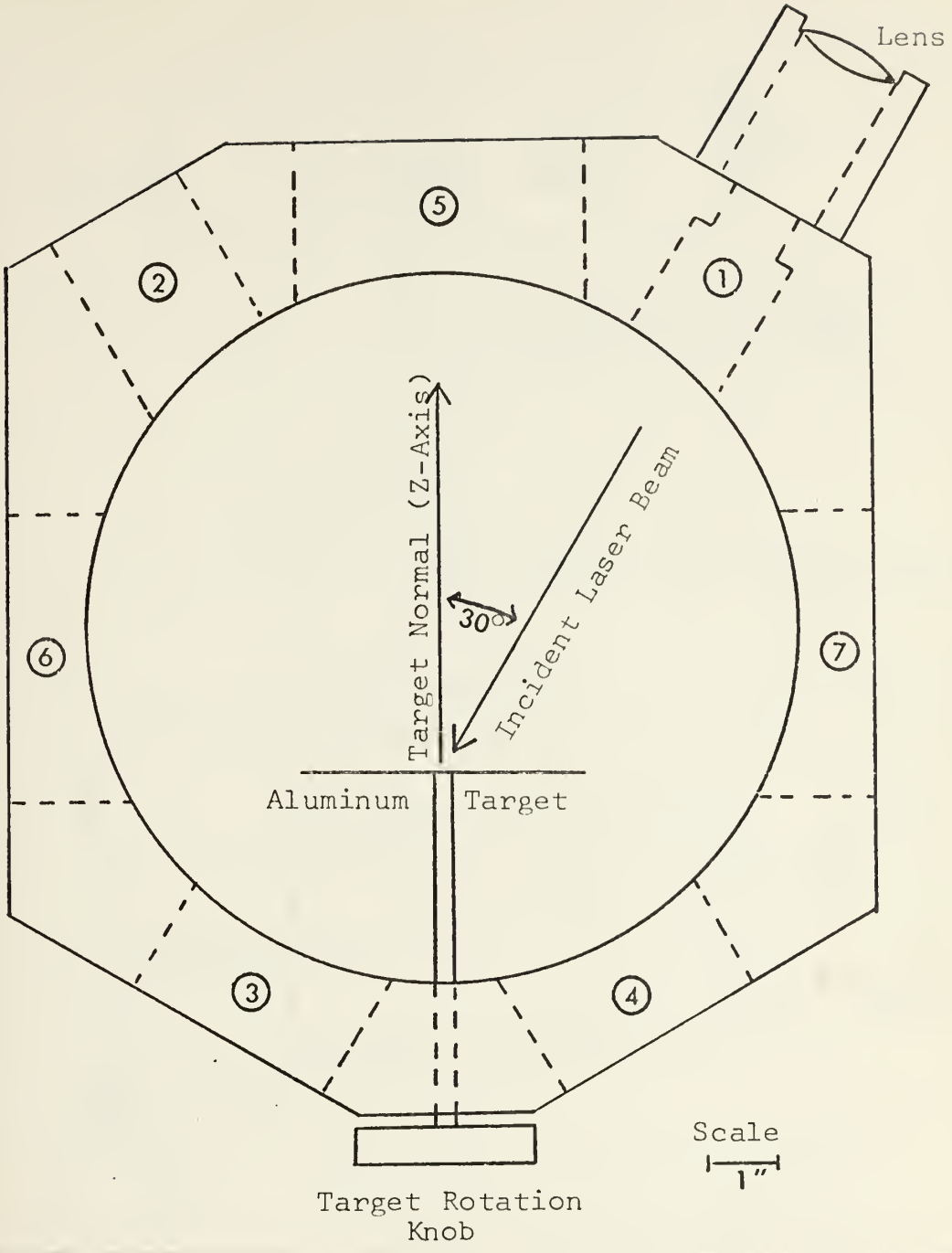

Figure 3. Top view of vacuum chamber. Port #1 is the laser beam entry port, #2 is the reflected laser beam observation port, #3 is the transmitted laser beam observation port, #4 is an optical observation port, #5 is the forward optical/probe observation port and #6 and #7 are the side optical/probe observation ports.

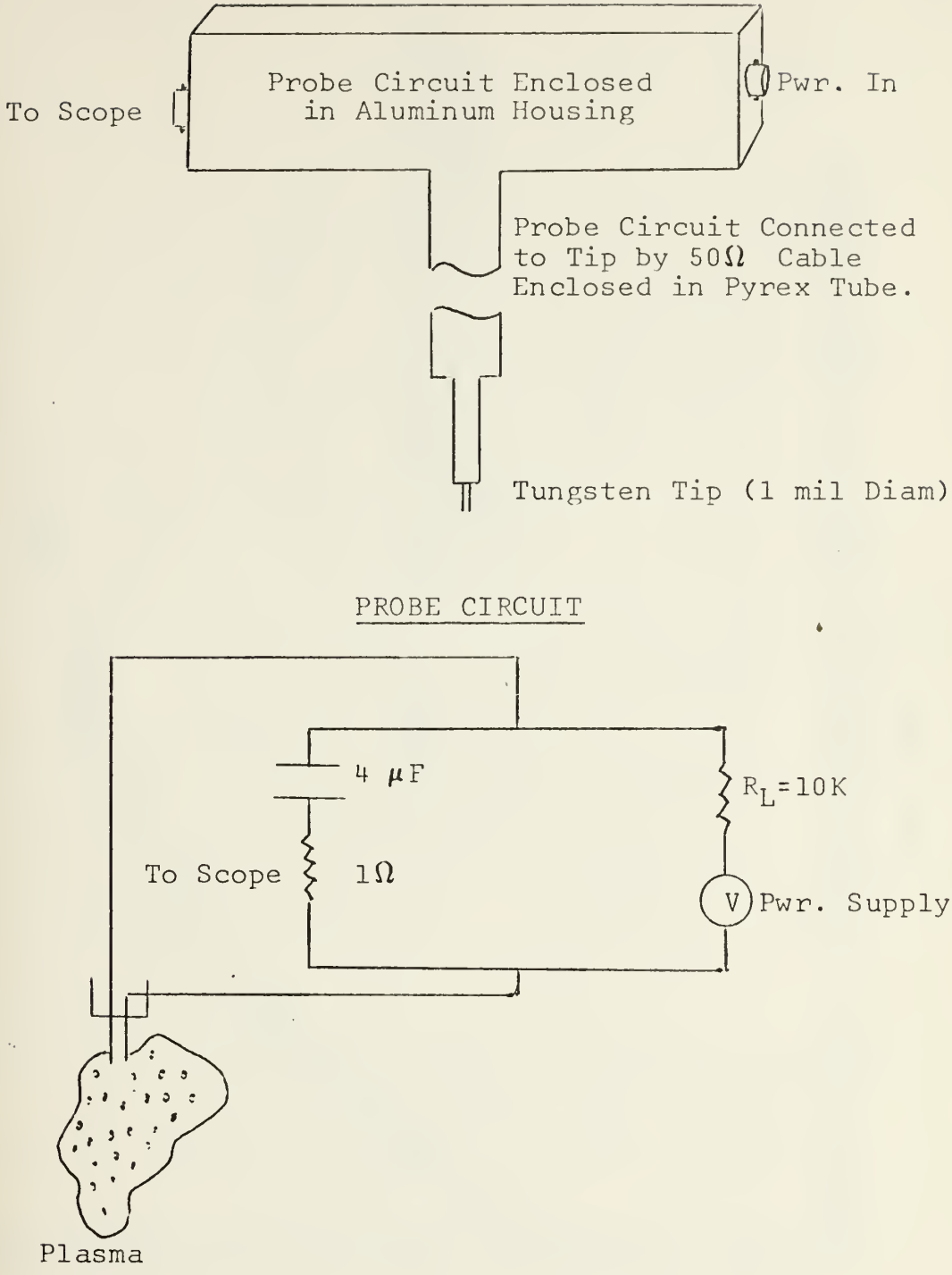

Figure 4. The electric double probe circuit.

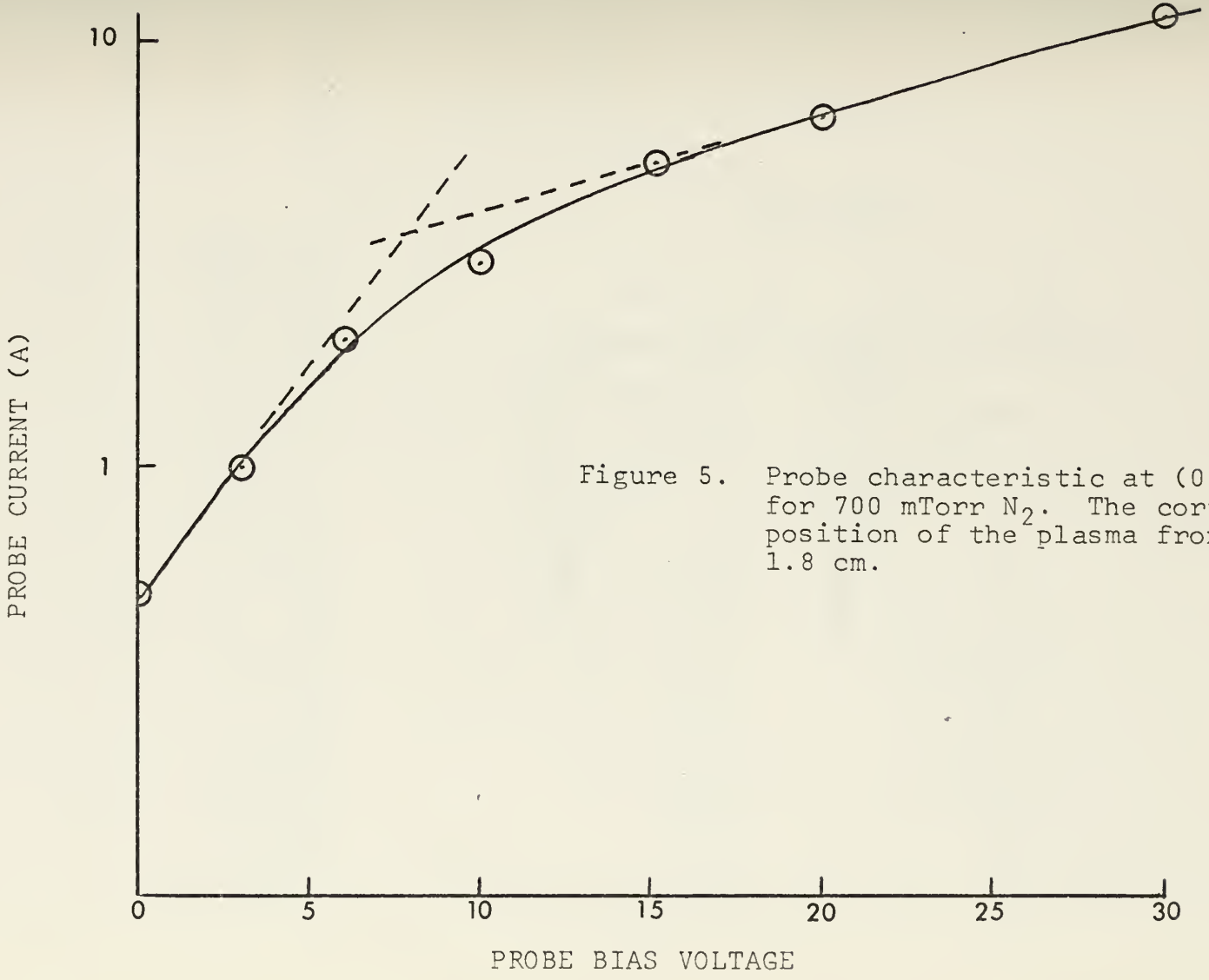

Figure 5. Probe characteristic at (0.4,0,1.5) for 700 mTorr N_2. The corresponding position of the plasma front is 1.8 cm.

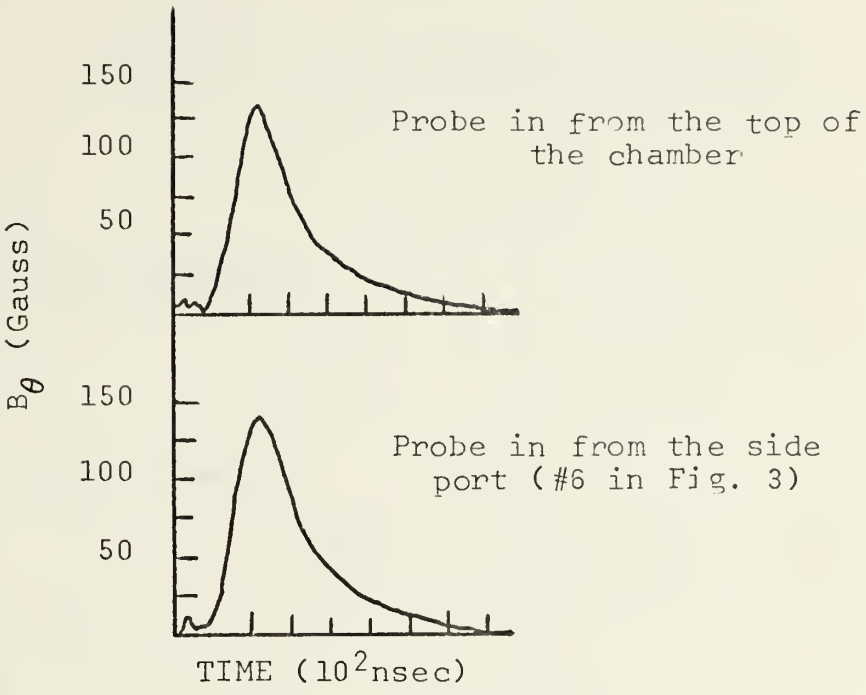

Figure 6. B_θ signal for a background pressure of 0.1 mTorr N_2. The horizontal scale is 100 nsec per divisions. The coil of the magnetic probe is located at the position (0.4, 0, 1.0).

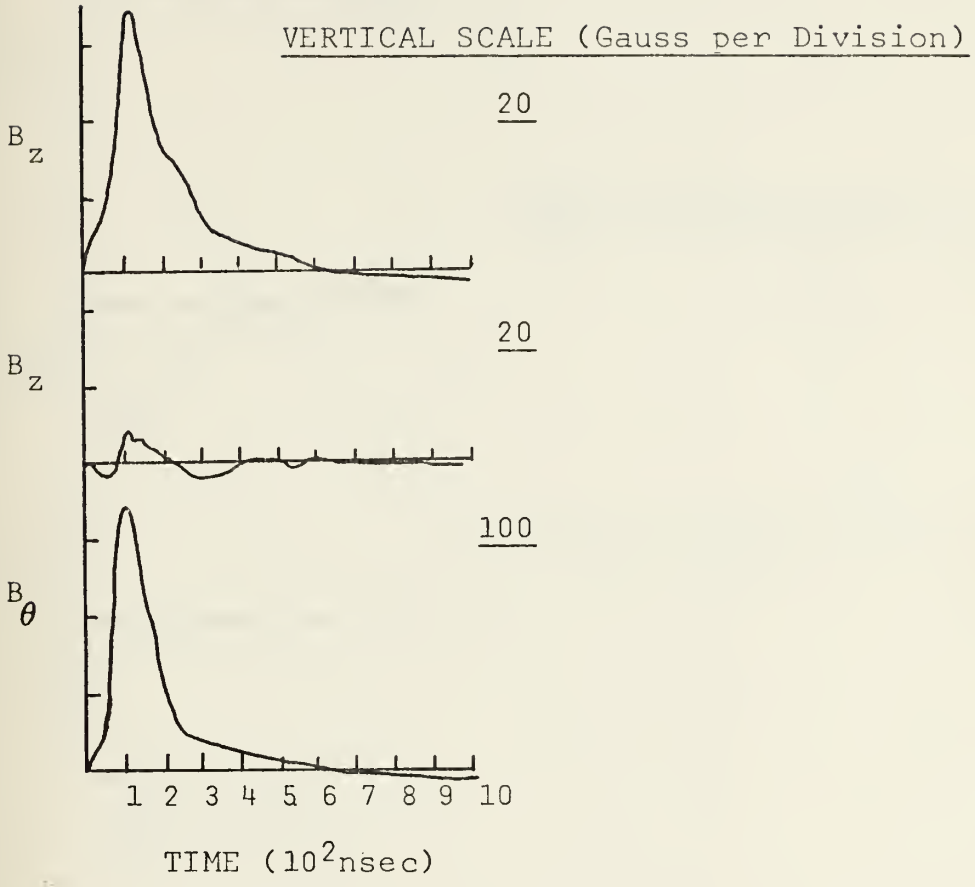

Figure 7. Magnetic field at (0.5, 0, 0.5) for a background pressure of 250 mTorr N_2. The top trace was obtained using a magnetic probe with a glass-enclosed tip while the lower traces were obtained using an open (unshielded) tip. The probe was inserted from the top of the chamber.

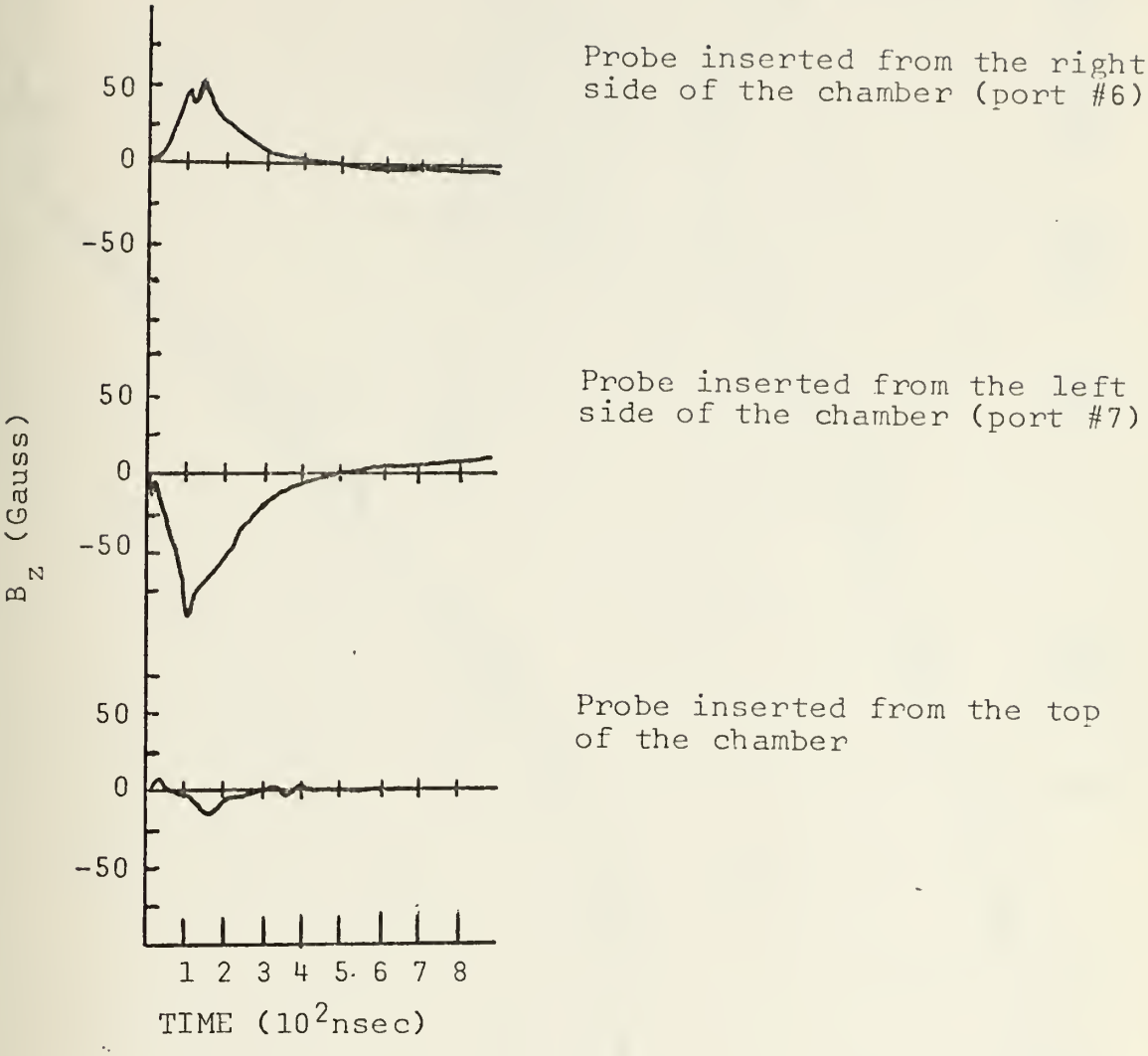

Figure 8. Magnetic field at (0.4, 0, 0.7) for a background pressure of 250 mTorr N_2 (open probe).

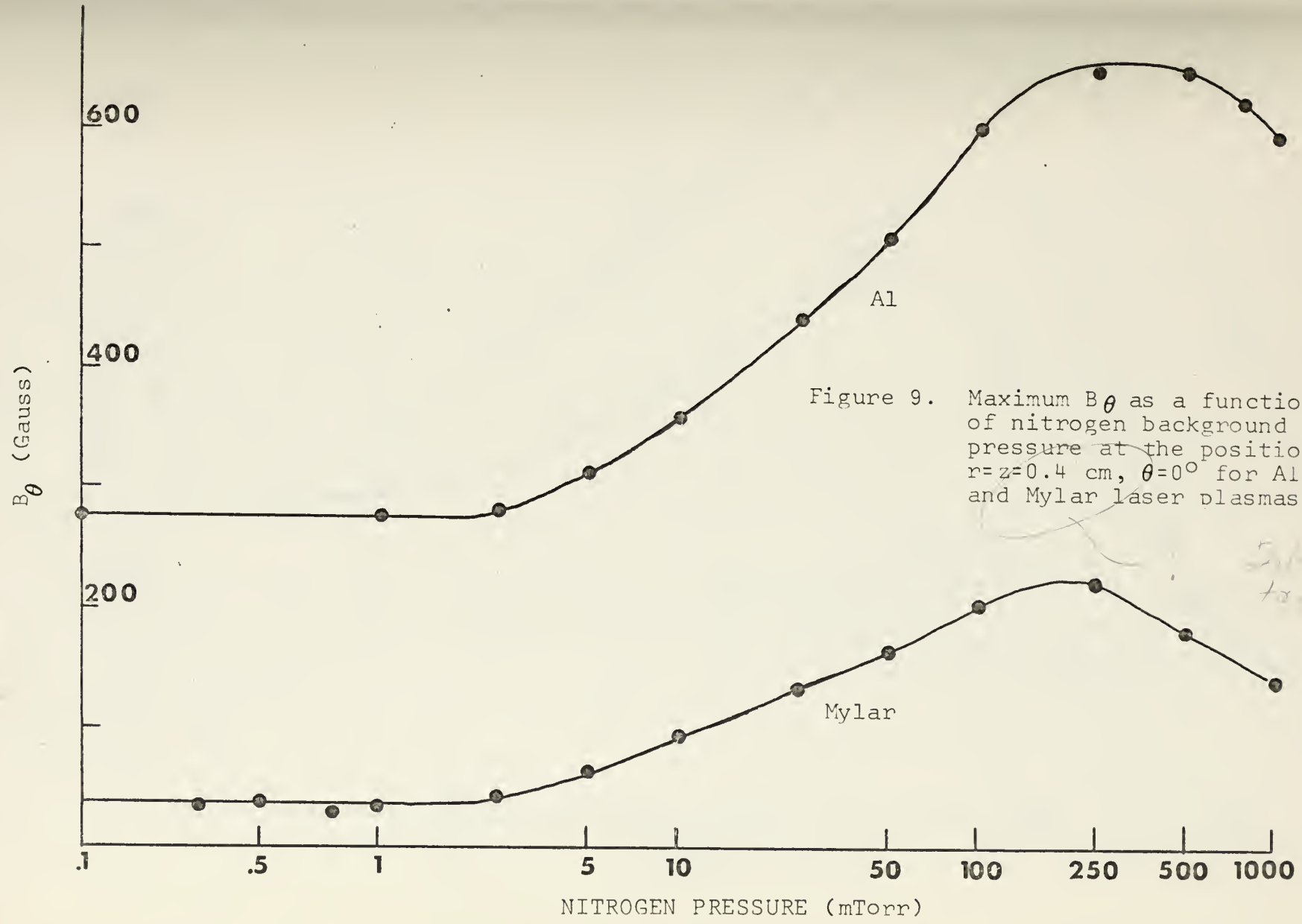

Figure 9. Maximum B_θ as a function of nitrogen background pressure at the position $r=z=0.4$ cm, $\theta=0^\circ$ for Al and Mylar laser plasmas.

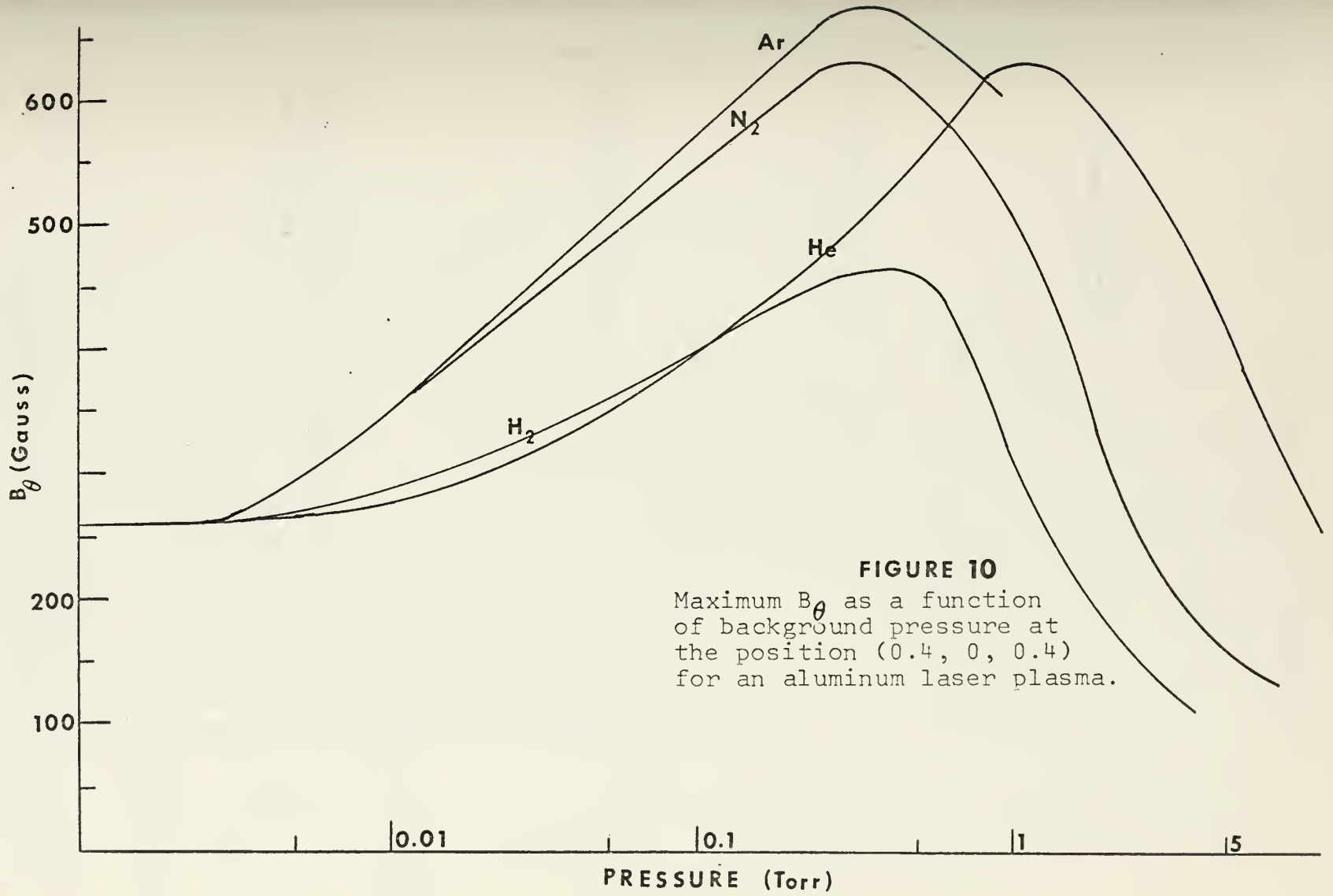

FIGURE 10

Maximum B_θ as a function of background pressure at the position (0.4, 0, 0.4) for an aluminum laser plasma.

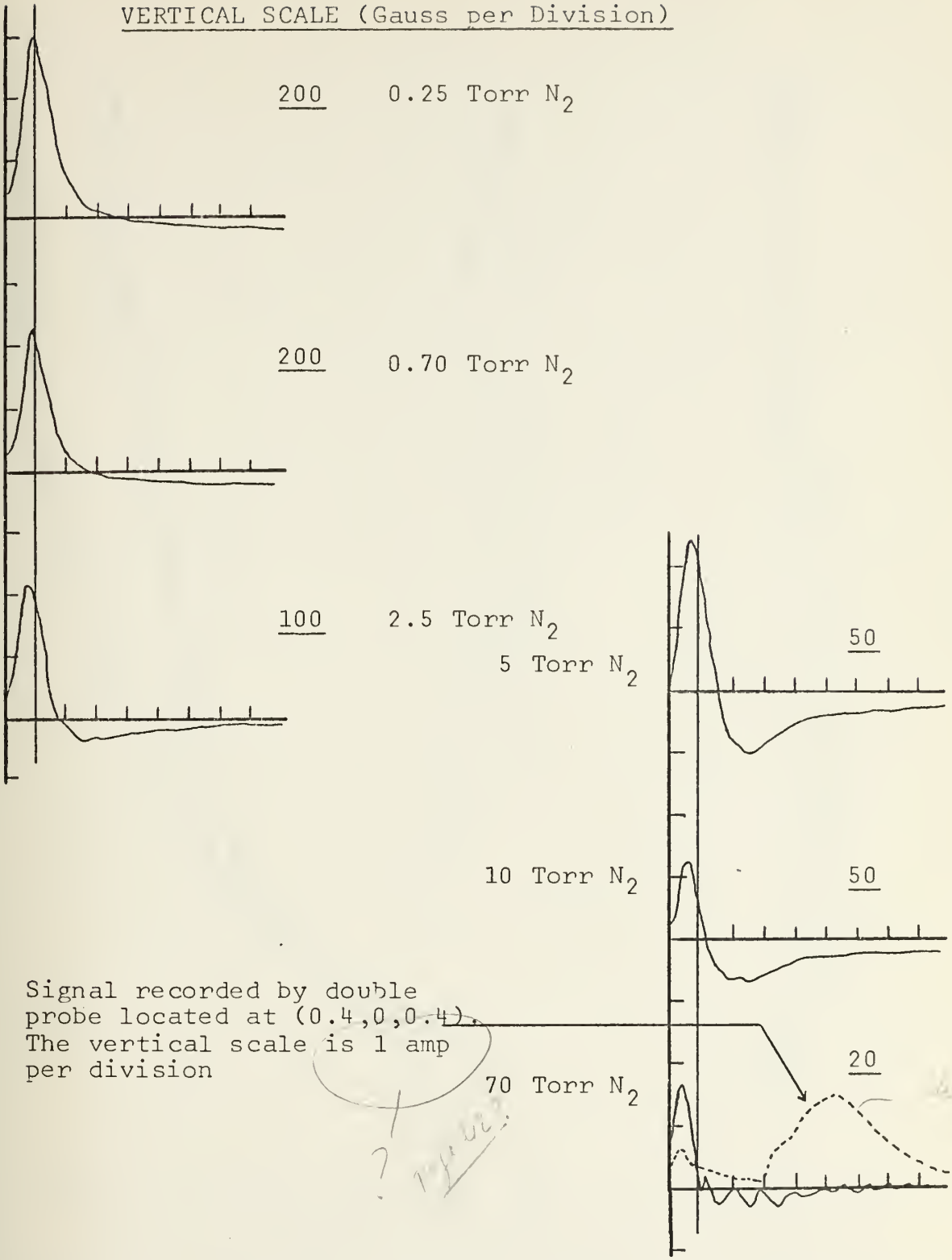

Figure 11. B_θ signal at the position r=z=0.4 cm, θ=0° as a function of nitrogen background pressure. The horizontal scale is 100 nsec per division.

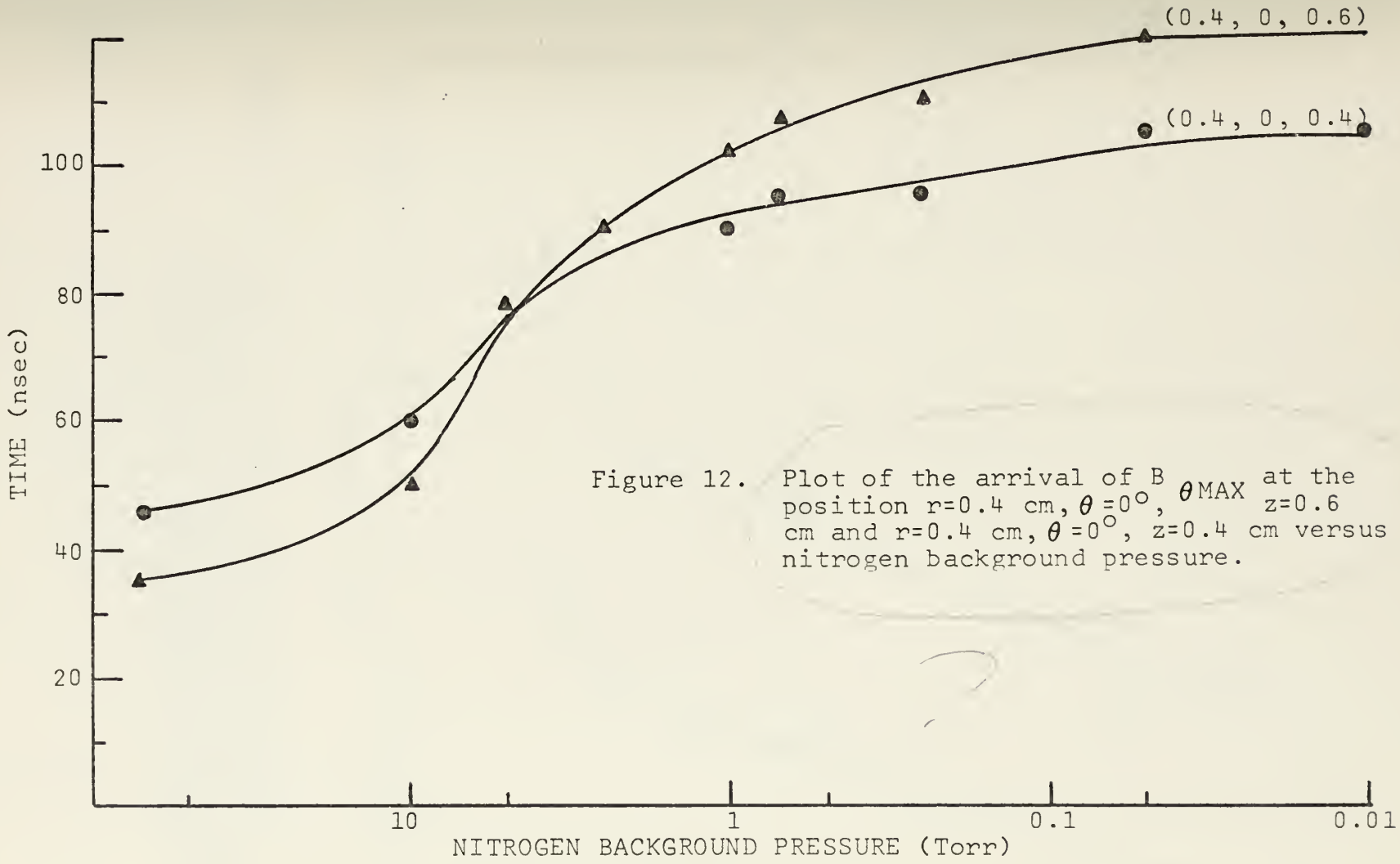

Figure 12. Plot of the arrival of $B_{\theta MAX}$ at the position r=0.4 cm, θ=0°, z=0.6 cm and r=0.4 cm, θ=0°, z=0.4 cm versus nitrogen background pressure.

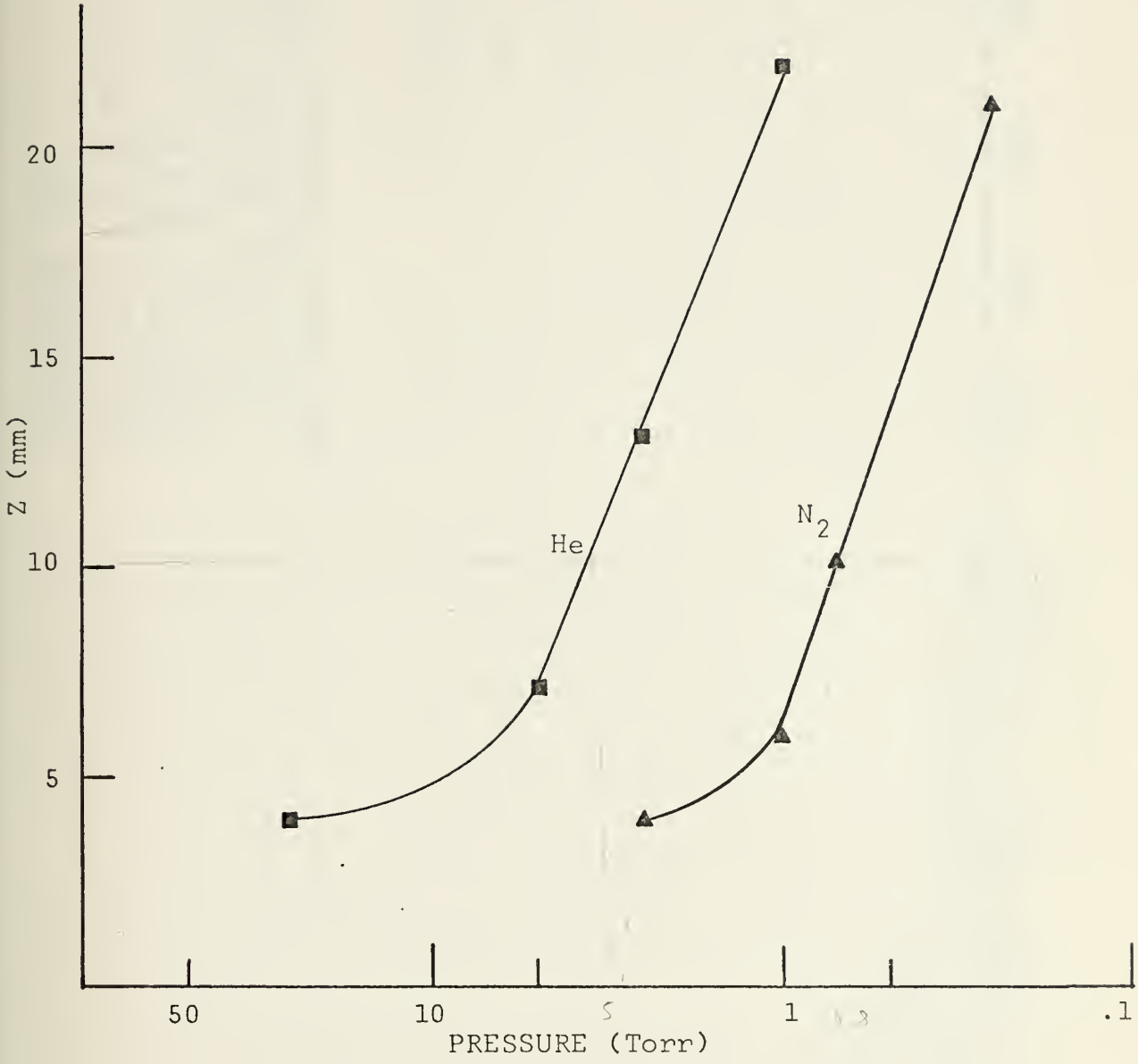

Figure 13. Onset of "strong" field reversal as a function of background pressure along the line r=0.4 cm, $\theta = 0^{\circ}$ for He and N_2. The vertical scale represents the z coordinate of the magnetic probe position in mm.

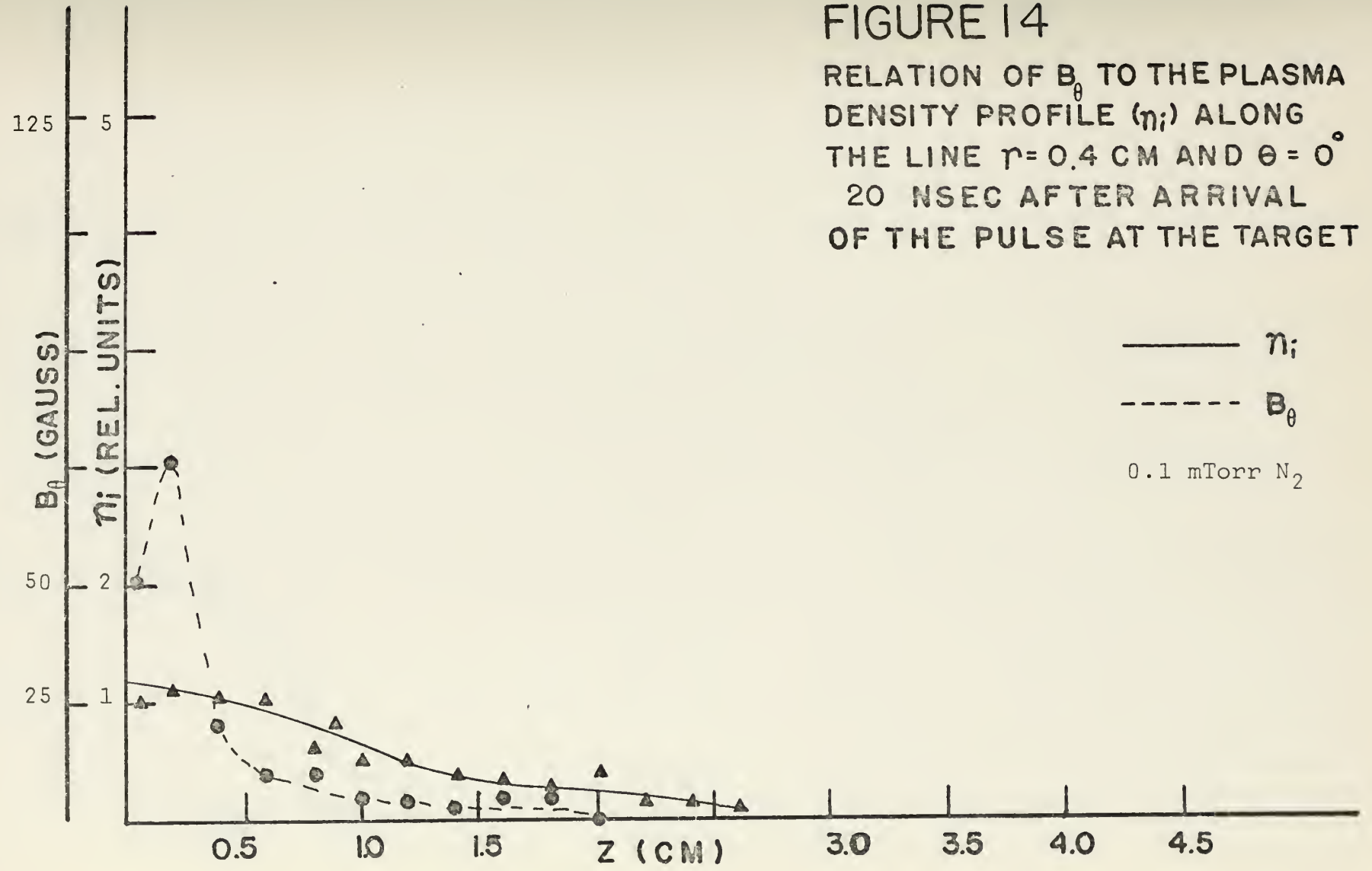

FIGURE 14

RELATION OF B_θ TO THE PLASMA DENSITY PROFILE (n_i) ALONG THE LINE $r = 0.4$ CM AND $\theta = 0^\circ$ 20 NSEC AFTER ARRIVAL OF THE PULSE AT THE TARGET

——— n_i

------ B_θ

0.1 mTorr N_2

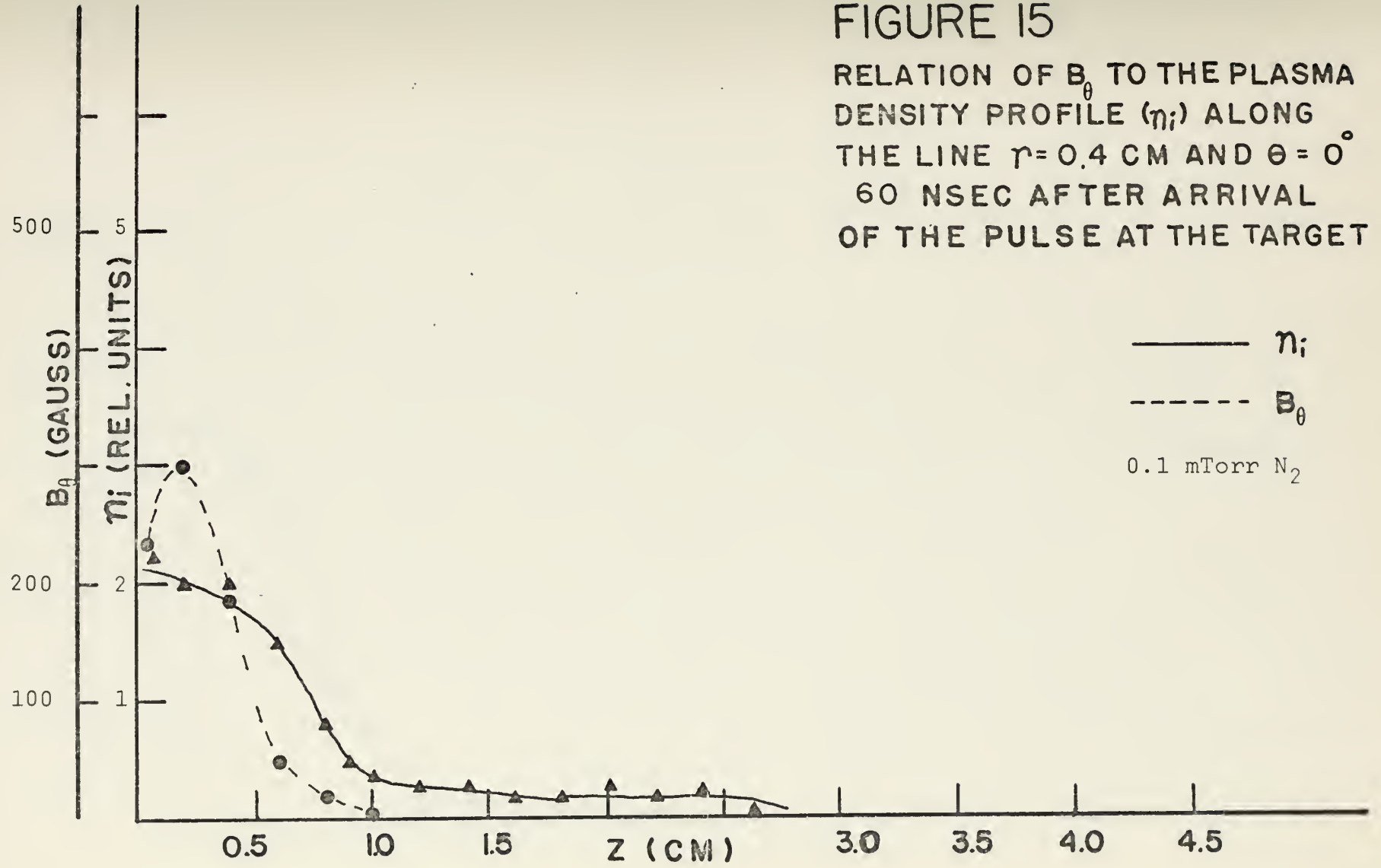

FIGURE 15

RELATION OF B_θ TO THE PLASMA DENSITY PROFILE (n_i) ALONG THE LINE $r = 0.4$ CM AND $\theta = 0^\circ$ 60 NSEC AFTER ARRIVAL OF THE PULSE AT THE TARGET

FIGURE 16

RELATION OF B_θ TO THE PLASMA DENSITY PROFILE (n_i) ALONG THE LINE $r = 0.4$ CM AND $\theta = 0^\circ$ 100 NSEC AFTER ARRIVAL OF THE PULSE AT THE TARGET

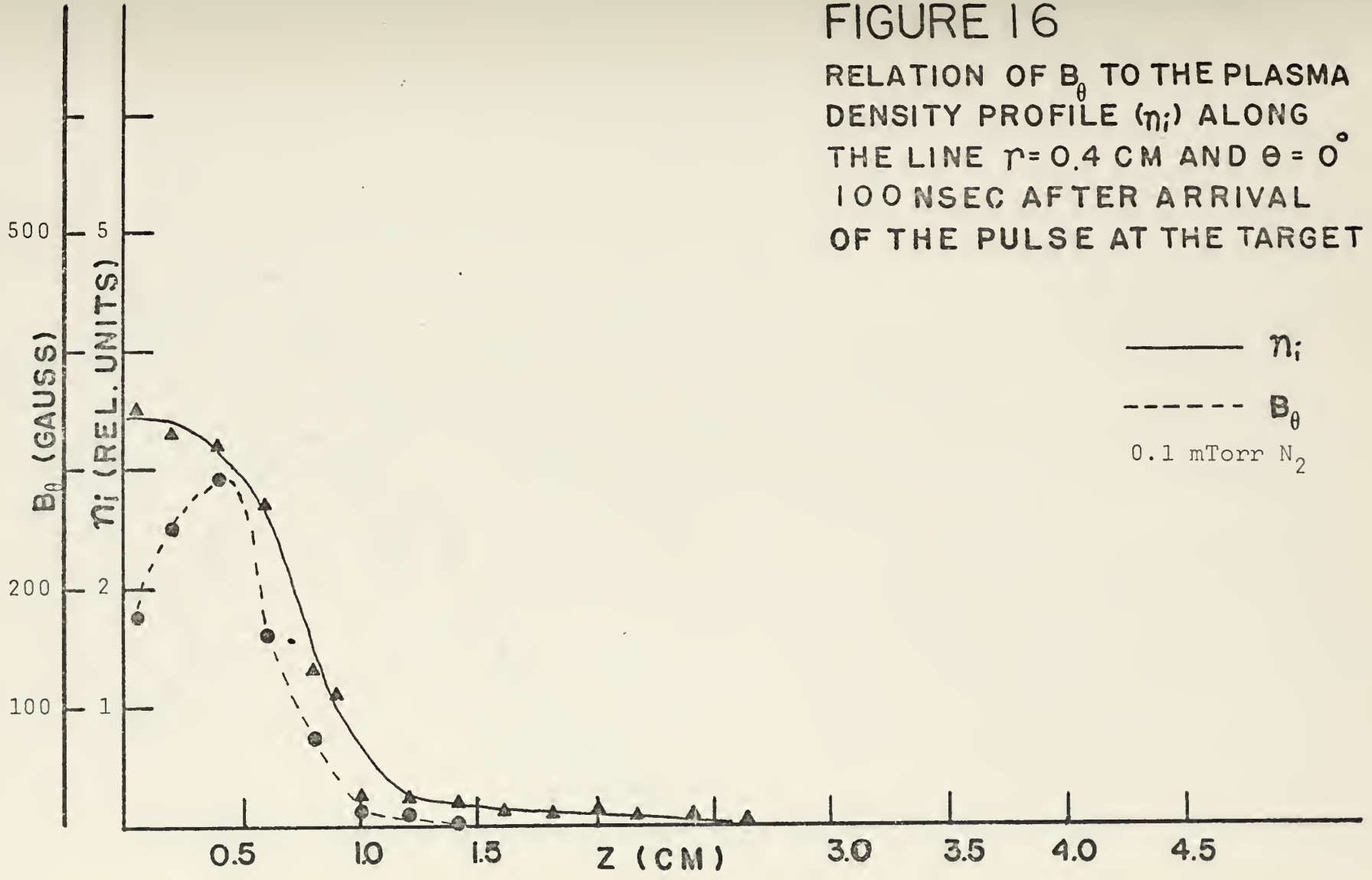

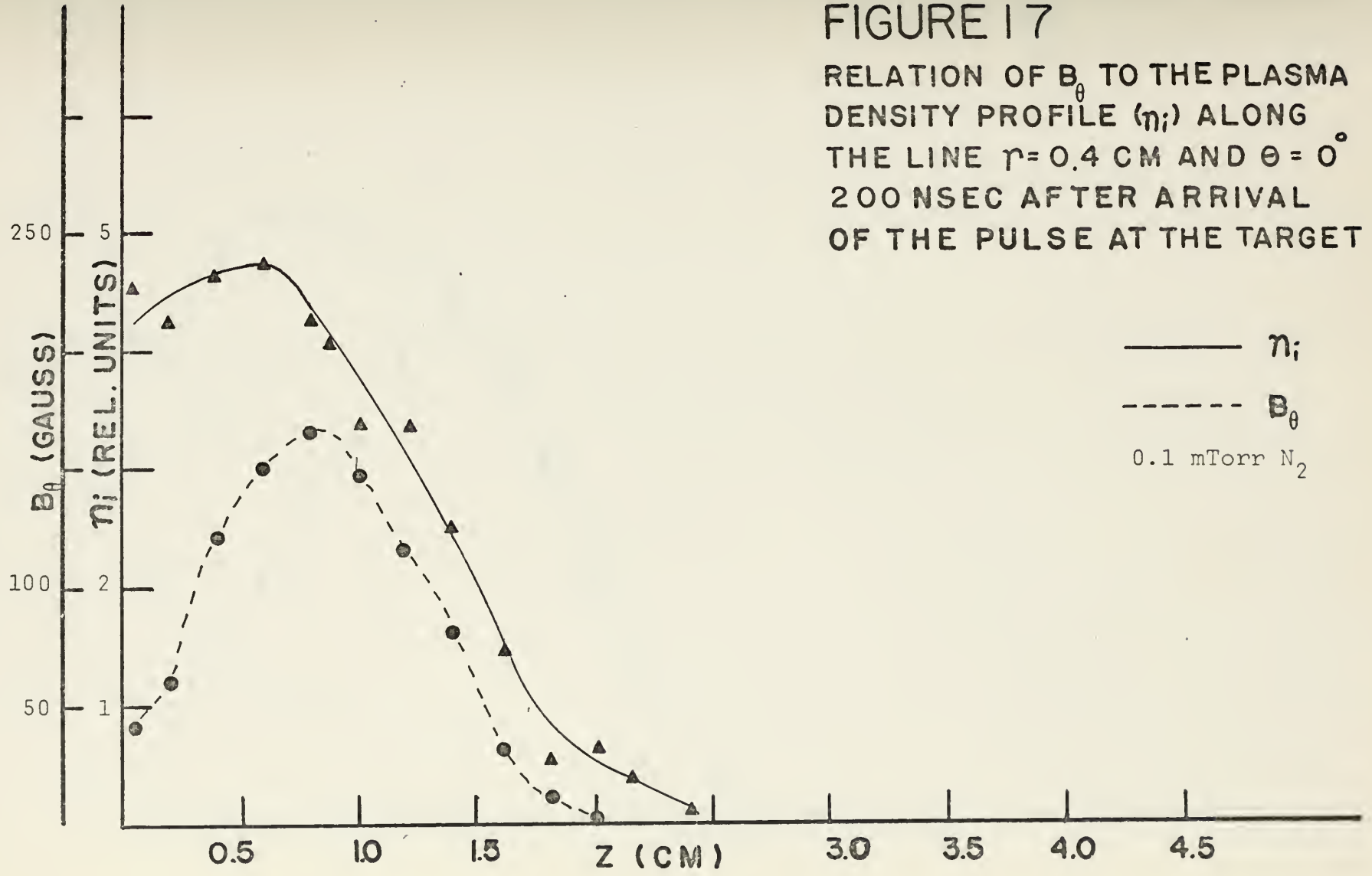

FIGURE 17

RELATION OF B_θ TO THE PLASMA DENSITY PROFILE (n_i) ALONG THE LINE $r = 0.4$ CM AND $\theta = 0^\circ$ 200 NSEC AFTER ARRIVAL OF THE PULSE AT THE TARGET

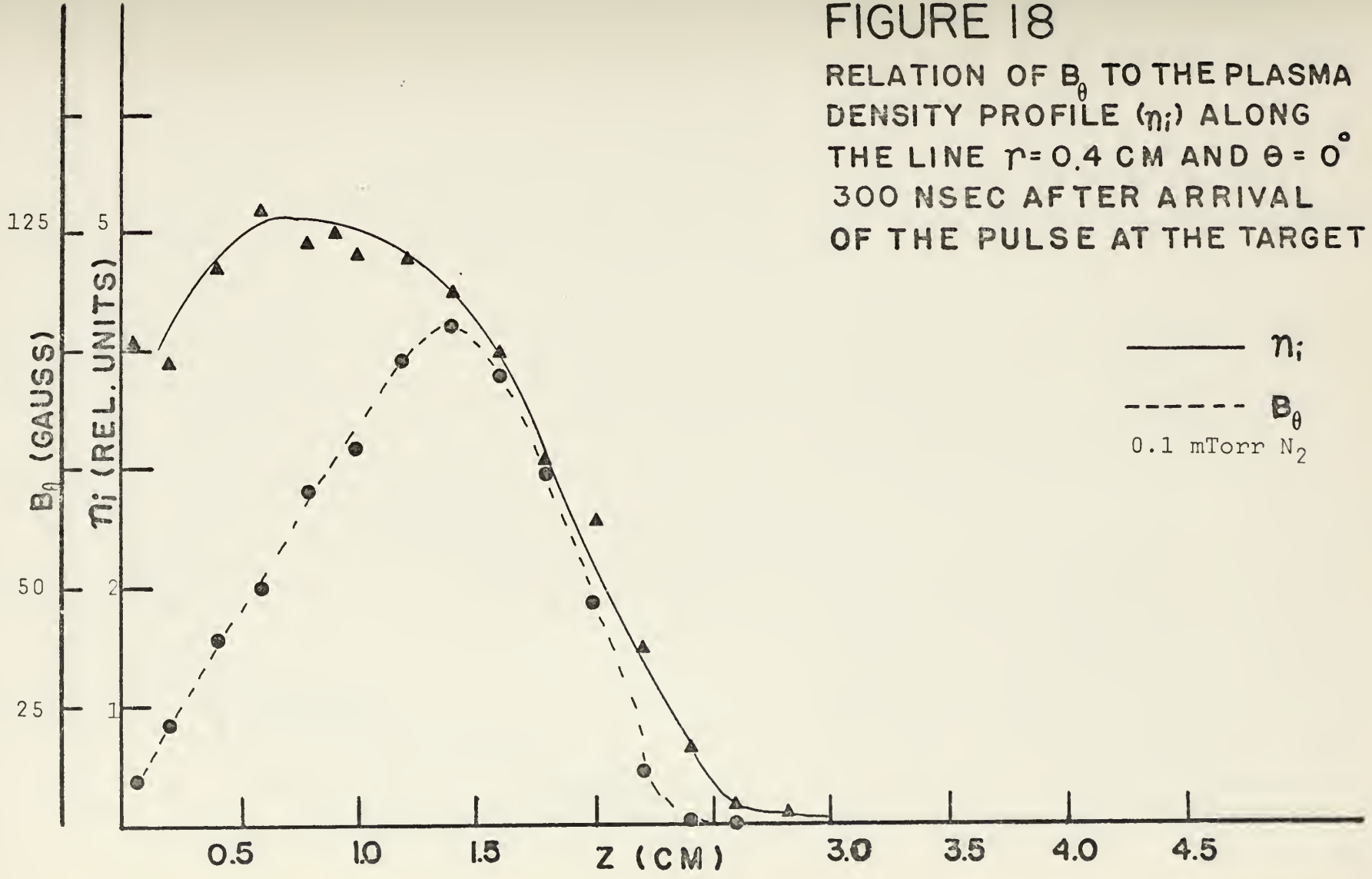

FIGURE 18

RELATION OF B_θ TO THE PLASMA DENSITY PROFILE (n_i) ALONG THE LINE $r = 0.4$ CM AND $\theta = 0^\circ$ 300 NSEC AFTER ARRIVAL OF THE PULSE AT THE TARGET

FIGURE 19

RELATION OF B_θ TO THE PLASMA DENSITY PROFILE (η_i) ALONG THE LINE $r = 0.4$ CM AND $\theta = 0^\circ$ 20 NSEC AFTER ARRIVAL OF THE PULSE AT THE TARGET

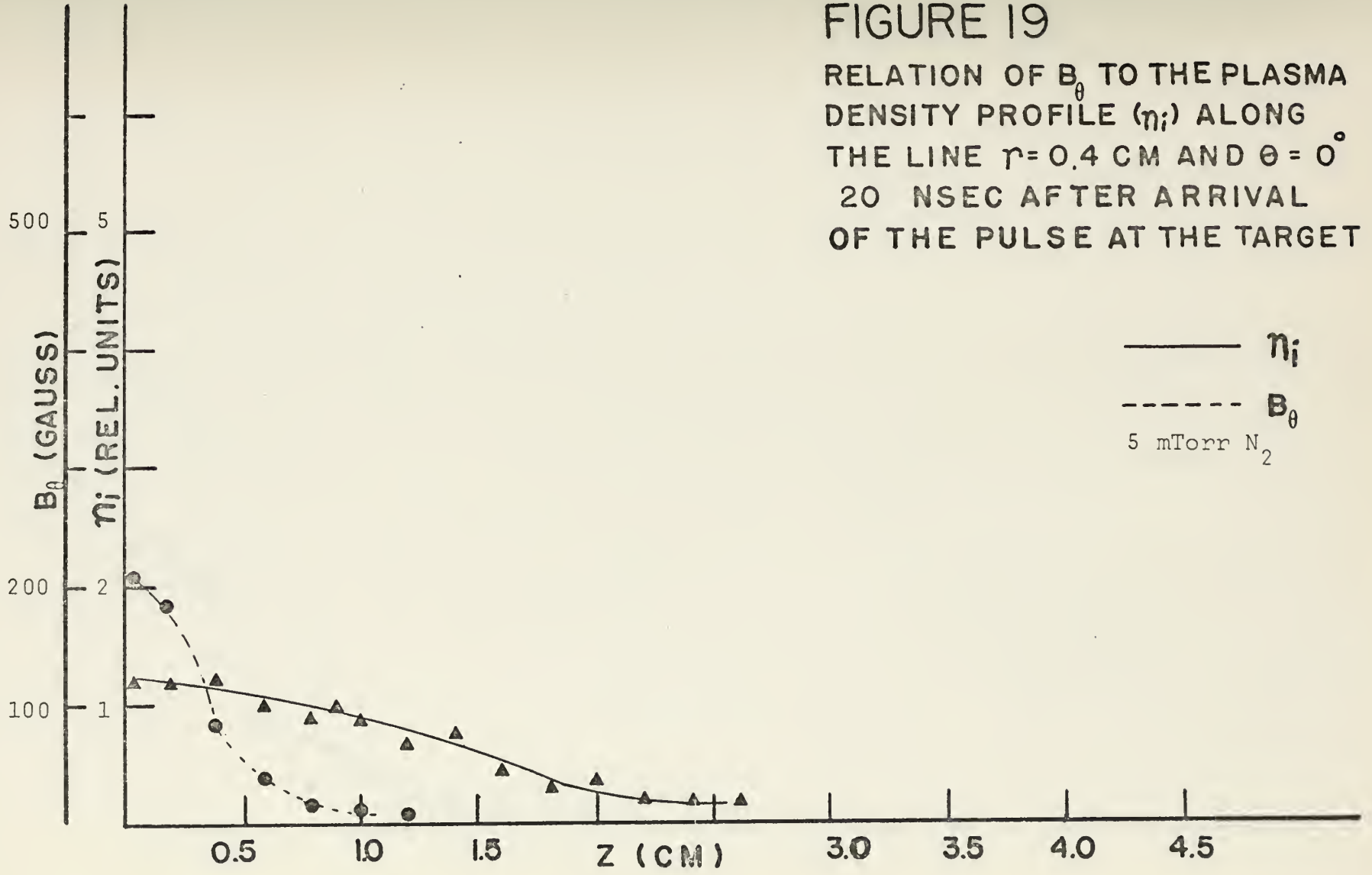

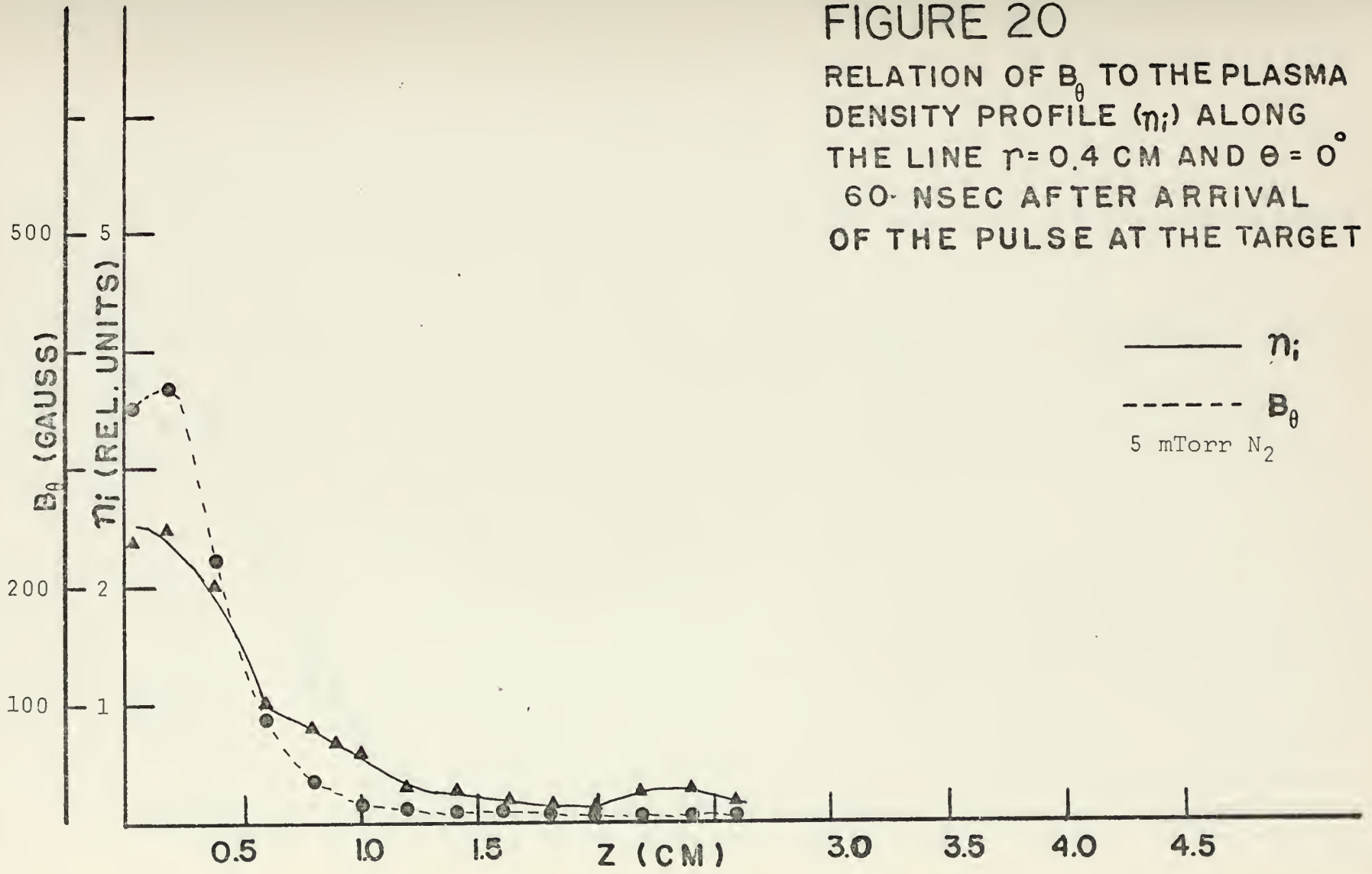

FIGURE 20

RELATION OF B_θ TO THE PLASMA DENSITY PROFILE (n_i) ALONG THE LINE $r = 0.4$ CM AND $\theta = 0^\circ$ 60 NSEC AFTER ARRIVAL OF THE PULSE AT THE TARGET

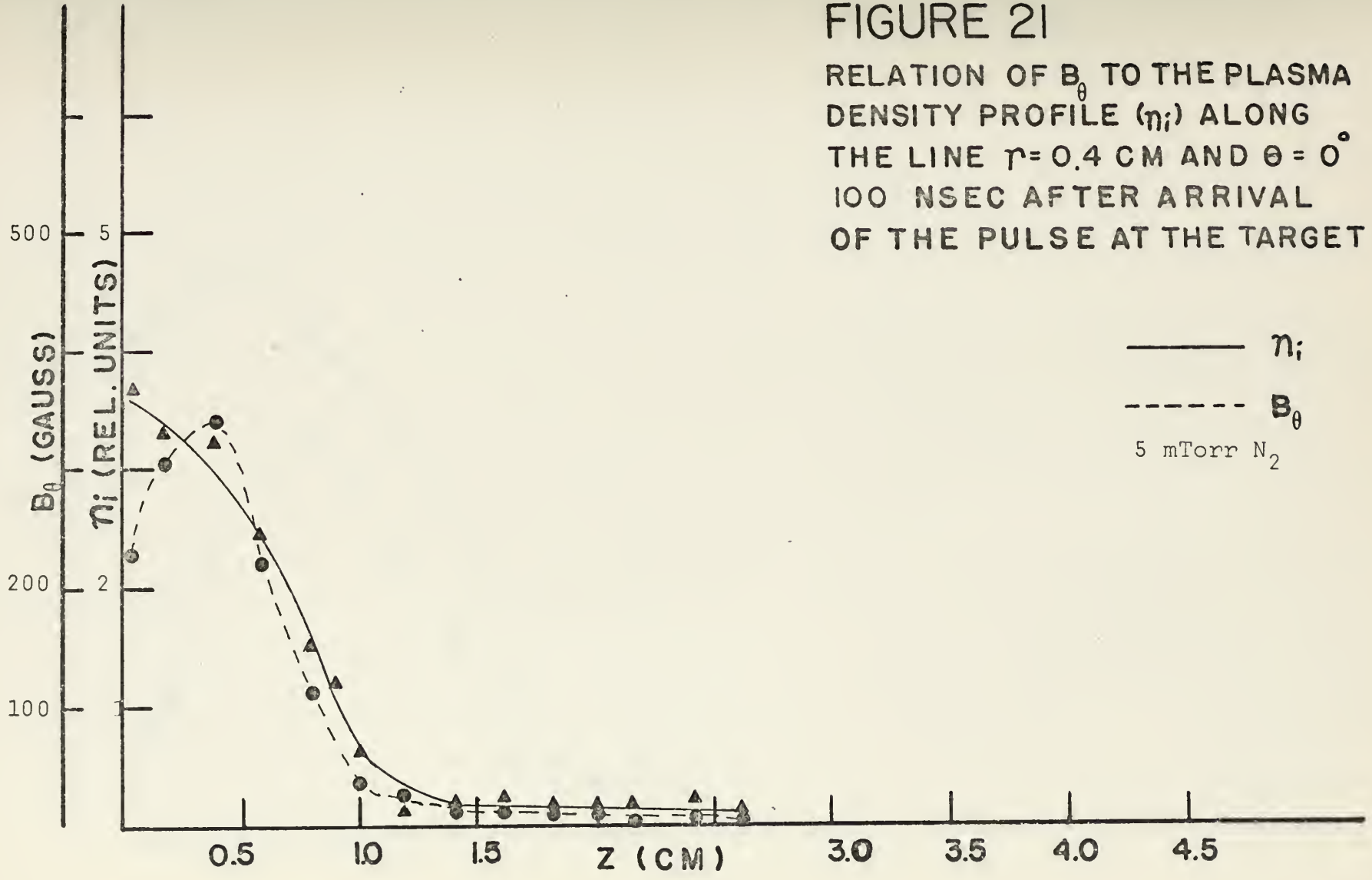

FIGURE 21

RELATION OF B_θ TO THE PLASMA DENSITY PROFILE (n_i) ALONG THE LINE $r = 0.4$ CM AND $\theta = 0^\circ$ 100 NSEC AFTER ARRIVAL OF THE PULSE AT THE TARGET

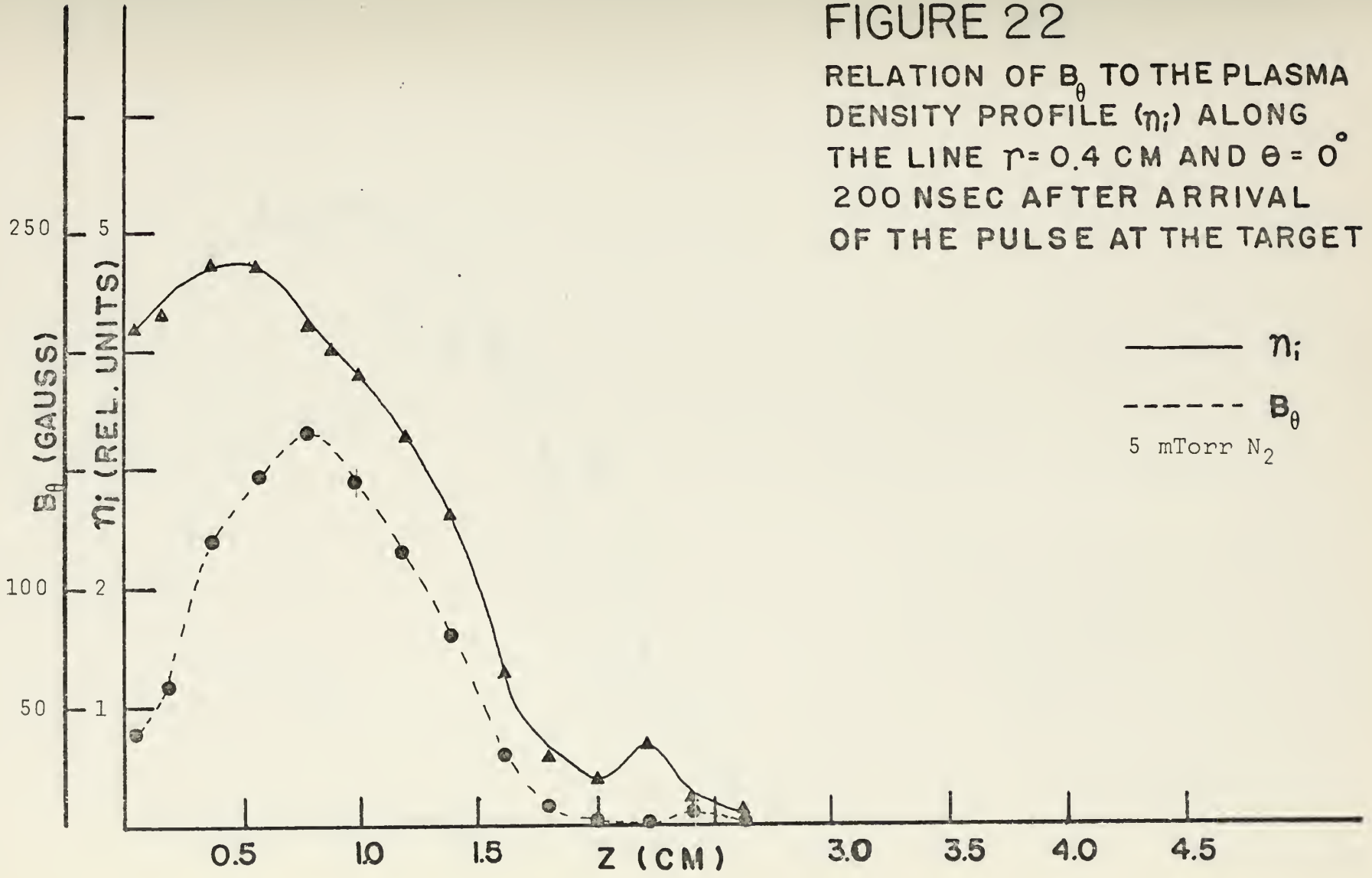

FIGURE 22

RELATION OF B_θ TO THE PLASMA DENSITY PROFILE (n_i) ALONG THE LINE $r = 0.4$ CM AND $\theta = 0^\circ$ 200 NSEC AFTER ARRIVAL OF THE PULSE AT THE TARGET

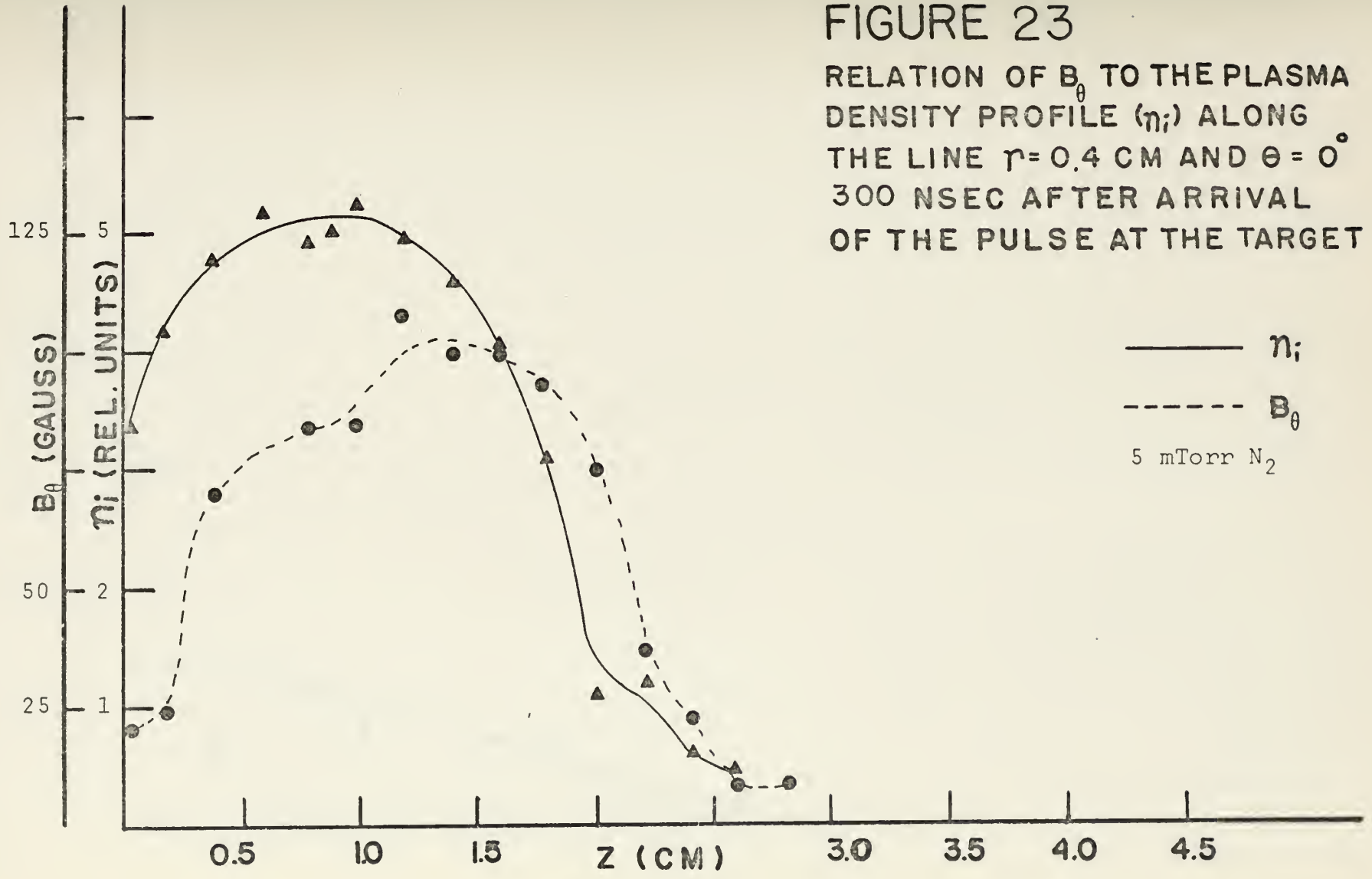

FIGURE 23

RELATION OF B_θ TO THE PLASMA DENSITY PROFILE (n_i) ALONG THE LINE $r = 0.4$ CM AND $\theta = 0°$ 300 NSEC AFTER ARRIVAL OF THE PULSE AT THE TARGET

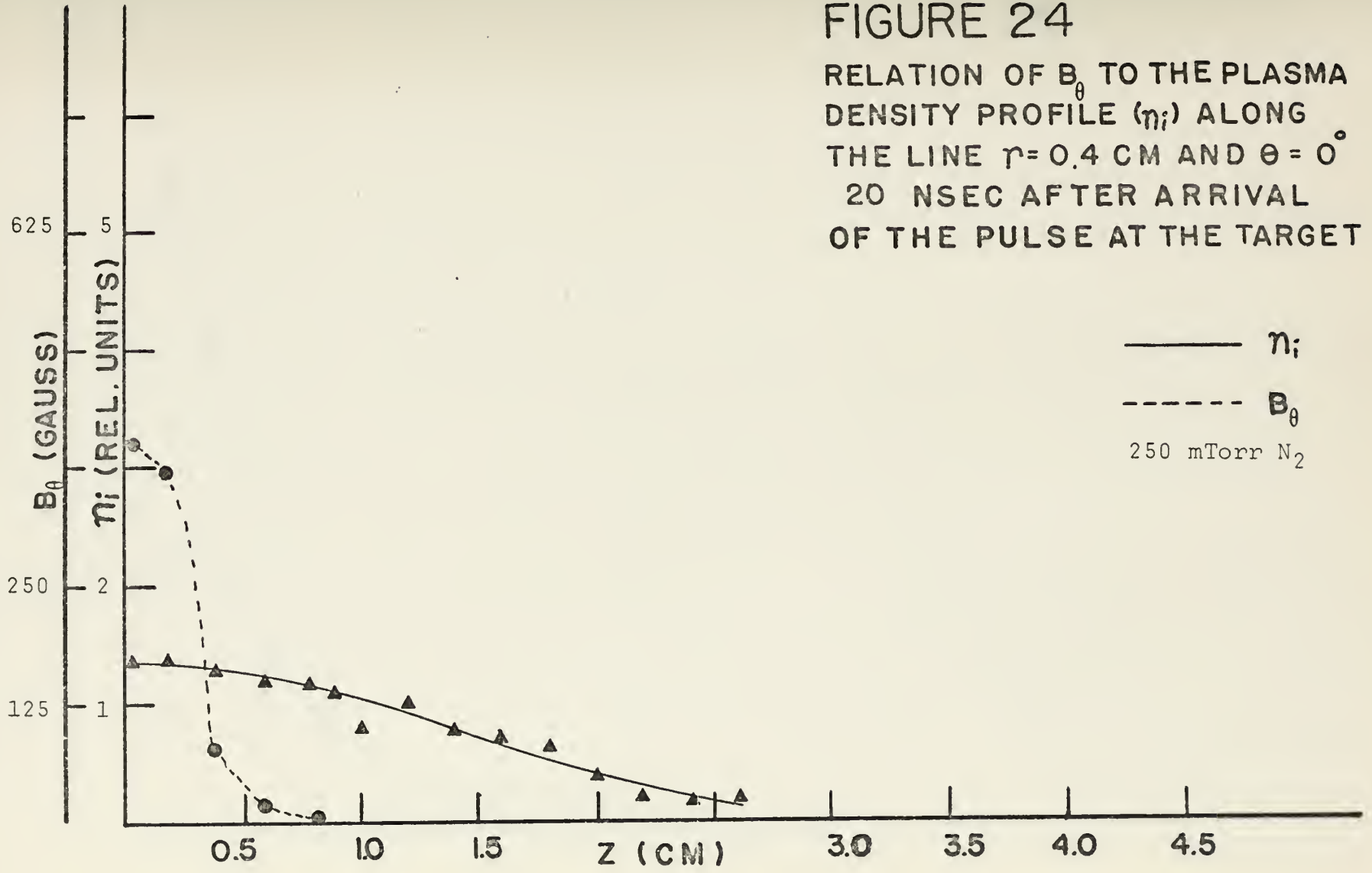

FIGURE 24

RELATION OF B_θ TO THE PLASMA DENSITY PROFILE (n_i) ALONG THE LINE $r = 0.4$ CM AND $\theta = 0^\circ$ 20 NSEC AFTER ARRIVAL OF THE PULSE AT THE TARGET

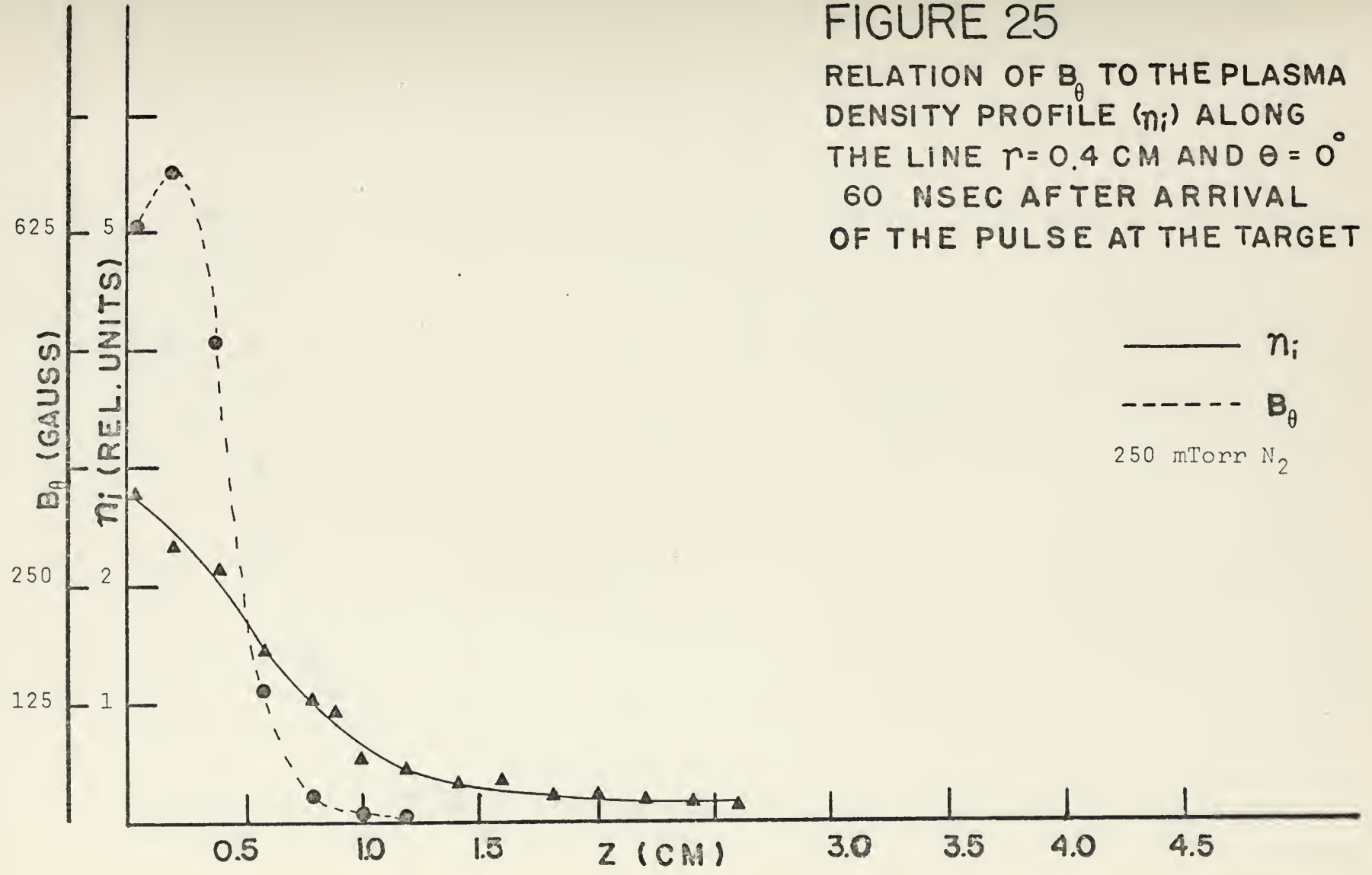

FIGURE 25

RELATION OF B_θ TO THE PLASMA DENSITY PROFILE (n_i) ALONG THE LINE $r = 0.4$ CM AND $\theta = 0^\circ$ 60 NSEC AFTER ARRIVAL OF THE PULSE AT THE TARGET

FIGURE 26

RELATION OF B_θ TO THE PLASMA DENSITY PROFILE (n_i) ALONG THE LINE $r = 0.4$ CM AND $\theta = 0^\circ$ 100 NSEC AFTER ARRIVAL OF THE PULSE AT THE TARGET

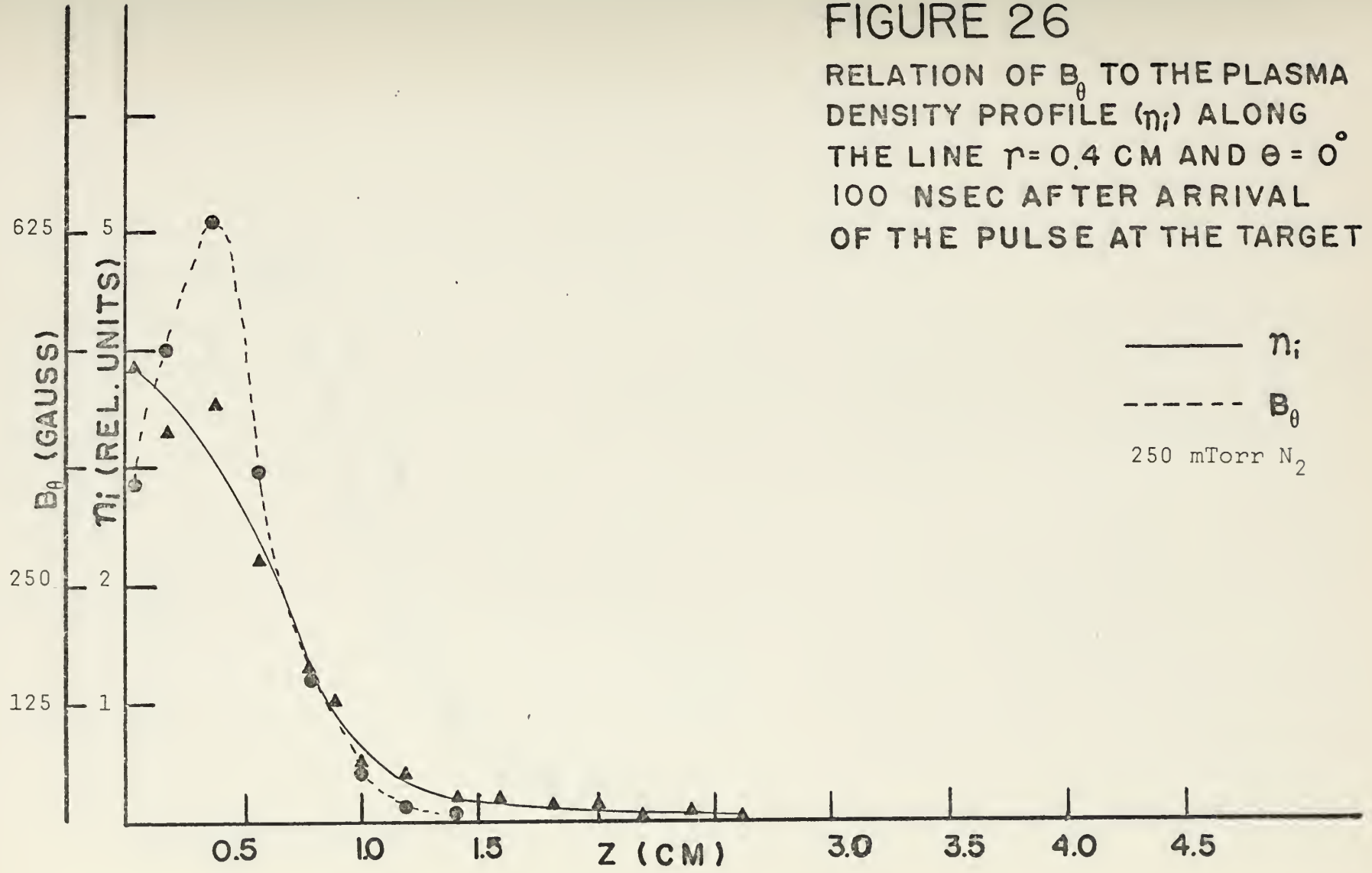

FIGURE 27

RELATION OF B_θ TO THE PLASMA DENSITY PROFILE (n_i) ALONG THE LINE $r = 0.4$ CM AND $\theta = 0^\circ$ 200 NSEC AFTER ARRIVAL OF THE PULSE AT THE TARGET

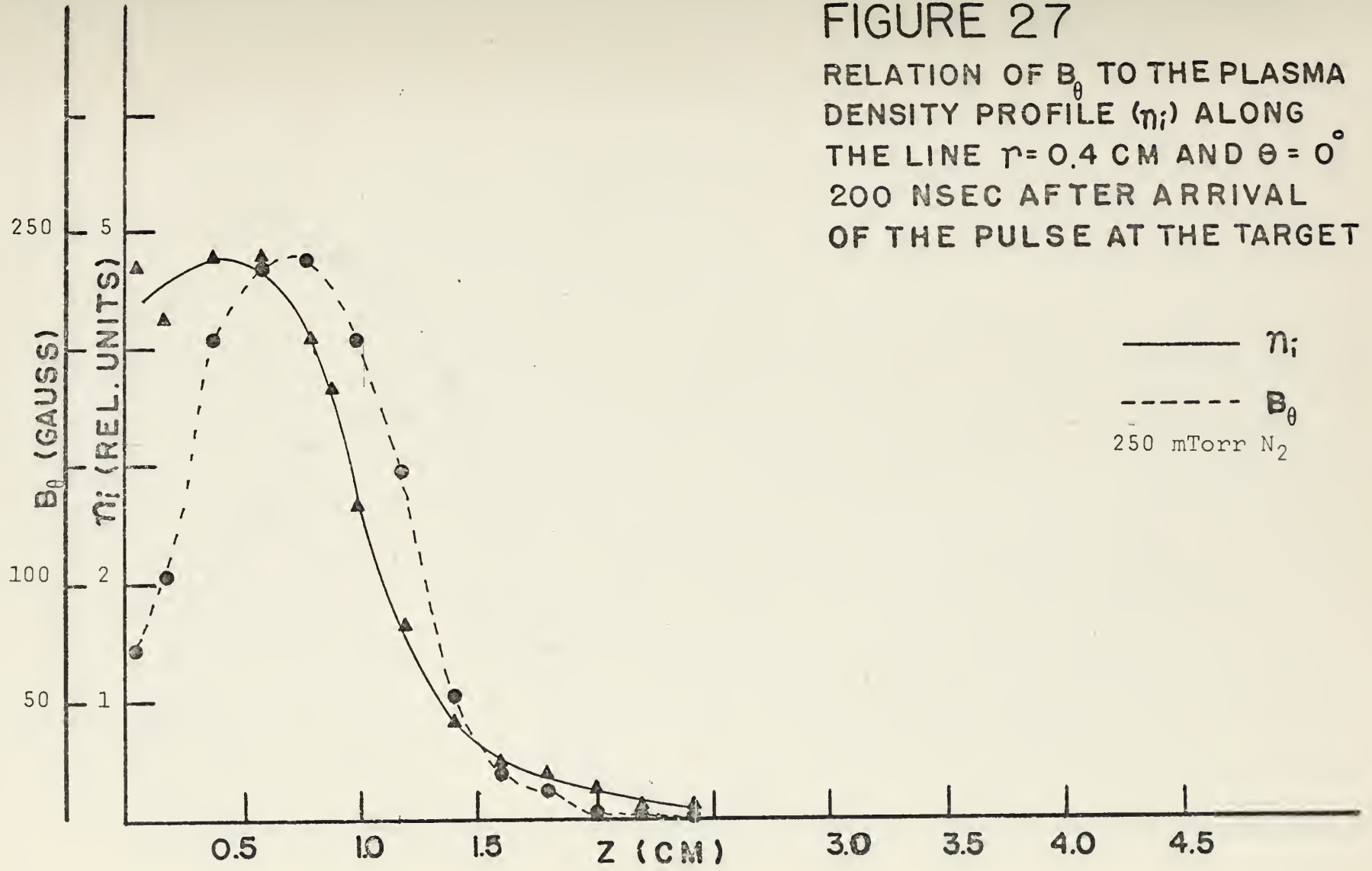

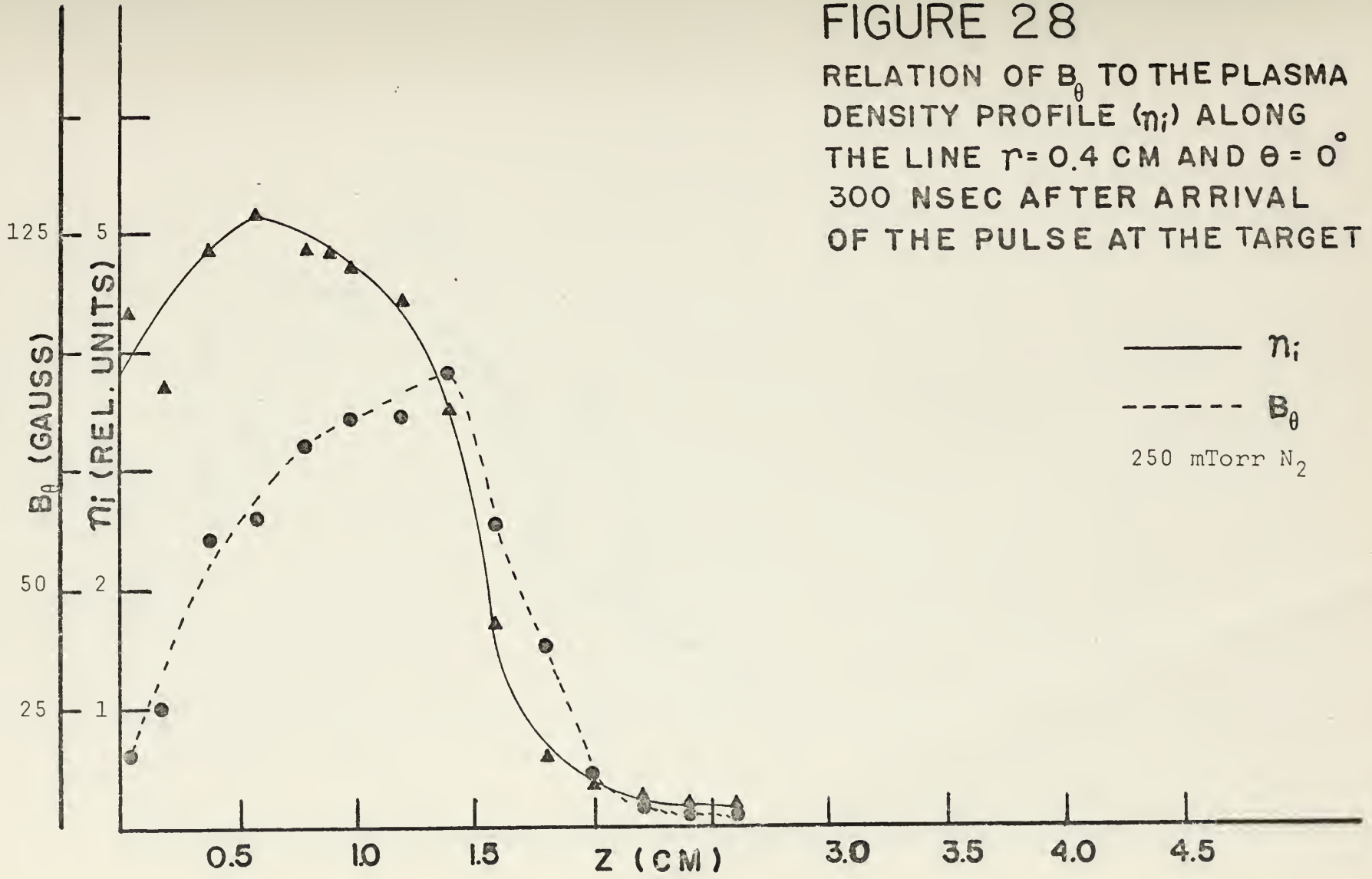

FIGURE 28

RELATION OF B_θ TO THE PLASMA DENSITY PROFILE (n_i) ALONG THE LINE r= 0.4 CM AND θ = 0° 300 NSEC AFTER ARRIVAL OF THE PULSE AT THE TARGET

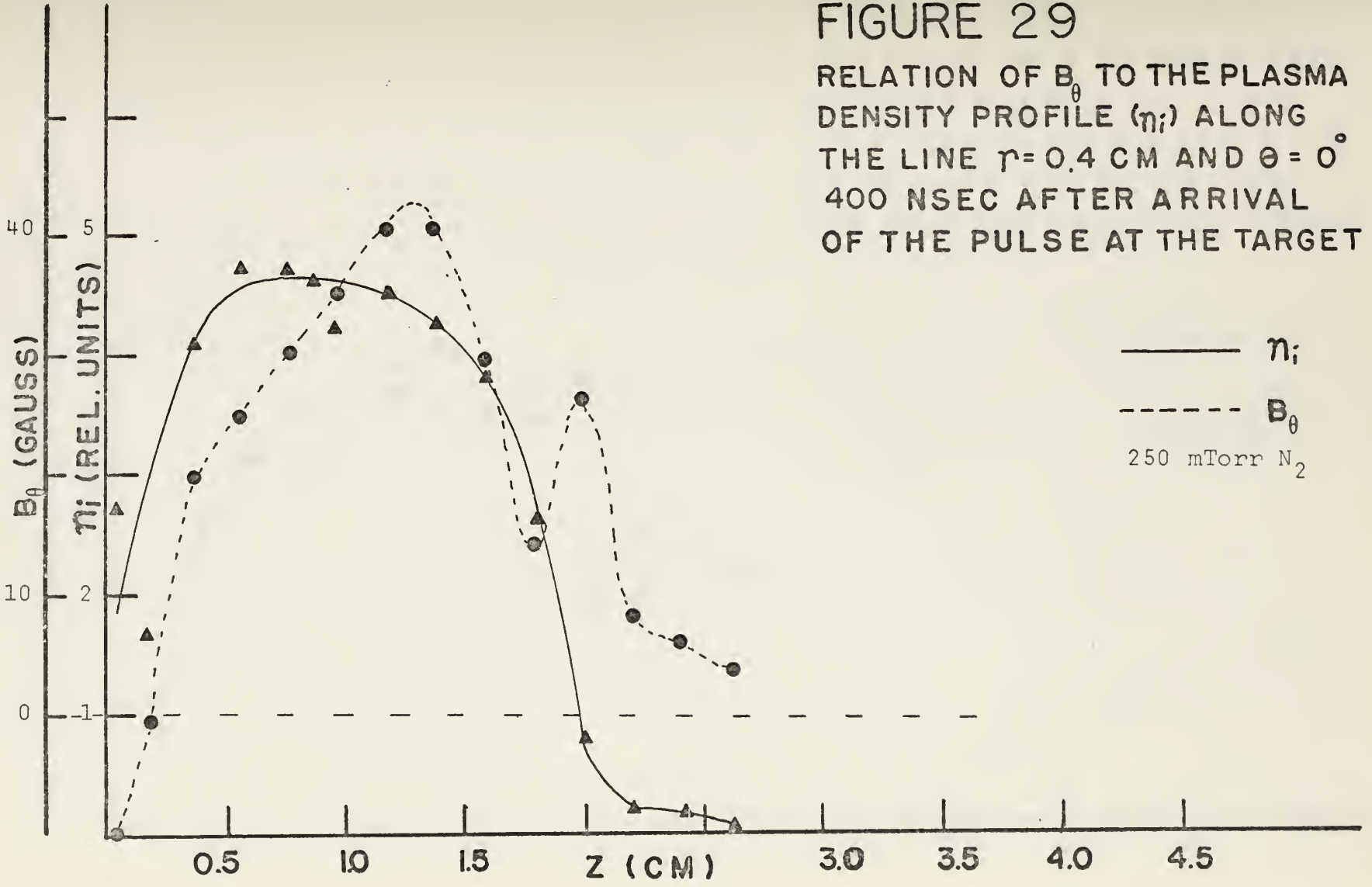

FIGURE 29

RELATION OF B_θ TO THE PLASMA DENSITY PROFILE (n_i) ALONG THE LINE $r = 0.4$ CM AND $\theta = 0^\circ$ 400 NSEC AFTER ARRIVAL OF THE PULSE AT THE TARGET

FIGURE 30

RELATION OF B_θ TO THE PLASMA DENSITY PROFILE (n_i) ALONG THE LINE $r = 0.4$ CM AND $\theta = 0^\circ$ 500 NSEC AFTER ARRIVAL OF THE PULSE AT THE TARGET

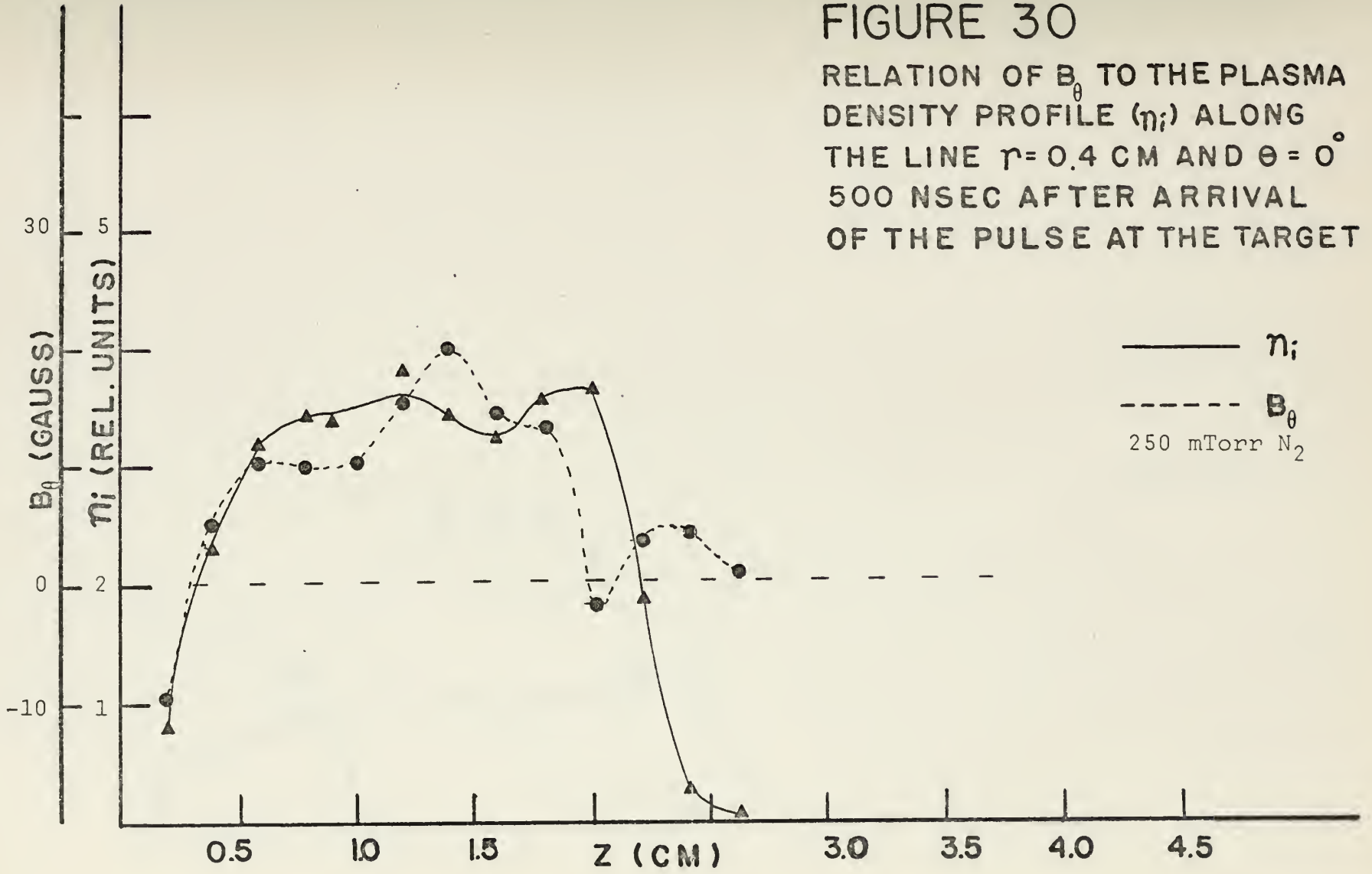

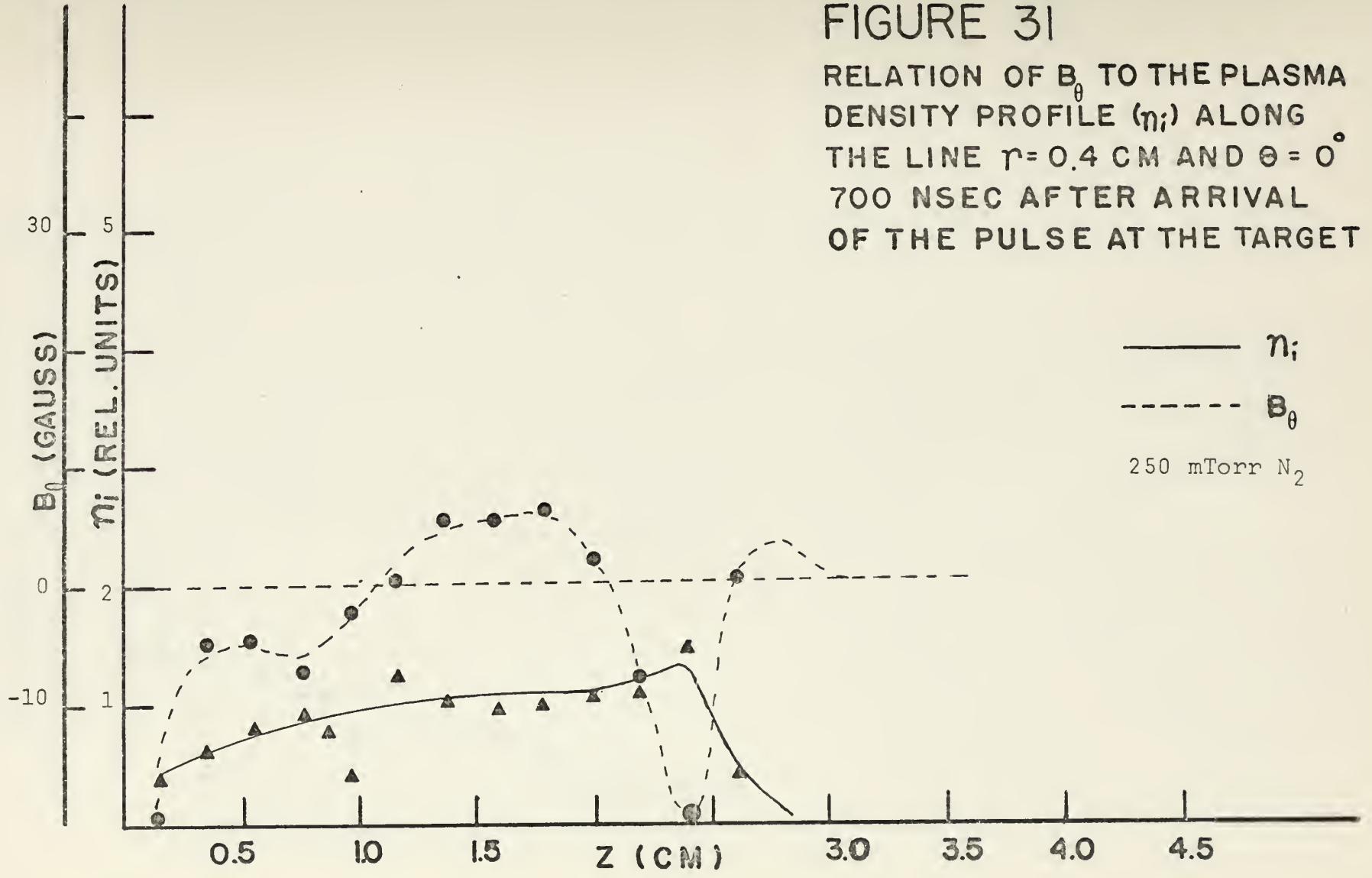

FIGURE 31

RELATION OF B_θ TO THE PLASMA DENSITY PROFILE (n_i) ALONG THE LINE $r = 0.4$ CM AND $\theta = 0^\circ$ 700 NSEC AFTER ARRIVAL OF THE PULSE AT THE TARGET

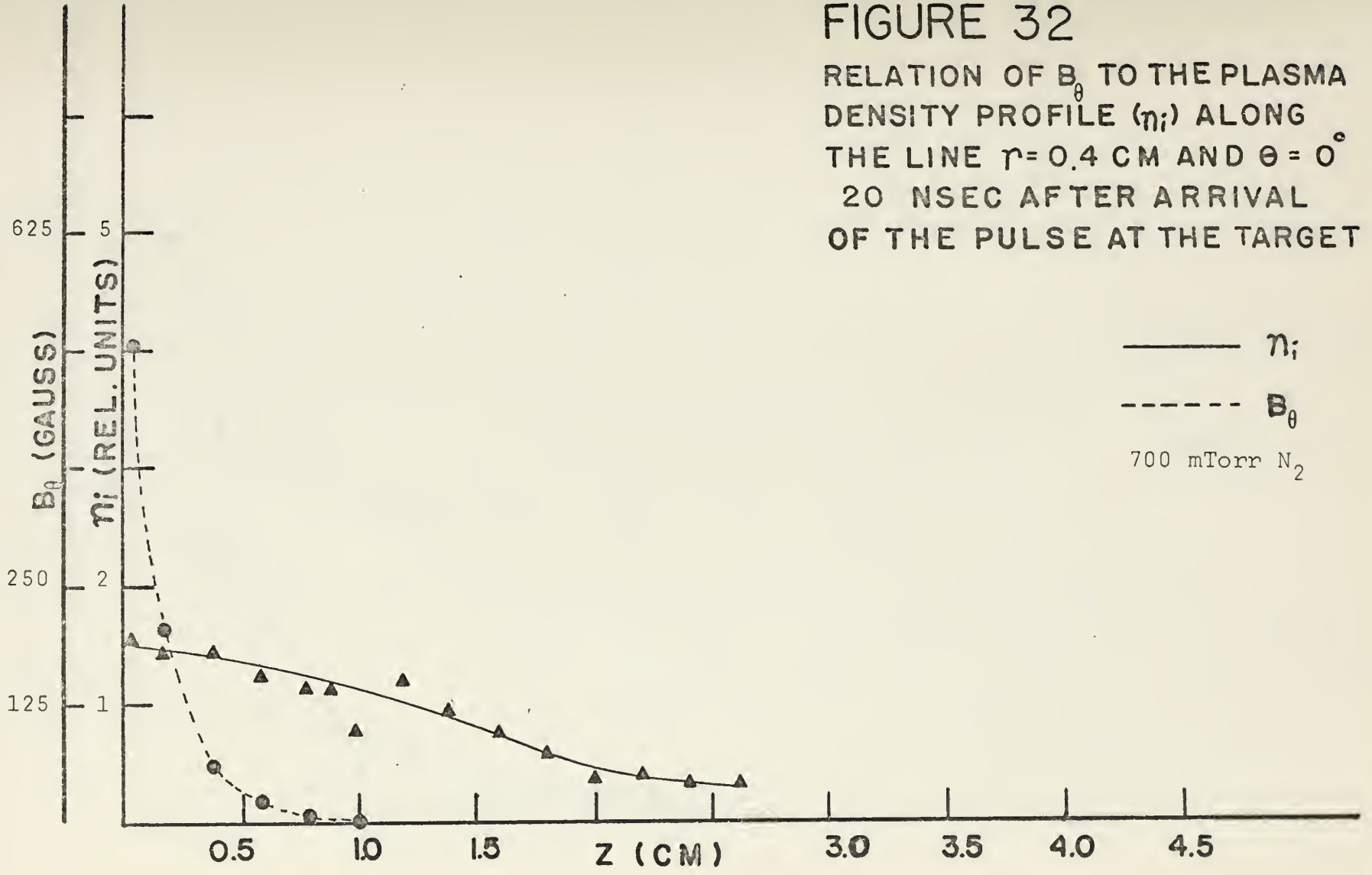

FIGURE 32

RELATION OF B_θ TO THE PLASMA DENSITY PROFILE (n_i) ALONG THE LINE $r = 0.4$ CM AND $\theta = 0^\circ$ 20 NSEC AFTER ARRIVAL OF THE PULSE AT THE TARGET

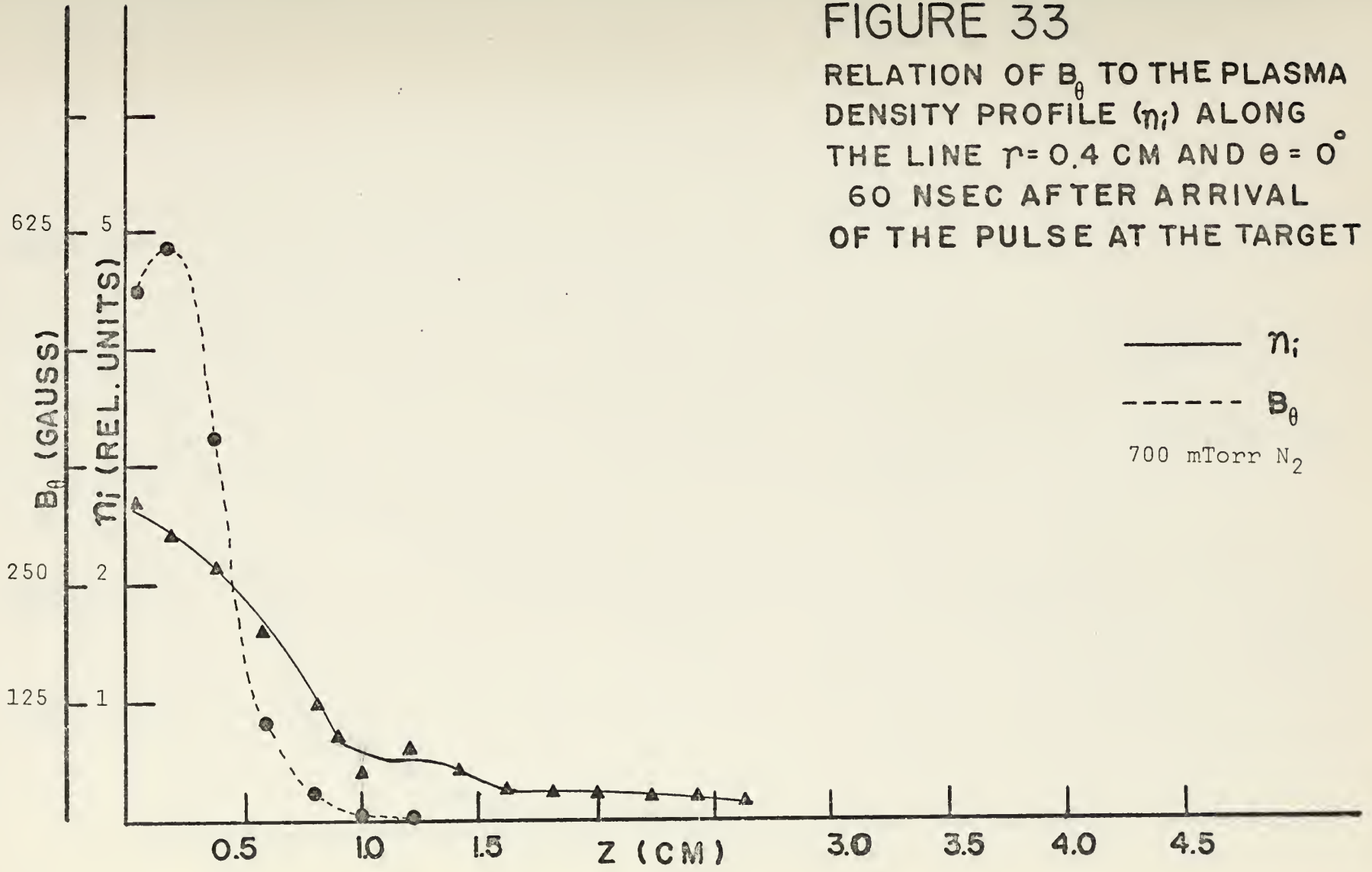

FIGURE 33

RELATION OF B_θ TO THE PLASMA DENSITY PROFILE (n_i) ALONG THE LINE $r = 0.4$ CM AND $\theta = 0^\circ$ 60 NSEC AFTER ARRIVAL OF THE PULSE AT THE TARGET

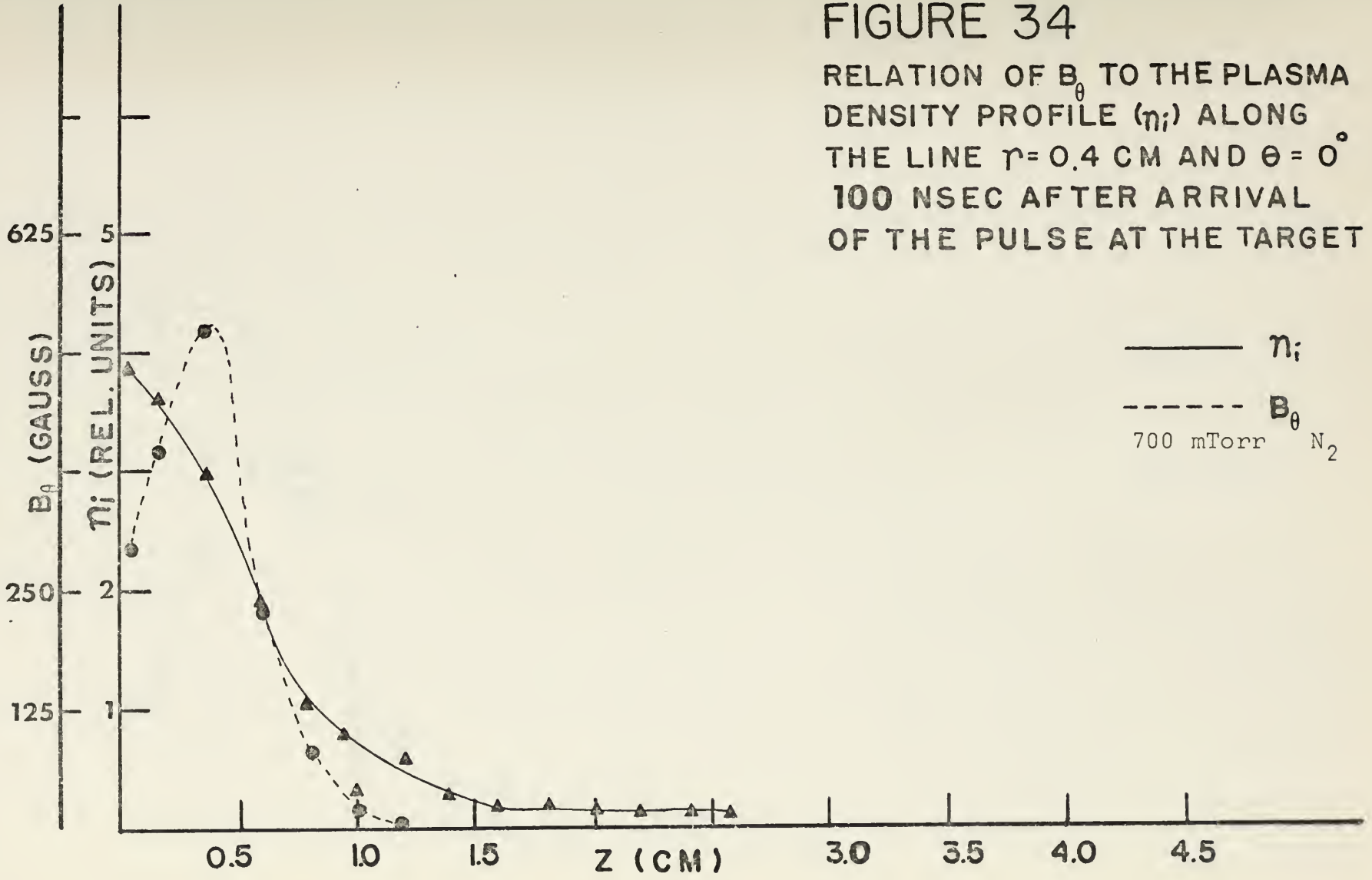

FIGURE 34

RELATION OF B_θ TO THE PLASMA DENSITY PROFILE (n_i) ALONG THE LINE $r = 0.4$ CM AND $\theta = 0^\circ$ 100 NSEC AFTER ARRIVAL OF THE PULSE AT THE TARGET

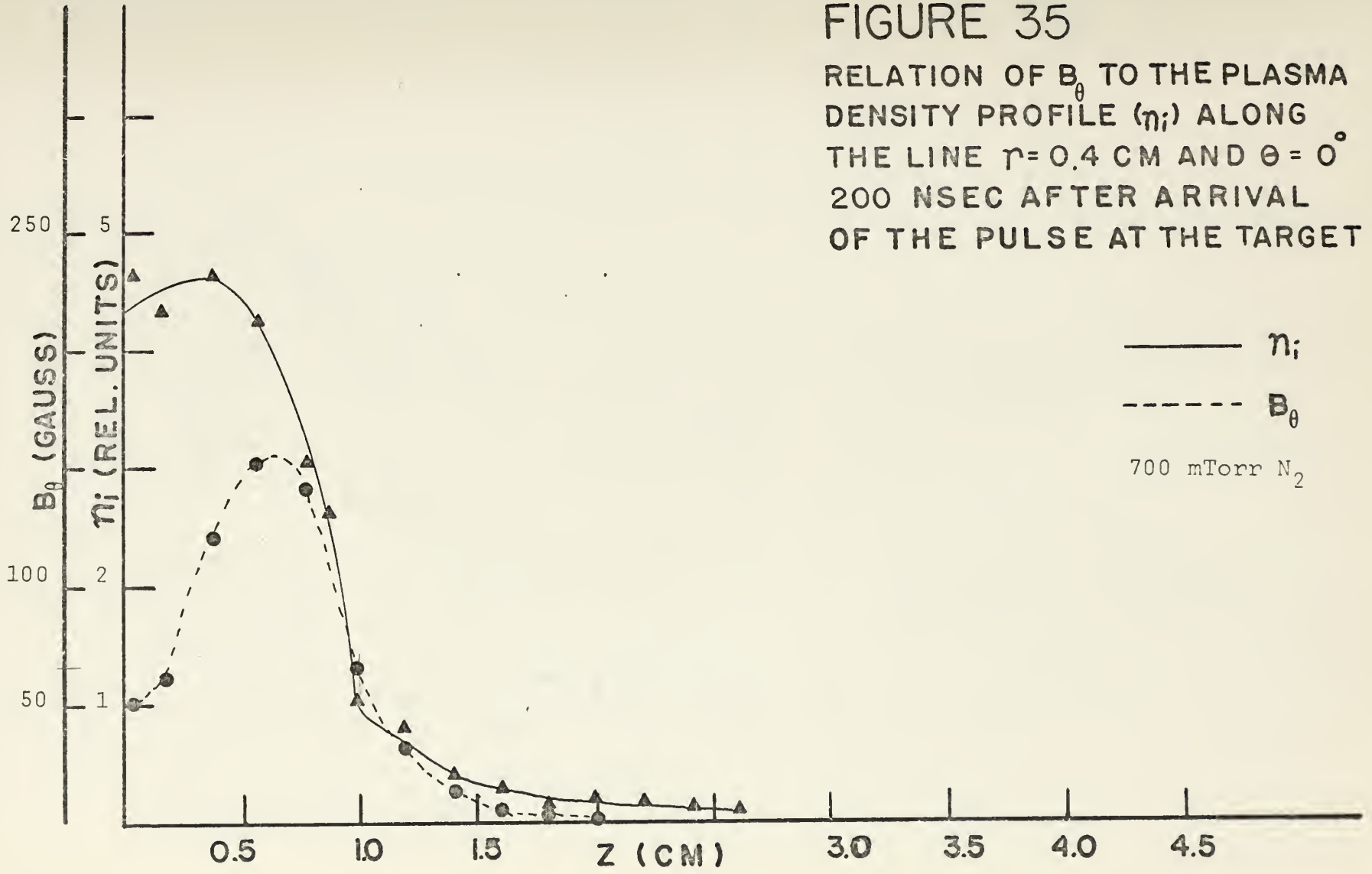

FIGURE 35

RELATION OF B_θ TO THE PLASMA DENSITY PROFILE (n_i) ALONG THE LINE $r = 0.4$ CM AND $\theta = 0^\circ$ 200 NSEC AFTER ARRIVAL OF THE PULSE AT THE TARGET

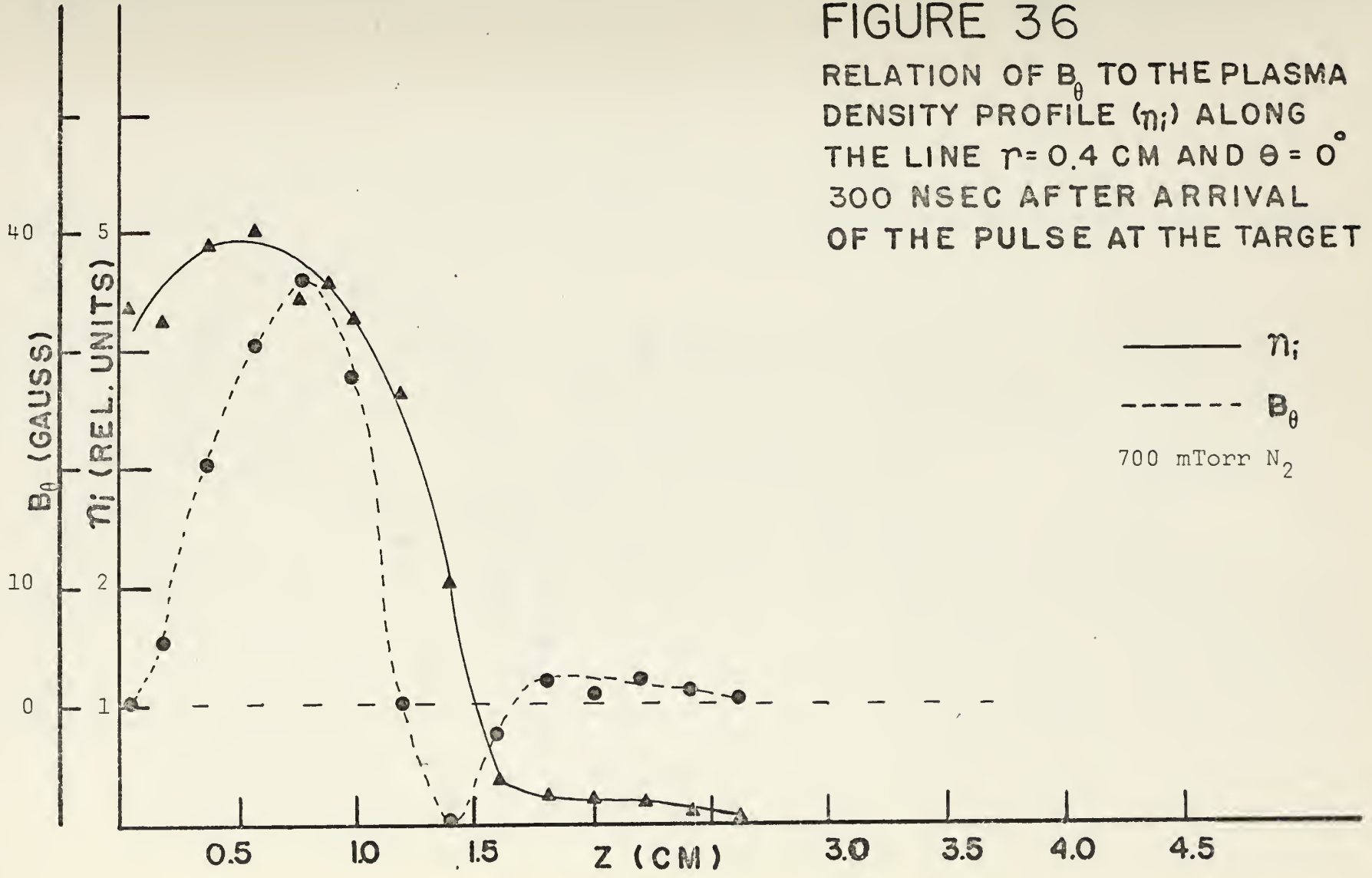

FIGURE 36

RELATION OF B_θ TO THE PLASMA DENSITY PROFILE (n_i) ALONG THE LINE $r = 0.4$ CM AND $\theta = 0^\circ$ 300 NSEC AFTER ARRIVAL OF THE PULSE AT THE TARGET

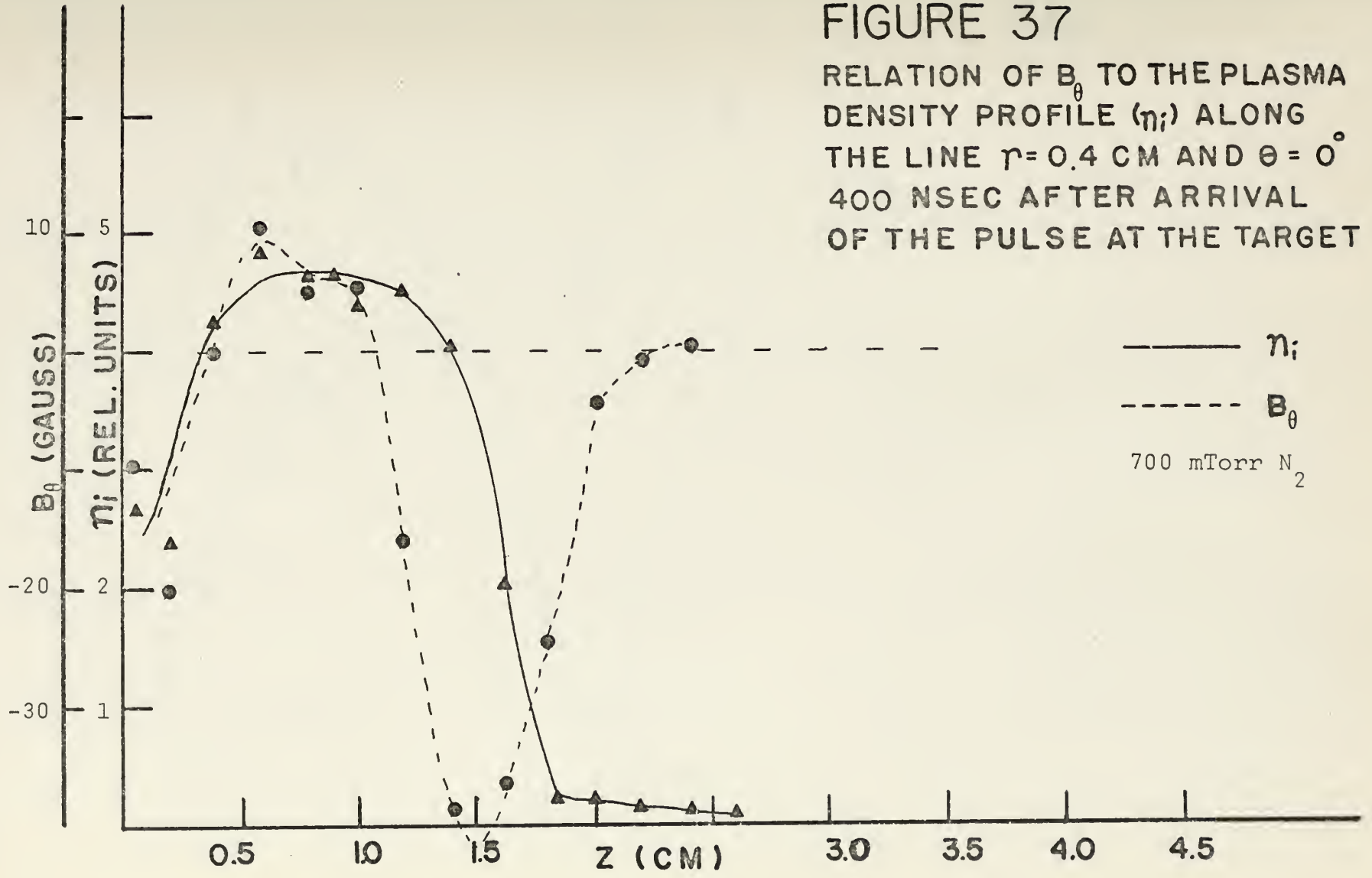

FIGURE 37

RELATION OF B_θ TO THE PLASMA DENSITY PROFILE (n_i) ALONG THE LINE $r = 0.4$ CM AND $\theta = 0°$ 400 NSEC AFTER ARRIVAL OF THE PULSE AT THE TARGET

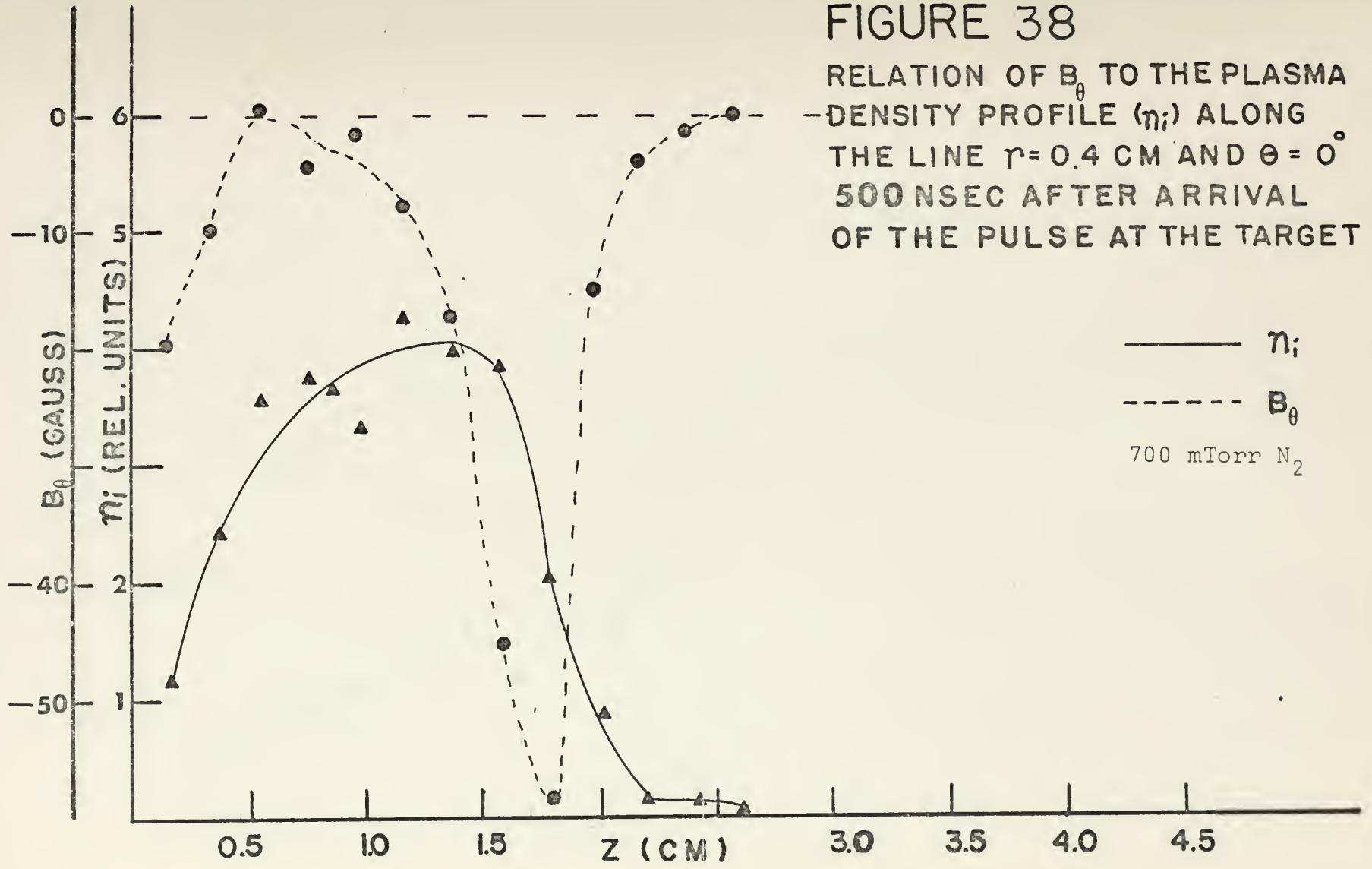

FIGURE 38

RELATION OF B_θ TO THE PLASMA DENSITY PROFILE (n_i) ALONG THE LINE $r = 0.4$ CM AND $\theta = 0°$ 500 NSEC AFTER ARRIVAL OF THE PULSE AT THE TARGET

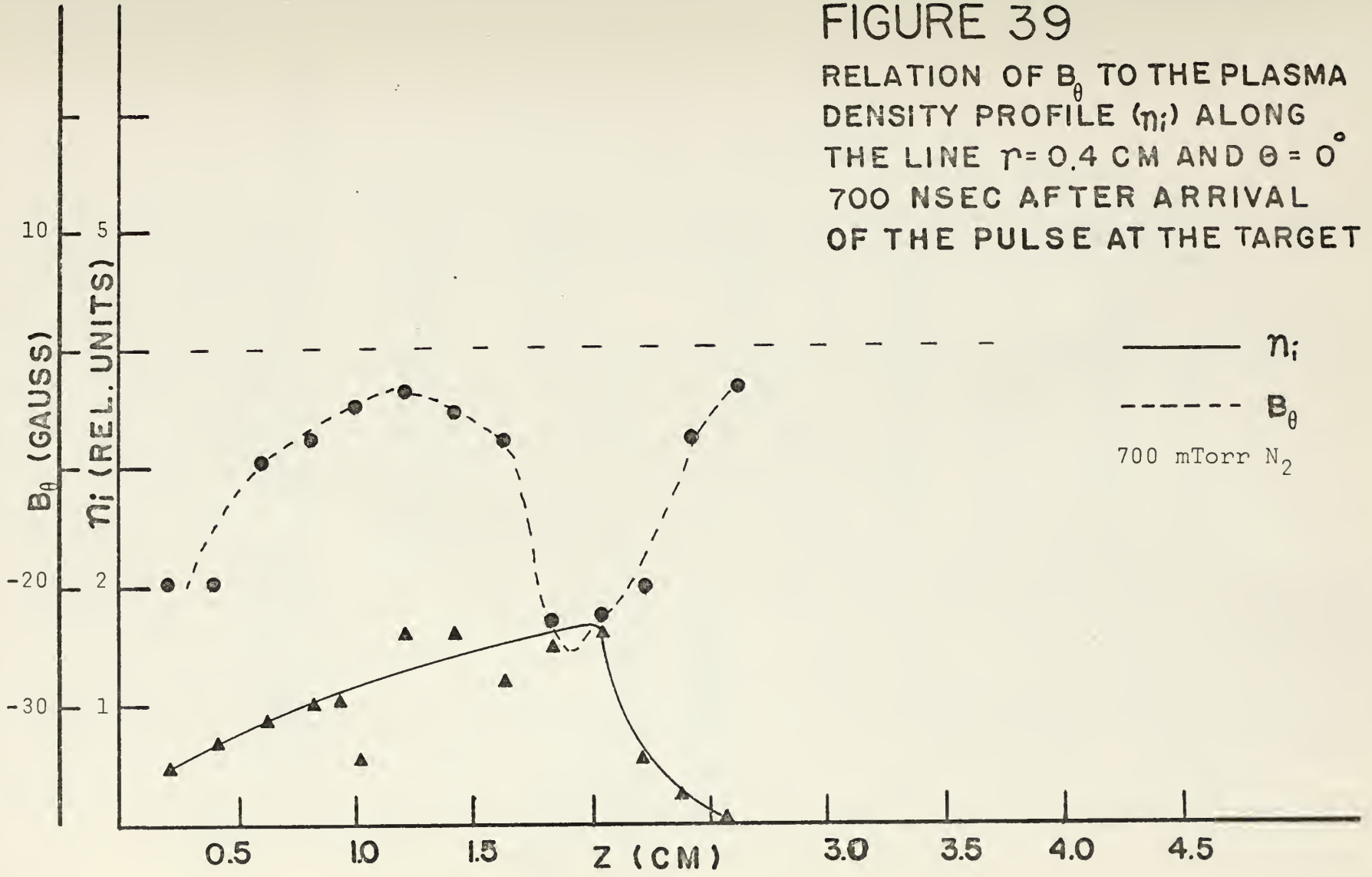

FIGURE 39

RELATION OF B_θ TO THE PLASMA DENSITY PROFILE (n_i) ALONG THE LINE $r = 0.4$ CM AND $\theta = 0^\circ$ 700 NSEC AFTER ARRIVAL OF THE PULSE AT THE TARGET

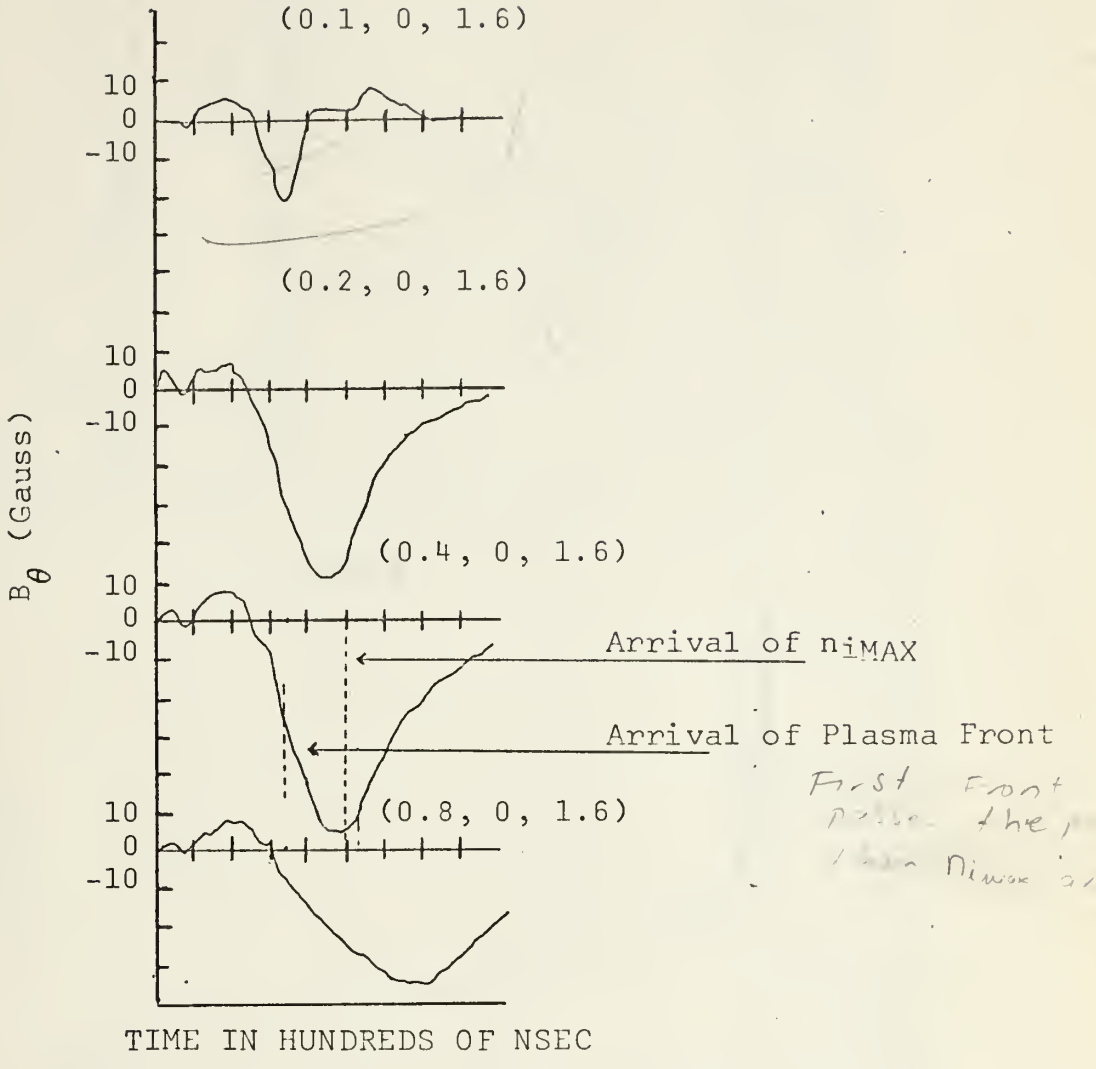

Figure 40. Magnetic field signals (B_θ) detected at various positions along the line z=1.6 cm, θ=0° for a background pressure of 700 mTorr N_2.

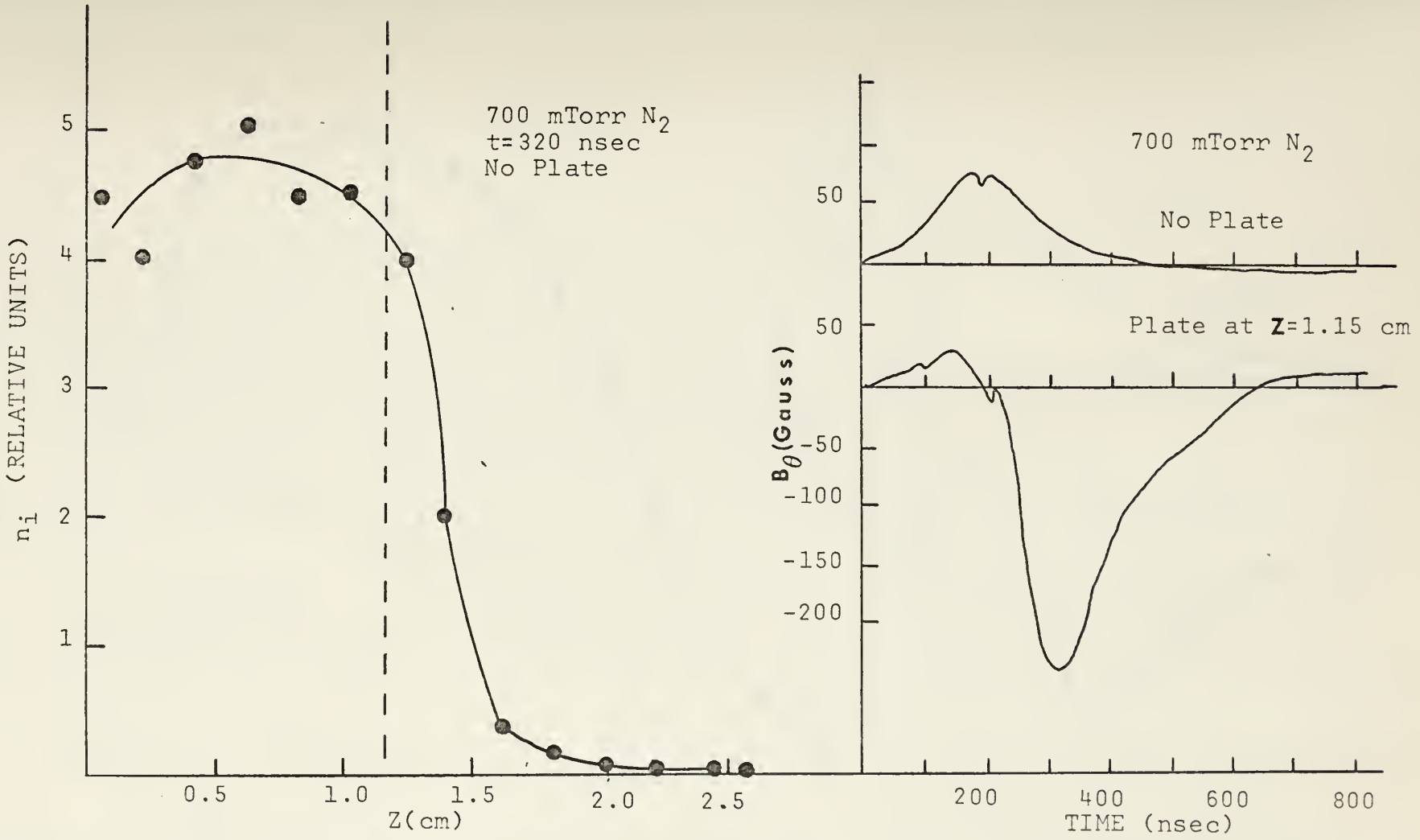

Figure 41. Plasma density profile along the line r=0.4 cm and $\theta = 0^\circ$ for an aluminum target; right-hand side: B_θ at r=0.4 cm, $\theta = 0^\circ$, z=1.0 cm.

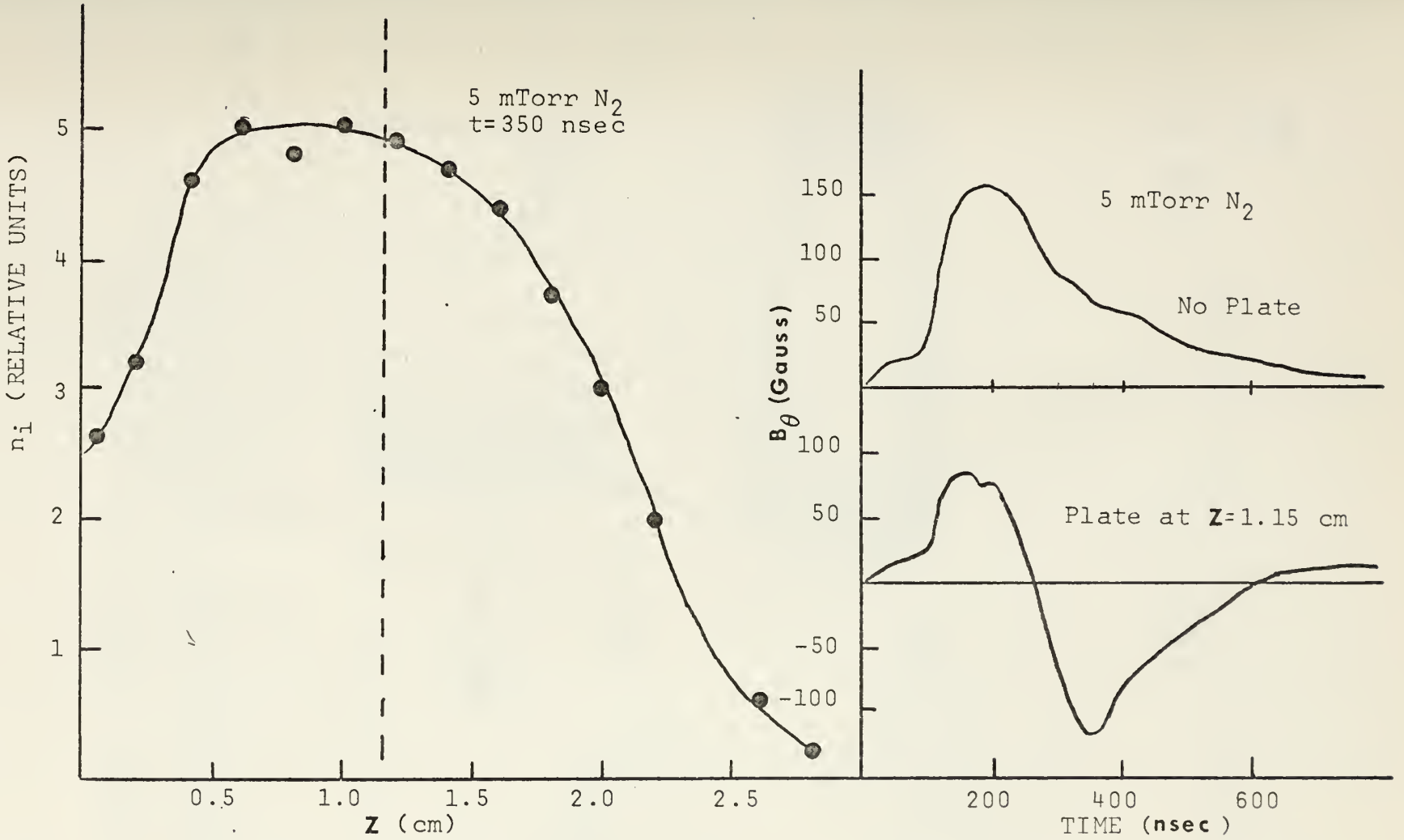

Figure 42. Plasma density profile along the line r=0.4 cm and $\theta = 0^\circ$ for an aluminum target; right-hand side: B_θ at r=0.4 cm, $\theta = 0^\circ$, z=1.0 cm.

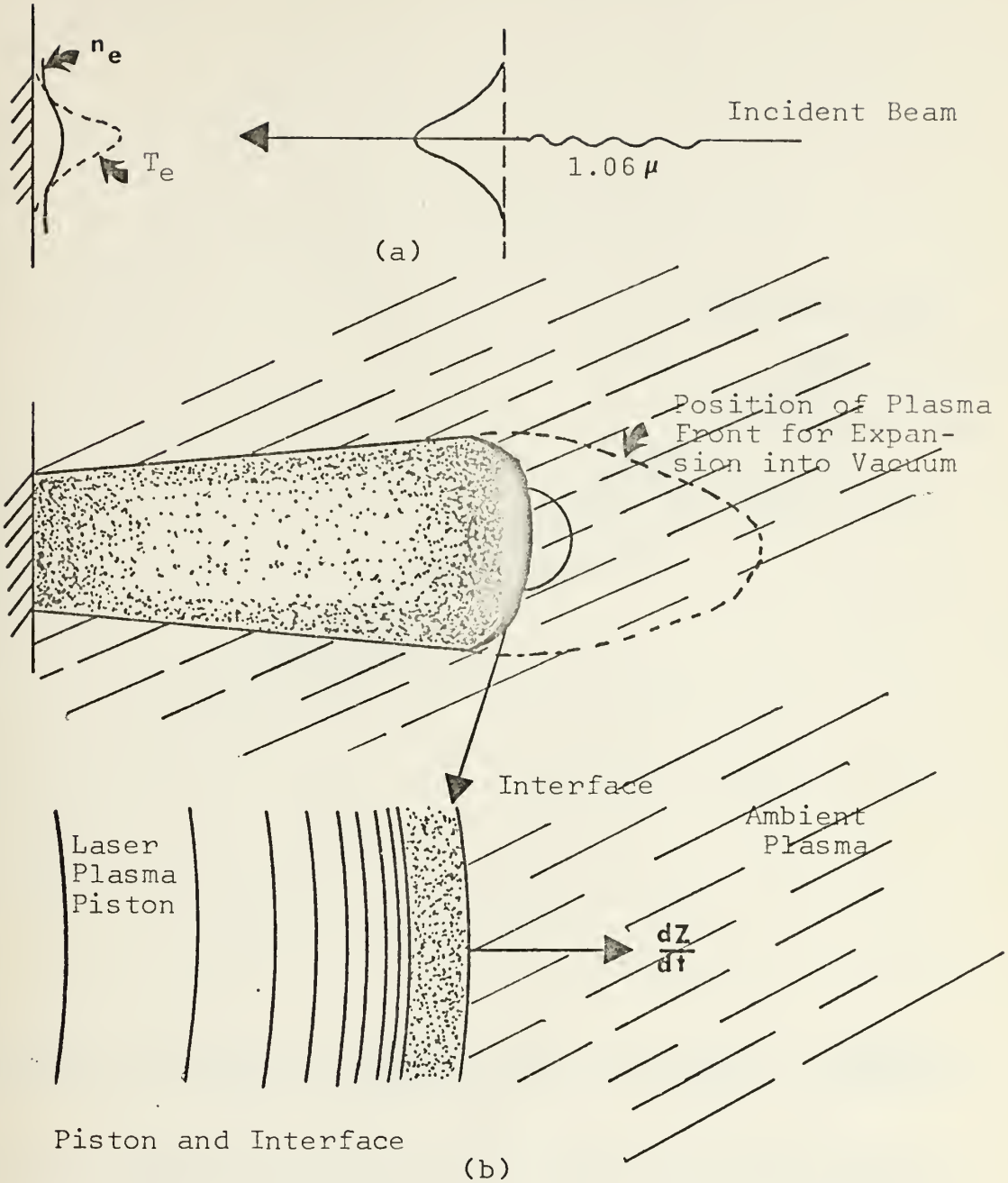

Figure 43. (a) The isothermal and iso-density contours existing near the target surface during the laser pulse.
(b) One dimensional expansion of the laser plasma piston into an ambient background plasma

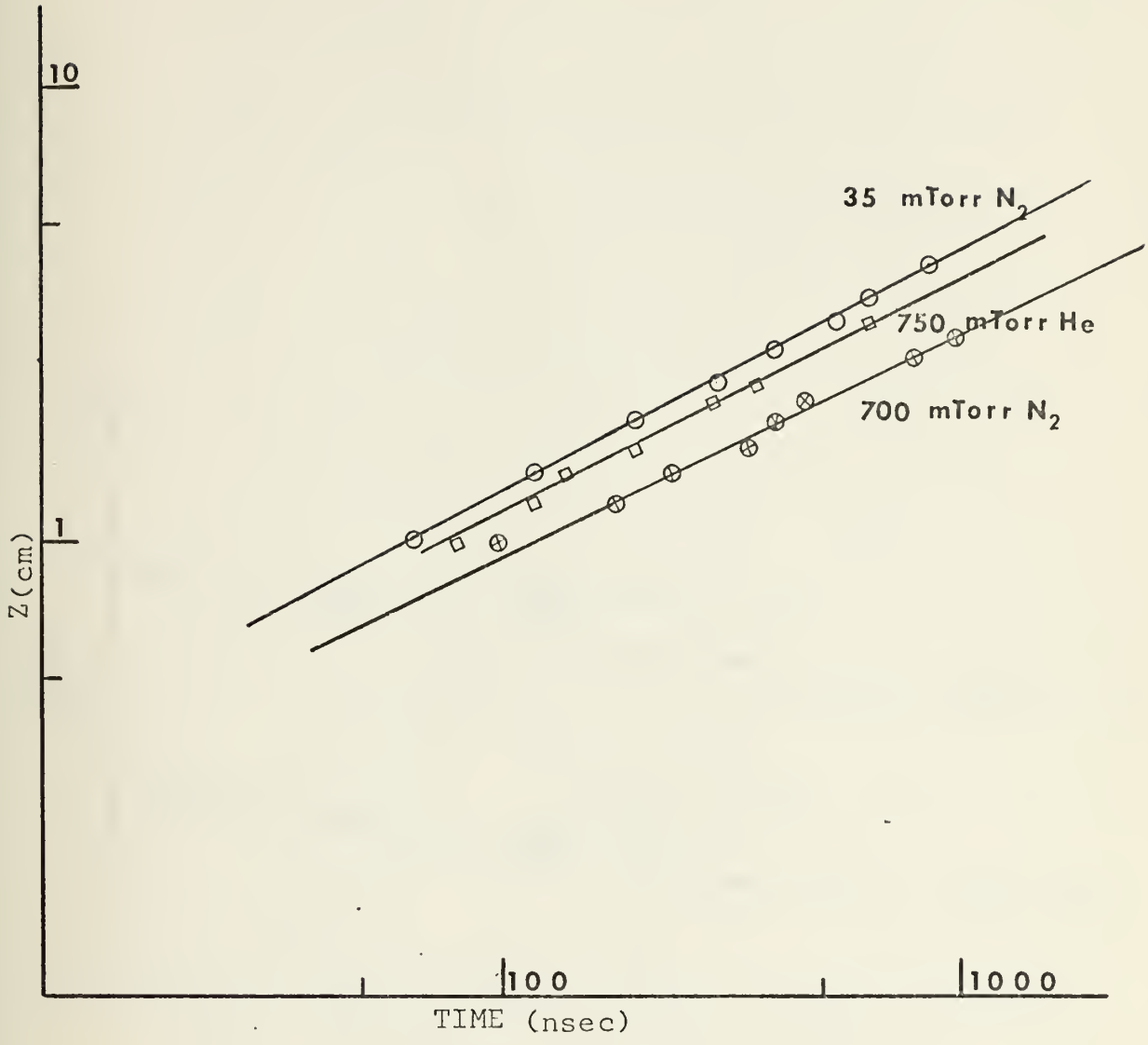

Figure 44. Position of the front of the expanding aluminum laser plasma versus time for various background gas pressures. The data was taken along the expansion axis with a Langmuir double probe.

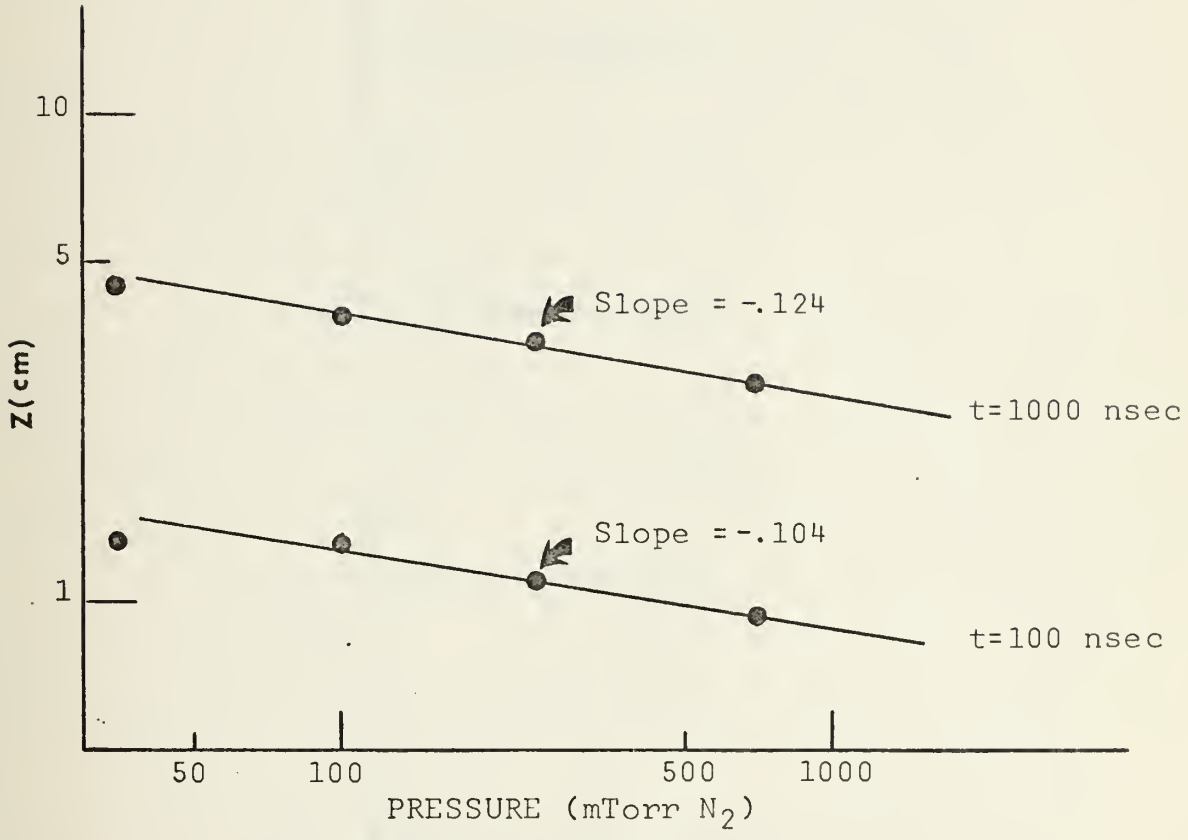

Figure 45. Axial position of the front of the expanding aluminum laser plasma versus nitrogen background pressure at t=100 nsec and t=1000 nsec.

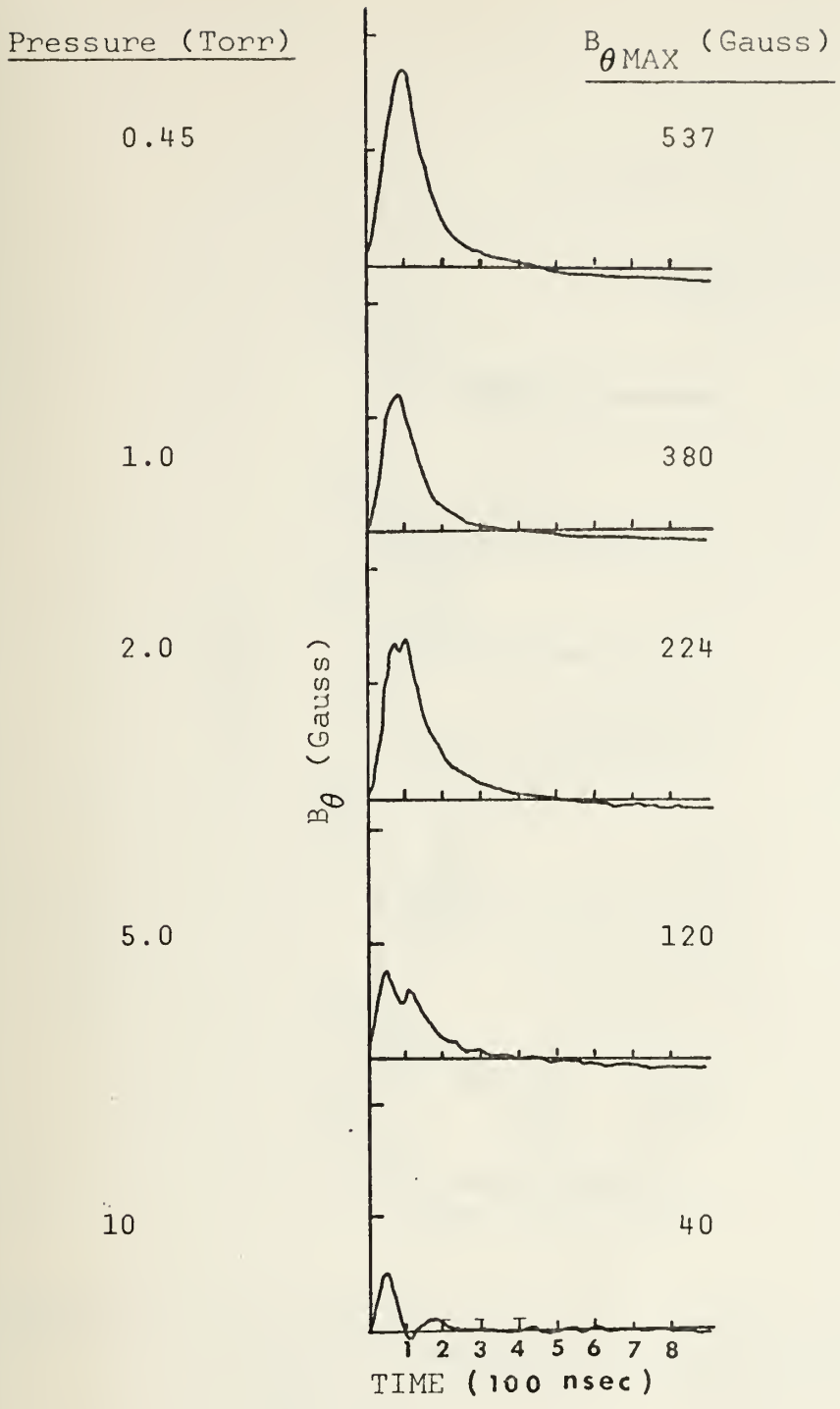

Figure 46. Magnetic probe signals (B_θ) detected at the position r=z=0.4 cm, $\theta=0^\circ$ for various hydrogen background gas pressures.

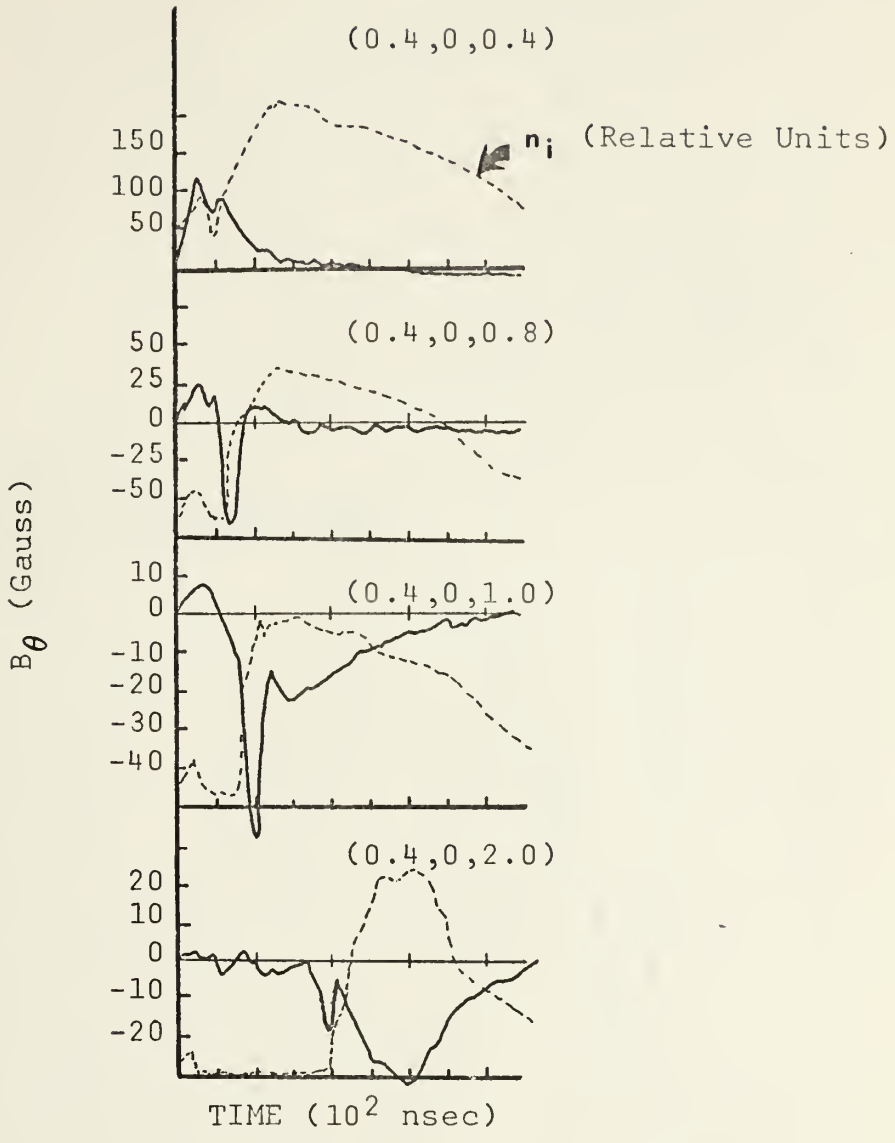

Figure 47. The magnetic field and density profiles detected at various positions along the line r=0.4 cm, $\theta = 0^\circ$ for a background pressure of 5 Torr H_2.

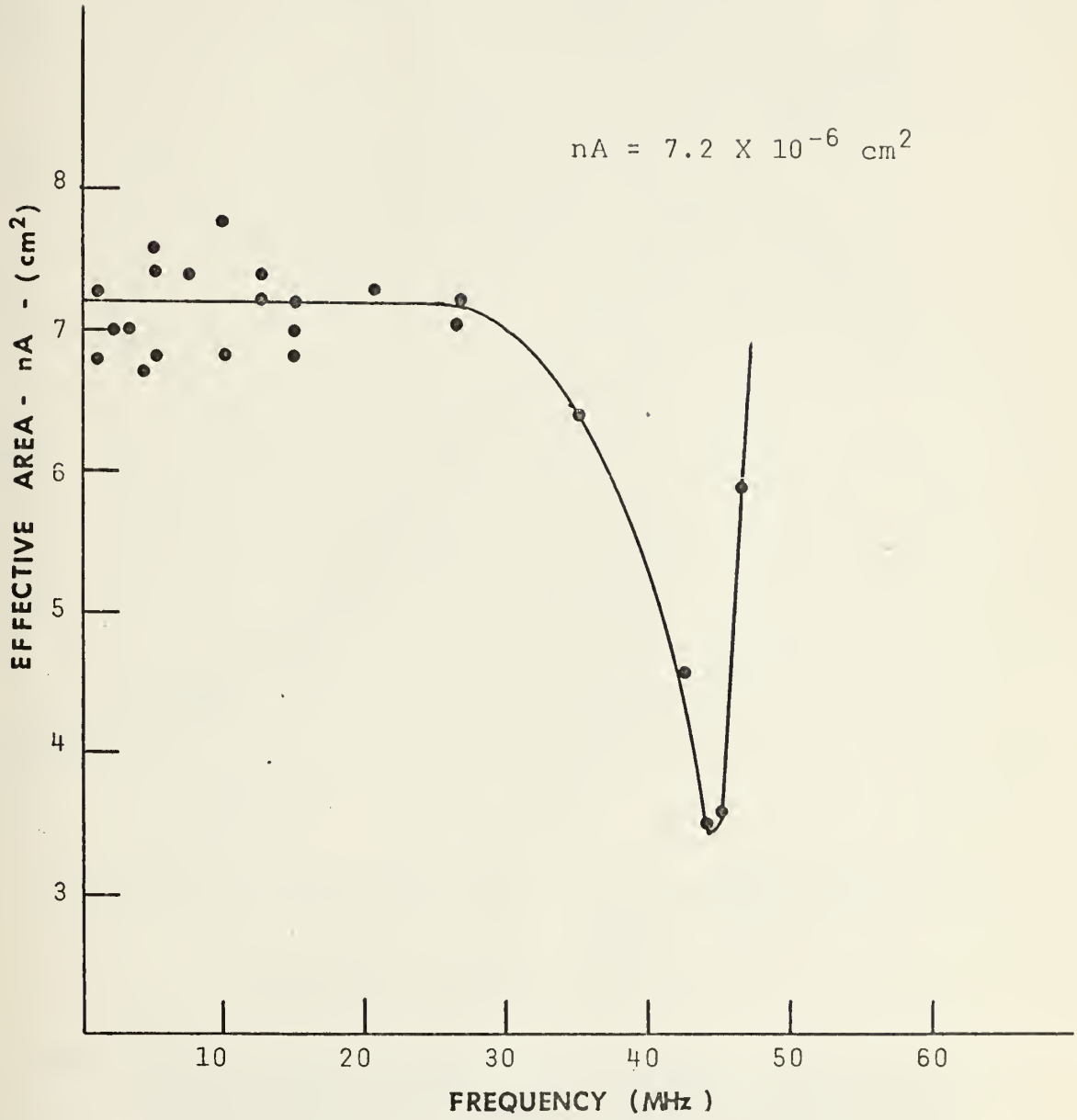

Figure 48. The effective area of the magnetic probe circuit as a function of the frequency of the detected signal

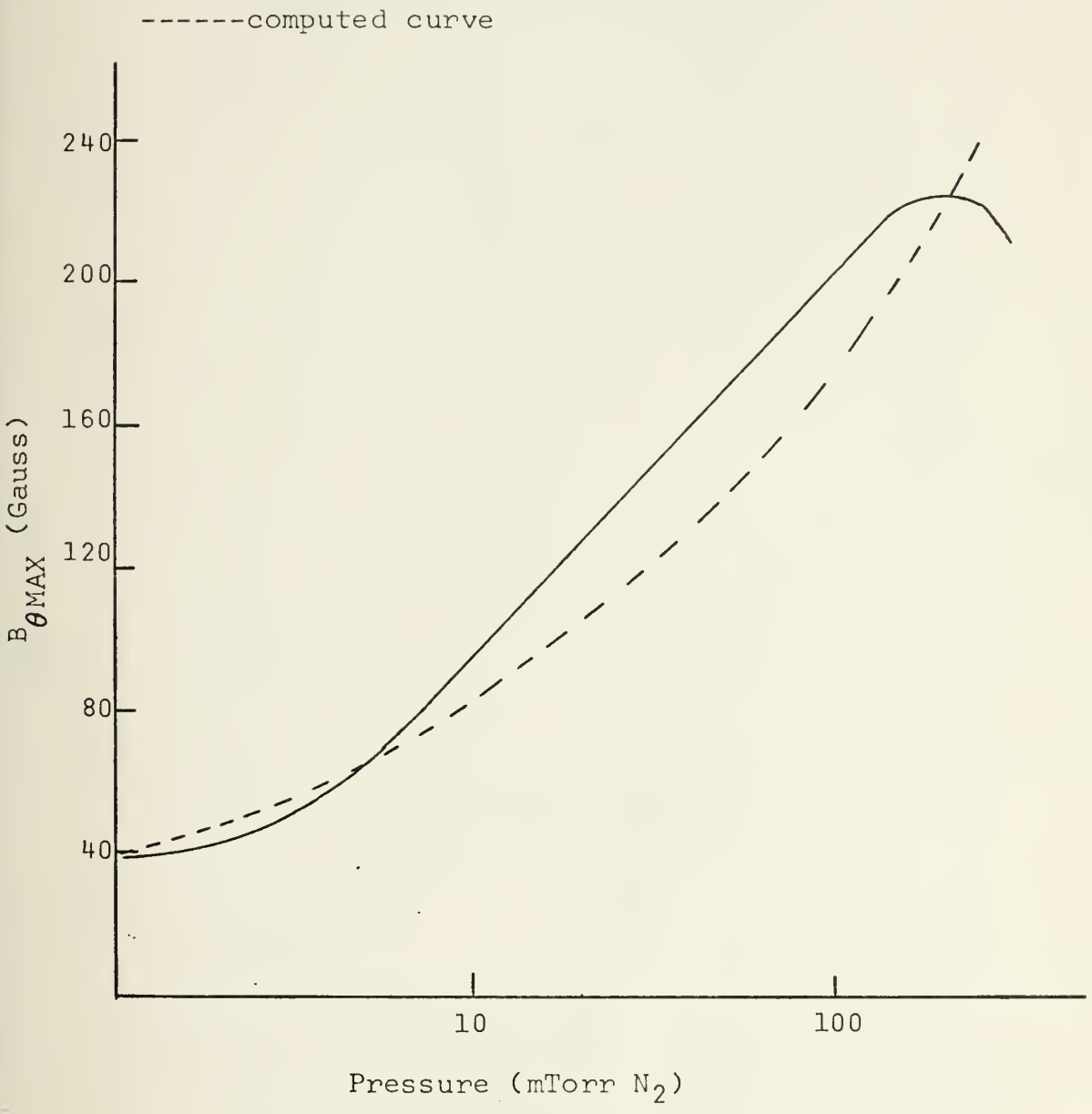

Figure 49. The maximum observed and computed (dashed line) values of $B_{\theta MAX}$ for a Mylar laser plasma as a function of nitrogen background gas pressure at the position $r=z=0.4$ cm, $\theta=0^{\circ}$.

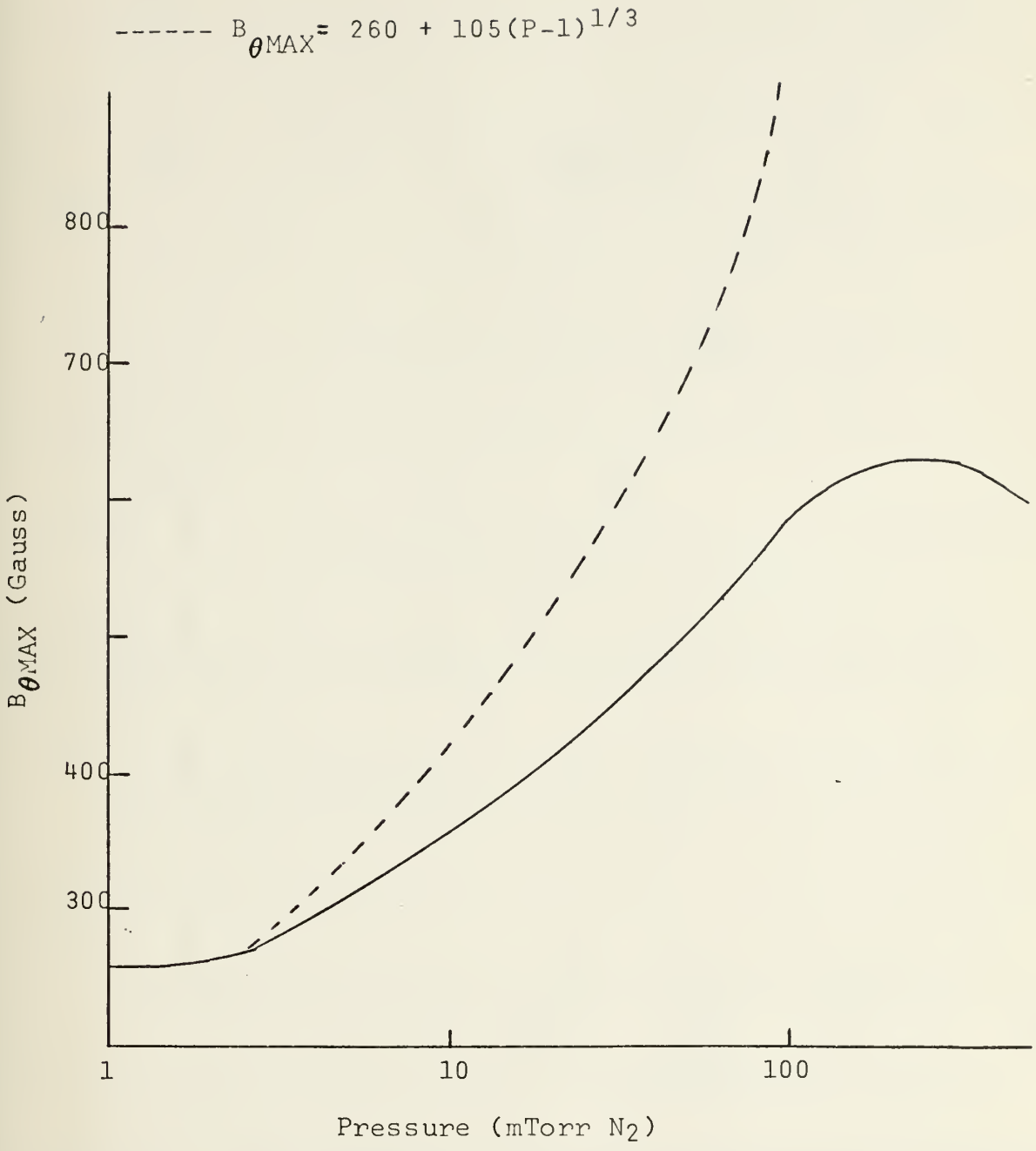

Figure 50. The maximum observed and computed (dashed line) values of $B_{\theta MAX}$ for an Al laser plasma as a function of nitrogen background gas pressure at the position r= z=o.4 cm, $\theta = 0^{\circ}$.

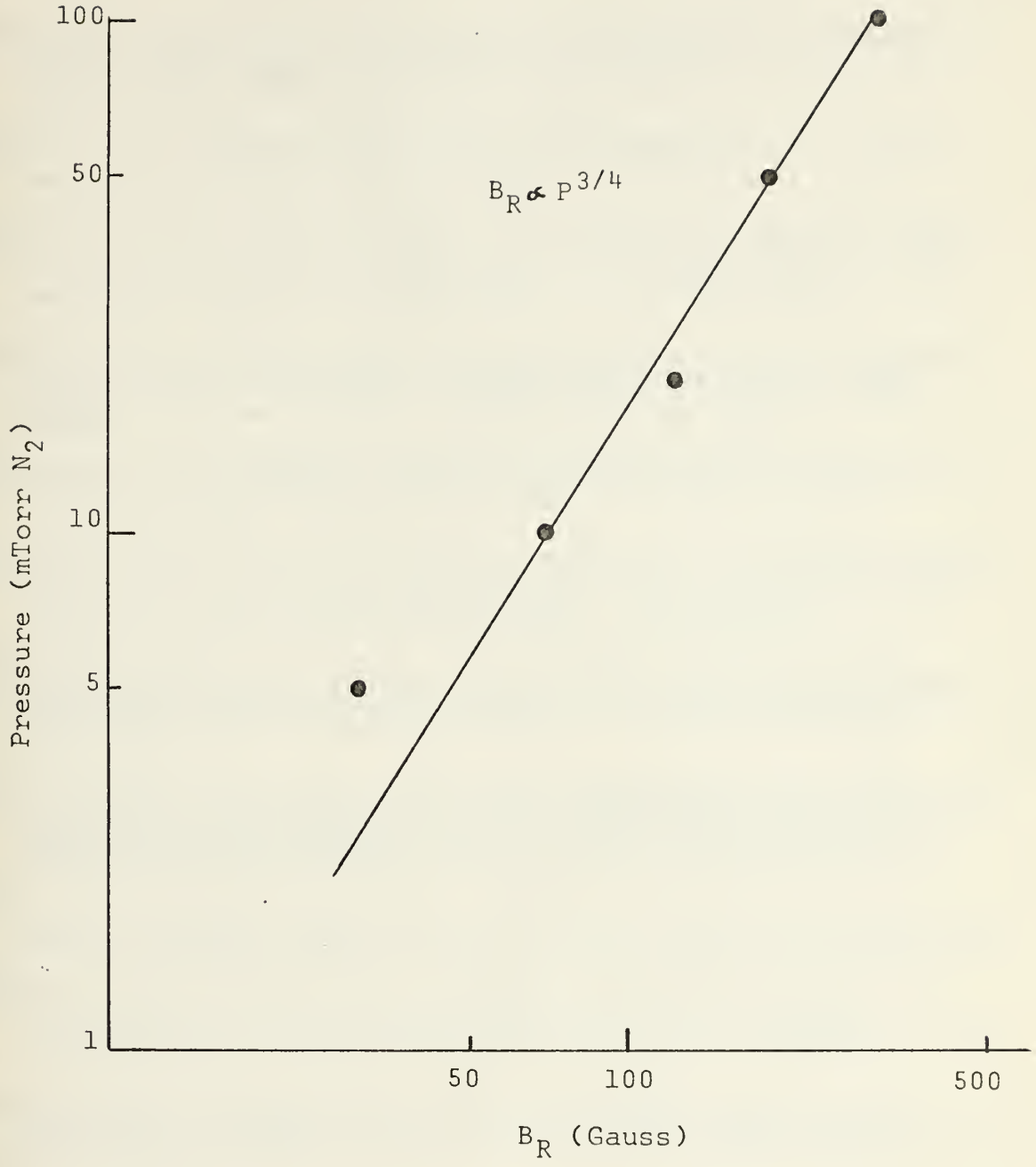

Figure 51. The difference between the observed and computed values of $B_{\theta MAX}$ plotted in Fig. 50 as a function of the nitrogen background gas pressure.

BIBLIOGRAPHY

1. DeMichelis, C., "Laser-Interaction with Solids--A Bibliographical Review," IEEE Journal of Quantum Electronics, v. 6, no. 10, pp. 630-641, October 1970.

2. Ready, J. F., Effects of High-Power Laser Radiation, pp. 109-116 and 161-207, Academic Press, 1971.

3. Bobin, J. L. and others, "Shock Wave Generation in Rarefied Gases by Laser Impact on Beryllium Targets," J. Appl. Phys., v. 39, no. 9, pp. 4184-4189, August 1968.

4. Haught, A. F. and Polk, D. H., "High-Temperature Plasmas Produced by Laser Beam Irradiation of Single Solid Particles," Phys. Fluids, v. 9, no. 10, pp. 2047-2056, October 1966.

5. Spitzer, L., Jr., Physics of Fully Ionized Gases, 2nd. Edition, Interscience Publishers, Inc., 1962

6. Koopman, D. W., "Momentum Transfer Interaction of a Laser-Produced Plasma with a Low-Pressure Background," Phys. Fluids, v. 15, no. 11, pp. 1959-1968, November 1972.

7. University of Maryland Technical Note BN-658, Experimental Study of Streaming Laser-Produced Plasmas, by David W. Koopman, June 1970.

8. Naval Research Laboratory Report 7301, Demonstration of Collisionless Interactions Between Counterstreaming Ions in a Laser-Produced Plasma Experiment, by S. O. Dean, 17 September 1971.

9. Hall, R. B., "Laser Production of Blast Waves in Low Pressure Gases," J. Appl. Phys., v. 40, no. 4, pp. 1941-1945, March 1969.

10. Ramsden, S. A. and Savic, P., "A Radiative Detonation Model for the Development of a Laser-Induced Spark in Air," Nature, v. 203, no. 4951, pp. 1217-1219, 19 September 1964.

11. Raizer, Yu. P., "Heating of a Gas by a Powerful Light Pulse," Soviet Physics JETP, v. 21, no. 5, pp. 1009-1017, November 1965.

12. McKee, L. L., An Investigation of the Self-Generated Magnetic Fields Associated with a Laser-Produced Plasma, Ph.D. Thesis, Naval Postgraduate School, 1972.

13. Stamper, J. A. and others, "Spontaneous Magnetic Fields in Laser-Produced Plasmas," Phys. Rev. Letters, v. 26, no. 17, pp. 1012-1015, 26 April 1971.

14. Dawson, J. M., "On the Production of Plasma by Giant Pulse Laser," Phys. Fluids, v. 7, no. 7, pp. 981-987, July 1964.

15. Bird, R. S. and others, "Pressure Dependence of Self-Generated Magnetic Fields in Laser-Produced Plasmas," The Physical Review, v. 7, no. 4, pp. 1328-1331, April 1973.

16. Wright, T. P. and Widner, M. M., "Some Geometrical Effects on the Source of Spontaneous Laser-Generated Magnetic Fields," Bull. Am. Phys. Soc., v. 17, p. 1027, 1972.

17. Giouvanielli, D. V. and McCall, T. H., "Spontaneously Generated Magnetic Fields in a Laser-Driven Plasma," to be published.

18. Braginski, S. I., Chapter in Reviews of Plasma Physics v. 1, Leontovich, M. A., ed., p. 232 and p. 273, (Consultants Bureau, New York), 1966.

19. McLaughlin, T. A., Inductive Magnetic Probe Diagnostics in a Plasma, MS Thesis, Naval Postgraduate School, 1970.

20. Chen, F. F., Chapter in Plasma Diagnostic Techniques, Huddlestone, R. H. and Leonard, S. L., eds., p. 178, Academic Press, New York, 1965.

21. Korobkin, V. V. and Serov, R. V., "Investigation of the Magnetic Field of a Spark Produced by Focusing Laser Radiation," JETP Letters, v. 4, no. 3, pp. 103-106, 1 August 1966.

22. Widner, M. M., "Self-Generated Magnetic Fields in Laser Plasmas," to be published.

23. Isenor, N. R., "Effect of Background Gas on Laser-Induced Electron Emission from Metal Targets," J. Appl. Phys., v. 36, no. 1, p. 316, January 1965.

24. Knecht, W. L., "Initial Energies of Laser-Induced Electron Emission from W," Appl. Phys. Lett., v. 6, no. 6, p. 99, March 1965.

25. Arifov, T. V., et al. "Laser-Induced Current Pulses from a Target in a Gas," Sov. Phys. JETP, v. 28, no. 2, p. 201, February 1969.

26. McDaniel, E. W., Collision Phenomena in Ionized Gases, pp. 629-677, Wiley, 1964.

INITIAL DISTRIBUTION LIST

		No. Copies
1.	Defense Documentation Center Cameron Station Alexandria, Virginia 22314	2
2.	Library, Code 0212 Naval Postgraduate School Monterey, California 93940	2
3.	Professor Alfred Cooper, Code 61Cr Department of Physics and Chemistry Naval Postgraduate School Monterey, California 93940	10
4.	Professor Fred Schwirzke, Code 61Sw Department of Physics and Chemistry Naval Postgraduate School Monterey, California 93940	1
5.	LCDR Ronald S. Bird, USN	1
	1342 Lady Marian Lane Dunedin, Florida 33528	1
6.	Captain Leslie L. McKee, III, USAF AFWL/DYS Kirtland AFB, New Mexico 87117	1

Security Classification

DOCUMENT CONTROL DATA - R & D

(Security classification of title, body of abstract and indexing annotation must be entered when the overall report is classified)

1. ORIGINATING ACTIVITY (Corporate author)

Naval Postgraduate School
Monterey, California 93940

2a. REPORT SECURITY CLASSIFICATION

Unclassified

2b. GROUP

3. REPORT TITLE

The Pressure Dependence of Spontaneous Magnetic Fields in Laser Produced Plasmas.

4. DESCRIPTIVE NOTES (Type of report and, inclusive dates)

Doctor of Philosophy, June 1973

5. AUTHOR(S) (First name, middle initial, last name)

Ronald S. Bird

6. REPORT DATE	7a. TOTAL NO. OF PAGES	7b. NO. OF REFS
June 1973	146	26

8a. CONTRACT OR GRANT NO.	9a. ORIGINATOR'S REPORT NUMBER(S)
b. PROJECT NO.	
c.	9b. OTHER REPORT NO(S) (Any other numbers that may be assigned this report)
d.	

10. DISTRIBUTION STATEMENT

Approved for public release; distribution unlimited.

11. SUPPLEMENTARY NOTES	12. SPONSORING MILITARY ACTIVITY
	Naval Postgraduate School Monterey, California 93940

13. ABSTRACT

A plasma has been produced by irradiation of an aluminum slab with a 6.6 joule, 22 nanosecond (10^{10} watt/cm^2) pulse of 1.06 micron radiation. Magnetic fields were observed to arise spontaneously when the laser-produced plasma was formed. The space and time behavior of the spontaneous magnetic fields and their relationship to the plasma density profile for expansion into various background pressures of H_2, He, N_2 and Ar was investigated using magnetic and electrostatic (double) probes. The magnitude and direction of the magnetic fields was found to depend on the background gas pressure. The generation of spontaneous magnetic fields at the front of the expanding laser plasma was observed long after laser irradiation ceased. These fields were axially symmetric and in a direction opposite to the initial field direction. Reverse fields were observed only above a "critical" background gas pressure. Magnetic fields were also observed to arise when a laser plasma impinged on a glass plate.

The observed increase of the magnitude of the initial spontaneous magnetic fields is interpreted as arising from the momentum interaction between the expanding laser plasma and the pre-ionized ambient background plasma. The reverse field is attributed to the development of an axial electron temperature gradient at the plasma front due to snowplowing of the ambient plasma.

DD FORM 1 NOV 68 1473 (PAGE 1)

S/N 0101-807-6811

Security Classification

A-31408

KEY WORDS	LINK A		LINK B		LINK C	
	ROLE	WT	ROLE	WT	ROLE	WT
Self-Generated Magnetic Fields						
Laser-Produced Plasma						
Magnetic Probe Signal						
Ambient Background Gas						
Photoionization						
Counterstreaming Plasmas						
Diffusion Time						

145233
Thesis
B5438 Bird
c.1 The pressure dependence of spontaneous magnetic fields in laser produced plasmas.